Universidade Federal do Paraná

Marina Elaine Wosniack

A Statistical Mechanics Approach to Random Searches

Curitiba
2016

Universidade Federal do Paraná
Programa de pós-graduação em Física

Marina Elaine Wosniack

A Statistical Mechanics Approach to Random Searches

Thesis submitted to the *Curso de Pós-graduação em Física* of the *Setor de Ciências Exatas* of the *Universidade Federal do Paraná*, in partial fulfillment of the requirements for the degree of Doctor of Physics.
Advisor: *Prof. Dr. Marcos Gomes E. da Luz.*

Curitiba
2016

W928s Wosniack, Marina Elaine
A statistical mechanics approach to random searches / Marina Elaine Wosniack. – Curitiba, 2016.
131f. . : il. [algumas color.] ; 30 cm.

Tese (doutorado) - Universidade Federal do Paraná, Setor de Ciências Exatas, Programa de Pós-Graduação em Física, 2016.

Orientador: Marcos Gomes E. da Luz

1. Física estatística. 2. Mecânica estatística I. Universidade Federal do Paraná. II. Luz, Marcos Gomes E. da. III. Título.

CDD: 530.13

MINISTÉRIO DA EDUCAÇÃO
UNIVERSIDADE FEDERAL DO PARANÁ
SETOR DE CIÊNCIAS EXATAS
CURSO DE PÓS-GRADUAÇÃO EM FÍSICA

Fone: (41) 3361-3096 **Fax:** (41) 3361-3418
E-mail: posgrad@fisica.ufpr.br

ATA DE DEFESA DE TESE DE DOUTORADO

"A Statistical Mechanics Approach to Random Searches".

ALUNA

MARINA ELAINE WOSNIACK

Em sessão pública iniciada às treze horas do dia 18 de fevereiro de 2016, após um seminário sob o título acima e posterior arguição, esta banca examinadora decidiu aprovar a candidata com o conceito global A.

Banca Examinadora	Assinatura	Conceito
Prof. Dr. Marcos Gomes Eleutério da Luz (UFPR)		A
Prof. Dr. Gilberto Medeiros Kremer (UFPR)		A
Prof. Dr. Wilson Marques Junior (UFPR)		A
Profª Dra. Celia Beatriz Anteneodo de Porto (PUC-RJ)		A
Prof. Dr. Iberê Luiz Caldas (USP)		A

MINISTÉRIO DA EDUCAÇÃO
UNIVERSIDADE FEDERAL DO PARANÁ
SETOR DE CIÊNCIAS EXATAS
CURSO DE PÓS-GRADUAÇÃO EM FÍSICA

Fone: (41) 3361-3096 **Fax:** (41) 3361-3418
E-mail: posgrad@fisica.ufpr.br

PARECER

Os abaixo-assinados, membros da banca examinadora de Defesa de Tese de Doutorado da aluna ***MARINA ELAINE WOSNIACK***, consideram aprovada a redação final da tese, cujo título é: *"A Statistical Mechanics Approach to Random Searches"*.

Curitiba, 18 de fevereiro de 2016.

Banca Examinadora	**Assinatura**
Prof. Dr. Marcos Gomes Eleutério da Luz (UFPR)	
Prof. Dr. Gilberto Medeiros Kremer (UFPR)	
Prof. Dr. Wilson Marques Junior (UFPR)	
Profª. Dra. Celia Beatriz Anteneodo de Porto (PUC/RJ)	
Prof. Dr. Iberê Luiz Caldas (USP)	

To my loving grandfather, *nonno* Sileno, for his contagious *joie de vivre*.

Acknowledgements

First and foremost I would like to acknowledge my advisor Prof. Marcos Gomes Eleutério da Luz (Universidade Federal do Paraná). It has been a long time working under his supervision and I appreciate all his contributions in time, ideas and discussions to make my PhD experience productive and stimulating. I am also grateful to Prof. Marcos for the opportunity and encouragement to work abroad in different research fields under the supervision of high skilled scientists.

I am grateful to Prof. Gandhi M. Viswanathan (Universidade Federal do Rio Grande do Norte) and Prof. Ernesto P. Raposo (Universidade Federal de Pernambuco) for their support during my work and especially in the submission of my papers.

All the numerical simulations were realized with the computational support provided by Prof. Carlos de Carvalho (Universidade Federal do Paraná), to whom I am also grateful.

I also would like to acknowledge Prof. Lawrence Schulman (Clarkson University) for my inspiring split doctorate period in USA. Under Prof. Larry supervision I worked in different scientific problems and learned (a lot of) Physics. I am grateful to the Physics Department from Clarkson University for their support in my research and the stimulating working environment I had there.

I am grateful to Dr. Jimena Berni (Cambridge University) for the precious opportunity of developing an experimental part of my work under her supervision and using her laboratory in the Zoology Department. Many thanks to all the staff and colleagues that helped me in Cambridge.

Finally, I would like to thank CAPES for the scholarship that supported my graduate studies since 2010, CNPq for my *Science Without Borders* scholarship in Clarkson University (USA) and CAPES again for my *PDSE* scholarship in Cambridge University (UK). These fundings were very important in my career and I am very grateful to them.

Abstract

The topic of this thesis is the application of random search models in a collection of interdisciplinary problems. We developed simple models that can reproduce (at some extent) the complex behavior present in the problems that we have chosen. The first applications concerned animal foraging, where the robustness of the Lévy flight foraging hypothesis was numerically studied. We developed a model of a dynamic distribution of targets and studied the emergence of the stationarity in this new problem. A parallel optimization method was designed to reduce the computational costs in random search simulations, and was proved efficient in homogeneous search environments. In a direct application of random search models, we studied the dual foraging behavior of *Drosophila melanogaster* larvae with both a numerical and an experimental approach. A new procedure was applied in the study of random searches using a stochastic process formulation. In this problem, a spectral method was developed to reconstruct the geometry of the targets distribution using only the transition matrix of the search process. The last work was the study of a model that describes the evolutionary process using a statistical mechanics approach. We designed a thermodynamics interpretation of the transitions between stasis and hectic phases in the model and applied simulated annealing techniques to reach longer stasis configurations.

Keywords: random search, Lévy flights, statistical mechanics, stochastic processes.

Resumo

O tópico desta tese é a aplicação de modelos de busca aleatória em uma coleção de problemas multi-disciplinares. Foram desenvolvidos modelos simples que reproduzem (aproximadamente) o comportamento complexo dos problemas que escolhemos. As primeiras aplicações consideram o problema do forrageamento biológico, onde estudamos numericamente evidências que suportam a otimização por buscas de Lévy. Em seguida, desenvolvemos um modelo de distribuição de alvos dinâmica e estudamos a emergência da estacionariedade neste problema. Um modelo para a otimização computacional de buscas em ambientes homogêneos foi elaborado utilizando ferramentas de paralelização. Numa aplicação direta de buscas aleatórias, estudamos o forrageamento de larvas da mosca da fruta *Drosophila melanogaster* em um modelo numérico e através de uma abordagem experimental. Utilizamos um procedimento novo para caracterizar a busca aleatória através de processos estocásticos. Um método espectral foi aplicado na reconstrução do ambiente de busca utilizando a matriz de transição do processo. O último trabalho foi um estudo de um modelo que descreve, através da mecânica estatística, um processo evolucionário. Desenvolvemos um tratamento termodinâmico para interpretar as transições de fase do processo, bem como empregamos técnicas de *simulated annealing* para obter configurações mais robustas do modelo.

Palavras-chave: busca aleatória, vôos de Lévy, mecânica estatística, processos estocásticos.

Contents

List of Figures

List of Tables

Chapter 1

Introduction

Nature uses only the longest threads to weave her patterns, so each small piece of her fabric reveals the organization of the entire tapestry.

Richard P. Feynman

The present PhD thesis is a numerical and theoretical study of a class of practical problems involving random searches, Lévy flights and complex systems in general. This introductory Chapter motivates the importance of using computational models and statistical mechanics tools to understand very complex problems like animal foraging and evolution of species.

The understanding of the natural world is the utmost aim of scientific research. Surrounded by complex problems, scientists rely in simplification techniques to gather insights into their problems. Among the most used approaches, idealized simple models that are thoroughly studied in Physics (like the simple harmonic oscillator and the isotropic random walk) are widely used in inter-disciplinary fields such as Biology, Ecology, Economics and Chemistry.

Random walks, that are familiar to physicists in statistical mechanics, have been succesfully employed in the description of animal movement since the first studies on animal dispersal [1]. Surely it is an impossible task to generalize a single displacement model to a broad range of animal species, and several distinct random walk models have been introduced in the literature in the last decades [2–4]. One common hypothesis in these models is that the animals are constantly looking for something, like food, mates or shelter, that is, they are foraging in nature. The exact location of resources is unknown

to the animal during the foraging, and they rely on a good search strategy to locate these resources.

The movement pattern of an animal is the result of complex behavioral and biophysical responses to internal decisions, the interaction with environmental cues and constrains. Surely it is impossible to model all these internal and external factors, thus most animal displacement models add a certain degree of *stochasticity* to fulfill the description. Random search models have been used to describe animal foraging as a stochastic process [5]. In these models, the resources are represented as points in a landscape. The forager has a small perceptual radius, and uses it to detect resources. Since the location of resources is unknown to the forager, it moves through the space until a resource falls within its perceptual radius. The pattern executed by the forager in the search is its search strategy, and is closely related to its random walk.

Statistical mechanics is essentially the description of macroscopic phenomena that result from microscopic interactions among innumerable individual components. Thus, the macroscopic statistical mechanics properties of the search strategies are related to the microscopic steps performed by the organism. In the same way, the microscopic interactions between individuals result in the macroscopic evolution patterns, again a complex problem that can be approached by statistical mechanics methods. In this way, throughout this thesis we will use a statistical mechanics approach to a selection of complex problems that are characterized as random searches.

About this Thesis

The present thesis is divided in independent chapters corresponding to different problems studied during the PhD. Regardless of being very distinct subjects, all the problems were modeled using random searches. At the beginning of each Chapter a full introduction into the problem is presented with a review of the related works in the literature.

In Chapter 2 we present the fundamental concepts of random walks and random searches that are very important to the following chapters. We develop the connection between the isotropic one dimensional random walk and the diffusion equation, emphasizing the Brownian motion. The Lévy flights are discussed in terms of stable distributions, following the historical work by Paul Lévy. Finally, we present the search heuristics used in the thesis, altogether with a survey on the literature of random searches.

In Chapter 3 we propose a numerical investigation of an ongoing question in the literature: the presence of Lévy flights across so many animal species is the result of an evolutive pressure or just an emergent pattern? We show the robustness of optimal Lévy flights in a variety of fragmented landscapes that resemble the distribution of resources

in nature. Further, we obtain an emergent Brownian motion pattern in a very dense environment explored by a Lévy walker.

In Chapter 4 a dynamic distribution of targets is the subject of the work. In this model, we increase the number of targets periodically in a destructive search process. We want to characterize the stationarity in the process, that is, when the searcher eliminates targets to the same extent in which new ones are created. We show that the stationarity is achieved first for the ballistic strategy and later for the Brownian searcher. Finally, we discuss the correspondence between the dynamic and static models.

In Chapter 5, a practical problem is considered: how to reduce the computational cost of random search simulations? Our approach uses parallelization techniques in the original algorithm with a new procedure that implements the sequential features in the parallel solution. We obtained a significant reduction in the computational time and discuss the limitations of our method.

In Chapter 6, a numerical and experimental work concerning the efficiency of distinct foraging strategies is presented. The numerical part was made comparing the performance of a composite search strategy and Lévy flights in a fragmented environment. Then, the experimental work was done tracking *Drosophila melanogaster* larvae trajectories foraging in a patchy environment. In nature, these larvae show a dual foraging strategy: approximately 70% of the population performs Lévy flights and the remaining 30% adopts a composite search strategy. We compare the numerical and experimental approaches and discuss the implications of the work.

In Chapter 7, we study the random search as a stochastic process. First we write a transition matrix corresponding to the evolution of states (in this case the locations of the random searcher). We apply a spectral method to the transition matrix, known as the observable representation, to visualize the geometry of the states space. Finally, we show that the information about the geometrical configuration of the environment (and the targets distribution) can be recovered by means of the transition matrix.

In Chapter 8 an evolutionary model is presented. We study the formation of stable evolutionary periods in the model and characterize it using thermodynamics quantities. We analyze the relevance of the interaction matrix to the model, showing that the interaction strengths and the network connectivity are essential parameters in the formation of stable periods. Further, we propose a simulated annealing approach to speed up the location of mutualistic pairs in the matrix, obtaining longer stable periods.

In Chapter 9 we outline our conclusions and final remarks.

Four Appendices are included in this thesis. Appendix A is a survey on probability and statistics, with definitions and theorems regarding random variables. In Appendix

B the experimental methodology used in Chapter 6 is described. In Appendix C we present a survey regarding the properties of stochastic matrices used in Chapter 7. Finally, Appendix D contains the analytical calculations of Chapter 8.

Chapter 2

Random Walks and the Random Search Problem

A review of the theory of random walks and some mathematical results are presented in this chapter. The one-dimensional random walk is discussed in details and the connection with the diffusion equation is emphasized. The mathematical formalism of Lévy walks is made using the Lévy alpha-stable distributions and its main mathematical properties are outlined. Finally, we address the relation between Lévy walks and animal foraging in the random search model.

2.1 Random Walks

The development of the theory of random walks was made independently in different scientific lines, as a prediction of its multidisciplinary applications. The most famous description of random walks was made in the biology context by Richard Brown (1828) [6], when he was observing the irregular movement of small polen particles in a liquid substance. In probability theory, the Bernoulli trials (1713) [7] are random walks where the probability to go forward is p and backwards is $1-p$. When analyzing stock options, Louis Bachelier (1900) [8] was the first scientist to present the Brownian motion as a stochastic process. Finally, in physics, Karl Pearson (1905) [9] brought the question about random walks to the scientific community, and Lord Rayleigh (1880) [10] presented a solution to the problem previously developed in a different context (superposition of sound waves). In a short period of time, Einstein (1905) [11] and von Smoluchowski (1906) [12] developed a rigorous approach for the dynamics of microscopic particles using macroscopic diffusion. Both of them obtained, independently, an important mathematical

relationship that allowed the calculation of the Avogadro's number, supporting the atomic theory.

The *random walk* concept was originally introduced by Karl Pearson in the following way [9]:

> A man starts from a point 0 and walks ℓ yards in a straight line; he then turns through any angle whatever and walks another ℓ yards in a straight line. He repeats this process n times. I require the probability that after these n stretches he is at a distance between r and $r+\delta r$ from his starting point 0.

Notice that the random walk proposed by Pearson is very simple: two-dimensional, isotropic and with fixed step lengths. More complex random walks have been developed in order to increase its range of applicability. For example, we have the generalization of random walks in higher dimensions, random walks that exhibit fractality and models using random walks with memory. Nowadays, random walks are successfully used in Physics and Chemistry (diffusion, reactions), Economics (price of a fluctuating stock), Biology (animal foraging), and many other disciplines [13–16].

2.1.1 The one-dimensional random walk and the diffusion equation

The simple one-dimensional random walk is used in several applications of diffusive processes. Here we will derive the probability distribution for the one-dimensional random walk when the number of steps gets very large and connect this result to the diffusion equation. In Appendix A we present a survey on fundamental concepts of probability and statistics that are used in this chapter.

Consider a random walker that can visit regularly spaced positions along a line that are separated by a distance Δx. The positions are labeled by whole numbers m and the walker starts to move at the position 0 at time 0. Then, after a fixed time interval Δt the walker moves either to the right with probability p or to the left with probability $q = 1-p$. We want to obtain the probability $p(m,N)$ that the walker will be at m after N time steps.

There are many ways to start a walk at the origin and arrive at m after N steps. But all the possibilities are *independent*, so we will add up all the probabilities. Let n_1 be the number of steps to the right and n_2 to the left ($N = n_1 + n_2$). To arrive at m, one has to give $n_1 = m + n_2$ jumps to the right and n_2 jumps to the left. Since $N = n_1 + n_2$, the

walker must have made:

$$n_1 = \frac{1}{2}(N+m) \quad \text{jumps to the right and}$$
$$n_2 = \frac{1}{2}(N-m) \quad \text{jumps to the left.} \tag{2.1}$$

The probability for a sequence of jumps to the left and to the right is the product of the probability of individual jumps. Since the jumps are independent, all the possibilities to start a walk at 0 and arrive at m after $N = n_1 + n_2$ steps have the same overall probability. This follows because the probability of making n_1 jumps to the right and n_2 jumps to the left must have n_1 factors p and n_2 factors q. Thus,

$$p^{n_1} q^{n_2} = p^{\frac{1}{2}(N+m)} q^{\frac{1}{2}(N-m)}, \tag{2.2}$$

and this probability has to be multiplied by the total number of paths with n_1 steps to the right and n_2 to the left. This problem is similar to the number of ways to put n_1 objects out of N in one box and $n_2 = N - n_1$ objects in another box. We have N ways to choose the first object, $N-1$ ways to choose the second, and so on. The total number of choices of n_1 objects becomes $N(N-1)(N-2)\ldots(N-n_1+1)$. However, the n_1 objects are identical and can be arranged in any order. The total number of distinguishable ways to choose n_1 steps to the right and n_2 steps to the left is

$$\frac{N!}{n_1! n_2!} = \frac{N!}{n_1!(N-n_1)!}, \tag{2.3}$$

and thus the probability of being at m after N time steps is given by:

$$p(m,N) = p^{\frac{1}{2}(N+m)} q^{\frac{1}{2}(N-m)} \frac{N!}{\left(\frac{N+m}{2}\right)!\left(\frac{N-m}{2}\right)!} = p^{\frac{1}{2}(N+m)} q^{\frac{1}{2}(N-m)} \binom{N}{\frac{N-m}{2}}. \tag{2.4}$$

The above result is the *binomial* distribution. Knowing the probability distribution $p(m,N)$ we can calculate the *statistical moments*[1] of m at a fixed time N. Writing the number of steps to the right $n_1 = n = (N+m)/2$ we have:

$$p(m,N) = p_N(n) = \frac{N!}{n!(N-n)!} p^n q^{N-n} = \binom{N}{n} p^n q^{N-n}. \tag{2.5}$$

[1] The definition of the statistical moments of a random variable can be consulted in Appendix A.

Then, noting that

$$(pu+q)^N = \sum_{n=0}^{N} \binom{N}{n} u^n p^n q^{N-n}, \tag{2.6}$$

we identify $p_N(n)$ as the coefficient of u^n in this binomial expansion. First, we need to verify if $p_N(n)$ is normalized to 1:

$$p_N(n) = \left[(pu+q)^N\right]_{u=1} = 1, \tag{2.7}$$

so $p_N(n)$ is properly normalized. The expectation value of n (the first moment) is:

$$\begin{aligned} E[n] &= \sum_{n=0}^{N} n p_N(n) = \sum_{n=0}^{N} n \left[\binom{N}{n} u^n p^n q^{N-n}\right]_{u=1} && (2.8)\\ &= \sum_{n=0}^{N} \left[\binom{N}{n} u \frac{\mathrm{d}}{\mathrm{d}u}(u^n p^n q^{N-m})\right]_{u=1} = \left[u \frac{\mathrm{d}}{\mathrm{d}u} \sum_{n=0}^{N} \binom{N}{n} u^n p^n q^{N-n}\right]_{u=1} && (2.9)\\ &= \left[u \frac{\mathrm{d}}{\mathrm{d}u}(pu+q)^N\right]_{u=1} = Np. && (2.10) \end{aligned}$$

In the same way, the second moment is given by:

$$E[n^2] = \sum_{n=0}^{N} n^2 p_N(n) = \left[\left(u \frac{\mathrm{d}}{\mathrm{d}u}(pu+q)^N\right)\right]_{u=1} = Np + N(N-1)p^2, \tag{2.11}$$

and the variance σ^2 is

$$\sigma^2 = E[(n-E(n))^2] = E[n^2] - (E[n])^2 = Npq. \tag{2.12}$$

Finally, the expected position of the walker after N steps is given by:

$$E[m] = 2E[n] - N = N(p-q), \tag{2.13}$$

the second moment

$$E[m^2] = 4E[n^2] - 4E[n]N + N^2 = 4\sigma^2 + (E[n])^2, \tag{2.14}$$

and the variance of the displacement m is

$$\sigma_m^2 = 4\sigma^2 = 4Npq. \tag{2.15}$$

One special result concerning *isotropic* random walks ($p = q = \frac{1}{2}$) is that the square of the covered distance scales with N, that is,

$$E[m] = 0 \qquad \text{and} \qquad E[m^2] = N. \tag{2.16}$$

The above relation is the signature of a normal diffusion process, like the Brownian motion. Now we will study the continuous limit of the random walk. One possibility is employing Stirling's approximation in Eq. (2.4) and achieve a Normal distribution [14]. We will adopt another approach, writing the *master equation* [17] of the one-dimensional random walk and then obtaining Einstein's diffusion equation, whose solution is again a Normal distribution.

We will suppose a free particle that can move either to the right or to the left with equal probability ($p = q = \frac{1}{2}$). At each step the particle moves a distance Δ and the duration of the step is τ. Thus, $P_N(m)$ in Eq. (2.4) is the probability that the particle will be at a position $x = m\Delta$ at a given time $t = N\tau$. Only a particle that was at $x = (m+1)\Delta$ or $x = (m-1)\Delta$ by the time $t = (N-1)\tau$ can reach $x = m\Delta$ by the time t. Therefore, the recurrence relation for the process can be stated as [17]:

$$P_{N+1}(m) = \frac{1}{2}P_N(m-1) + \frac{1}{2}P_N(m+1). \tag{2.17}$$

If the number of steps is very large ($N \gg 1$), we can replace the discrete Eq. (2.17) for a continuous function $\eta(N\tau, m\Delta) = \eta(t,x)$:

$$P_{N+1}(m) = \eta((N+1)\tau, m\Delta) = \eta(N\tau + \tau, m\Delta) = \eta(t+\tau, x), \tag{2.18}$$

$$P_N(m+1) = \eta(N\tau, (m+1)\Delta) = \eta(N\tau, m\Delta + \Delta) = \eta(t, x+\Delta), \tag{2.19}$$

$$P_N(m-1) = \eta(N\tau, (m-1)\Delta) = \eta(N\tau, m\Delta - \Delta) = \eta(t, x-\Delta). \tag{2.20}$$

Replacing the second order Taylor's expansion around Δ and τ of Eq. (2.18), (2.19) and (2.20) into Eq. (2.17), we have the following result:

$$\tau^2 \frac{\partial^2 \eta}{\partial t^2} + \frac{\tau}{2}\frac{\partial \eta}{\partial t} = \Delta^2 \frac{\partial^2 \eta}{\partial x^2}, \tag{2.21}$$

and writing $D = \Delta^2/\tau < \infty$ we have the *generalized diffusion equation*:

$$\frac{\tau}{2}\frac{\partial^2\eta}{\partial t^2} + \frac{\partial\eta}{\partial t} = D\frac{\partial^2\eta}{\partial x^2}. \tag{2.22}$$

The connection with the normal diffusion equation is reached with the continuum limit ($\Delta \to 0, \tau \to 0$):

$$\frac{\tau}{2}\frac{\partial^2\eta}{\partial t^2} \ll \frac{\partial\eta}{\partial t}, \tag{2.23}$$

and Eq. (2.22) is simplified to:

$$\frac{\partial\eta}{\partial t} = D\frac{\partial^2\eta}{\partial x^2}. \tag{2.24}$$

The solution of the normal diffusion equation is the Normal distribution

$$\eta(x,t) = \frac{N}{\sqrt{4\pi Dt}}\exp\left\{-\frac{x^2}{4Dt}\right\}, \tag{2.25}$$

with mean 0 (walk started at the origin) and variance $2Dt$. The Normal distribution has a large number of applications, and the description of the Brownian motion is one of the most relevant. Also, this distribution is the limit of the sum of random variables with finite variance. This last result is known as the *central limit theorem* and is discussed in details in Appendix A.

2.2 Lévy Flights and Walks

Now, we will show that the Gaussian density, presented in the last section, is a particular case of a class of functions known as *Lévy stable* densities [18]. The special feature of these densities is that their low order moments (i.e., the mean and the variance) diverge. Lévy stable functions have been initially employed in the description of stochastic phenomena in physics, like the Cauchy distribution used in the description of atomic line shapes and the Holtsmark distribution of random fluctuations in the gravitational field of stars [19]. In the recent years, physicists employed Lévy stable distributions in turbulence models: the enhanced diffusion in turbulent flows requires a probability distribution with infinite moments, the hallmark of *Lévy flights*. Of special relevance in this thesis are the Lévy flights in animal foraging models [5].

2.2.1 Stable distributions

In short, we say that if two independent random variables X and Y are distributed according to the same type of *stable* density, then the sum $X+Y$ will be distributed conforming to the same density. This simple property has important implications, like the *Central Limit Theorem* and the *self-similarity* of Lévy walks that will be discussed later.

More precisely [18], a random variable X is stable if for X_1 and X_2 independent copies of X and any positive constants a and b the following relation holds for some positive c and some $d \in \mathbb{R}$:

$$aX_1 + bX_2 = cX + d. \tag{2.26}$$

X is said to be *strictly* stable if Eq. (2.26) holds for $d = 0$ and for all choices of a and b. These variables are called stable because the shape of its density function does not change under the sum in Eq. (2.26). The first mathematician to study stable distributions was Paul Lévy, so this distribution family is often referred to as *Lévy alpha-stable distributions* in the literature.

Stable distributions are very important in practical problems [19] and include distributions with skewness and heavy tails. As we will discuss further, there are only a few stable distributions with a closed formula for the densities, but computationally one can calculate approximate stable densities and distributions. The importance of stable distributions can be highlighted by the fact that some observed quantities are the sum of many small components, like the price of a stock or the displacements of a random walker. Several physical phenomena yield non-Gaussian distributions, like the distribution of hitting times of a Brownian walker resulting in a Lévy distribution (see [20] for more examples). Also, stable densities show an important role in the *generalized central limit theorem* that will be discussed further in the text. According to the aforementioned theorem, the only possible non-trivial limit of normalized sums of independent identically distributed terms is stable [18].

2.2.2 Lévy alpha-stable distributions

Before the work of Paul Lévy, the only stable distribution known was the Normal. The generalization includes distributions with divergence in the moments, so the Normal distribution is a particular case of the Lévy alpha-stable distributions. The probability density function for this class of distributions does not have a general analytical expression, and is usually defined in terms of its four-parameters characteristic function $\varphi(q)$ (see

Appendix A for definitions) [18]:

$$\ln\varphi(q)=\begin{cases} i\mu q-\gamma|q|^{\alpha}\left[1-i\beta\frac{q}{|q|}\tan\left(\frac{\pi}{2}\alpha\right)\right] & [\alpha\neq 1] \\ i\mu q-\gamma|q|\left[1+i\beta\frac{q}{|q|}\frac{2}{\pi}\ln|q|\right] & [\alpha=1], \end{cases} \tag{2.27}$$

with $0<\alpha\leq 2$, $\gamma>0$, $\mu\in\mathbb{R}$ and $\beta\in[-1,1]$. In Eq. (2.27) α is a stability parameter and concerns the distribution kurtosis. If $\alpha<2$ the variance of the distribution is infinite and for $\alpha>1$ the mean of the distribution exists and $\alpha=\mu$. β is the asymmetry parameter, and if $\beta=0$ the distribution is symmetric. The width of the distribution is governed by the scale parameter γ. Finally, μ is the location parameter and in special cases coincides with the distribution's mean.

The analytical form of the stable distributions is known only for three particular cases, that are shown in Fig. 2.1:

- Lévy-Smirnov: $\alpha=1/2$, $\beta=1$,

$$f(x)=\sqrt{\frac{\gamma}{2\pi}}\frac{1}{(x-\mu)^{3/2}}\exp\left(-\frac{\gamma}{2(x-\mu)}\right) \quad \text{for} \quad \mu<x<\infty. \tag{2.28}$$

- Cauchy: $\alpha=1$, $\beta=0$,

$$f(x)=\frac{1}{\pi}\frac{\gamma}{\gamma^2+(x-\mu)^2} \quad \text{for} \quad -\infty<x<\infty. \tag{2.29}$$

- Normal: $\alpha=2$,

$$f(x)=\frac{1}{\sigma\sqrt{2\pi}}e^{-\frac{1}{2}\left(\frac{x-\mu}{\sigma}\right)^2}, \quad x\in\mathbb{R}, \quad \mu\in\mathbb{R}, \quad \sigma>0. \tag{2.30}$$

In the following we will show the asymptotic form of the Lévy stable distributions, that is very important to practical applications, in special to Lévy flights.

2.2.3 The asymptotic behavior of the Lévy stable distributions

In many practical problems, it is common to use the asymptotic behavior of the symmetrical ($\beta=0$) stable distributions with $\mu=0$. Under these conditions, the characteristic function for the Lévy stable distributions is characterized only by α and γ in the following equation:

$$\varphi(q)=\exp[-\gamma|q|^{\alpha}]. \tag{2.31}$$

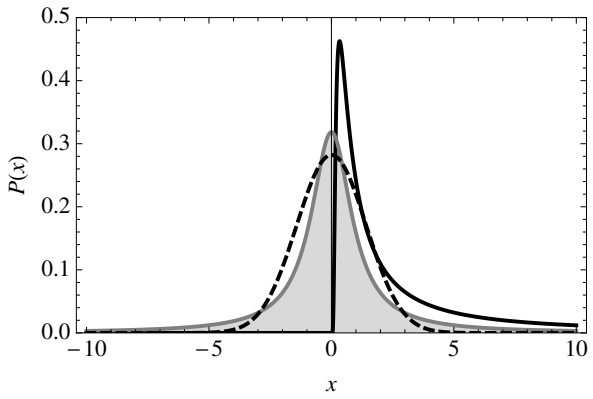

Figure 2.1 Lévy alpha-stable distributions with analytical probability density for $\mu = 0$. The asymmetric Lévy-Smirnov Eq. (2.28) (black solid line), and the symmetric Cauchy Eq. (2.29) (gray with shadow) and Normal Eq. (2.30) (dashed line). Notice the heavy tail behavior of the Lévy-Smirnov and the Cauchy distributions.

Since the characteristic function and the probability density function are connected through a Fourier transform (see Appendix A), we apply a cosine Fourier transform in Eq. (2.31), obtaining:

$$P_L(x) = \frac{1}{\pi}\int_0^\infty \exp[-\gamma|q|^\alpha]\cos(qx)\,\mathrm{d}q. \tag{2.32}$$

An integration by parts in the last equation gives:

$$P_L(x) = \frac{\gamma\alpha}{\pi}\int_0^\infty \frac{\sin(qx)}{x} q^{\alpha-1}\exp[-\gamma|q|^\alpha]\,\mathrm{d}q, \tag{2.33}$$

and after the change of variables $\zeta = qx$ $(\mathrm{d}\zeta = x\mathrm{d}q)$ we get

$$P_L(x) = \frac{\gamma\alpha}{\pi x^{\alpha+1}}\int_0^\infty \zeta^{\alpha-1}\sin(\zeta)\,\mathrm{d}\zeta. \tag{2.34}$$

The solution for the integral in Eq. (2.34) in the asymptotic limit $x \gg 1$ is written in terms of the Euler function $\Gamma(\alpha)\sin(\frac{\pi\alpha}{2})$:

$$P_L(x) \sim \frac{\gamma\alpha\Gamma(\alpha)\sin\left(\frac{\pi\alpha}{2}\right)}{\pi x^{\alpha+1}}. \tag{2.35}$$

Thus, the behavior of $P_L(x)$ when $x \gg 1$ is a power law with exponent $-(\alpha+1)$, that can be simplified as

$$P_L(x) \sim x^{-(1+\alpha)}. \tag{2.36}$$

The convention adopted in the literature uses $\mu = 1+\alpha$ as the power law exponent. In this way, the variance of Eq. (2.36) diverges when $1 < \mu < 3$, that is, it represents a super-diffusive process without a characteristic scale [21].

2.2.4 The self-similarity in the Lévy stable distributions

Self-similarity is the signature of a fractal process, and is recognized when a part of the object preserves the same features of the whole object [22]. The Lévy distributions are self-similar, and this property is explicitly used in the generation of the fractal targets distributions in Chapter 3.

Considering n random variables that are independent and identically distributed according to Eq. (2.31), we have (using the formula for the product of characteristic functions)

$$\varphi_n(q) = [\varphi(q)]^n = \exp[-n\gamma|q|^\alpha]. \tag{2.37}$$

Let S_n be the sum of these n random variables. In a random walk context, we can assign S_n as the final position of the walker after n steps in one dimension. The probability density function for S_n is given by:

$$P_n(S_n) = \frac{1}{2\pi}\int_{-\infty}^{\infty} \exp[-n\gamma|q|^\alpha - iqS_n]\mathrm{d}q. \tag{2.38}$$

The integral above does not have an analytical solution, but if we consider the probability that the walker returns to the origin after n steps, that is, $S_n = 0$, we have:

$$P_n(S_n = 0) = \frac{1}{2\pi}\int_{-\infty}^{\infty} \exp[-n\gamma|q|^\alpha]\mathrm{d}q = \frac{1}{\pi}\int_0^{\infty} \exp[-n\gamma q^\alpha]\mathrm{d}q, \tag{2.39}$$

and now the integral can be written in terms of $t = n\gamma q^\alpha$:

$$P_n(S_n = 0) = \frac{1}{\pi\alpha(n\gamma)^{\frac{1}{\alpha}}} = \int_0^{\infty} \exp(-t)t^{\frac{1}{\alpha}-1}\mathrm{d}t. \tag{2.40}$$

And the last integral corresponds to the function $\Gamma\left(\frac{1}{\alpha}\right)$. Thus, the probability that the walker returns to the origin after n steps is:

$$P_n(S_n = 0) = \frac{1}{\pi\alpha(n\gamma)^{\frac{1}{\alpha}}}\Gamma\left(\frac{1}{\alpha}\right), \tag{2.41}$$

and assuming $n = 1$:

$$P_1(S_n = 0) = \frac{1}{\pi\alpha\gamma^{\frac{1}{\alpha}}}\Gamma\left(\frac{1}{\alpha}\right) = n^{\frac{1}{\alpha}}P_n(S_n = 0). \tag{2.42}$$

That is, the probability density function has a scale factor of $n^{\frac{1}{\alpha}}$. This result is independent of the assumption $S_n = 0$ and a more general derivation can be found in [21]. Thus, for any n, one can write P_n in terms of P_1 through a simple change in the scale factor, the signature of a self-similar process.

2.2.5 The truncated Lévy distribution

The diverging variance in the Lévy distribution constitutes a problem when one tries to apply the distribution in real data. Even though the data show a good adjustment with the central part of the distribution, it is impossible to have infinitely long contributions. In animal foraging, for example, several empirical works use the asymptotic Lévy distribution to fit the displacement data. Still, one does not have arbitrarily long displacements that would be present in a distribution with diverging variance. The solution to this problem is a new form of the Lévy distribution that eliminates infinitely long outcomes. This distribution behaves like a proper Lévy distribution when the number of steps is small but tends to a Normal distribution (finite variance) when the number of steps is very big.

To eliminate the divergence in the variance, a truncation in the values from the distribution is assumed [23]:

$$P(x) = \begin{cases} 0 & x > l \\ cP_L(x) & -l \leq x \leq l \\ 0 & x < -l \end{cases} \tag{2.43}$$

where $P_L(x)$ is the usual Lévy distribution from Eq. (2.36) and c a normalizing constant. The constant l stands as the maximal value above which the truncation is applied. Eq. (2.43) characterizes the *truncated Lévy distribution*, and is widely used to fit data sets with Lévy flight properties.

2.2.6 The generalized central limit theorem

The generalized central limit theorem (G-CLT) is a very important result in Statistics and concerns the sum of random variables with infinite variance. The central limit theorem (whose demonstration can be found on Appendix A) is a less general result, because it requires that the variance of the random variables to be finite.

The generalized central limit theorem includes the variables whose distribution follow a Lévy stable distribution, and can be stated as:

Theorem 2.2.1 (The generalized central limit theorem). *Let $\{X_i\}$ be a set of n random variables and $S_n = \sum_{i=1}^{n}$ their sum. If $P(X_i)$ satisfies the following conditions:*

$$P(X_i) \sim \begin{cases} C_-|X_i|^{-(1+\alpha)} & \text{if} \quad X \to -\infty \\ C_+|X_i|^{-(1+\alpha)} & \text{if} \quad X \to \infty \end{cases}, \tag{2.44}$$

and defining:

$$\beta = \frac{C_+ - C_-}{C_+ + C_-}, \tag{2.45}$$

the distribution of the variables sum, $P(S_n)$, follows a Lévy stable distribution with the same parameters α and β.

The proof of the theorem is beyond the scope of this thesis, but can be consulted on [24, 25] and [20].

2.3 Random Walks and Animal Dispersal

The first studies that employed random walks in the description of animal movement adopted non-oriented random walks to model the dispersal of populations [26, 27]. In Skellam's model [26] the diffusion equation in two dimensions was employed to study the spatial distribution of a population that was initially released at a single point (resulting in a Normal distribution). Random walk models that are unbiased and uncorrelated will result in Brownian motion. These models did not include an explicit interaction between the individuals neither spatial heterogeneities.

Animal dispersal show a delicate balance between spreading and concentrating in the landscape to form groups or to stay in a preferred territory [28]. Thus, one needs models that can include spatial heterogeneities and a more complex diffusive movement. The random walk models in Biology thus increased in complexity: including correlations in the orientations [2] and using intermittent random walks to emulate animal foraging [4].

Lévy flights have been used in the description of animal foraging since a study of the flying behavior of fruit flies reported a power law tail in the flight sizes distribution [29]. The evidences for Lévy flight behavior include albatrosses [3], spider monkeys [30], fishing boats [31], jellyfishes [32], and several marine species [33]. Lévy flights are superdiffusive and non-oriented random walks that provide intensive search behavior during the execution of small flights and an extensive search in the long flights that relocate the searcher.

Regarding the search environment features, initially the works were based on patch-use models [34]. Patches are limited regions with resources that have a neighborhood with distinct properties (like the absence of resources). These models are focused almost exclusively on how foragers determine when to leave a patch and the details concerning how the foragers find the patches are usually neglected. Besides this, models like these are *deterministic*, and the optimal solution to the foraging task is determined before the search begins. Thus, in these models the forager is not influenced by its experiences in the search environment.

The major problem of deterministic approaches to foraging is that it demands a full set of rules describing the animal behavior. Such a deterministic model would describe with certainty how the animal responds to any given set of environmental conditions. It is an impossibly complex task to track all the variables of an organism and its environment. In random search models, the unknown factors about the forager and its environment are treated probabilistically, and this formulation has been proved a very good description to the problem.

2.4 Random Search Problem

In this section we will expose the analytical formulation of the random search problem according to [35]. The random walker has its steps ℓ chosen according to

$$P(\ell) = A\ell^{-\mu}, \tag{2.46}$$

where A is a normalization constant and $1 < \mu \leq 3$. The μ exponent controls the relative frequency between short and long flights, and is associated with the search strategy. When $\mu \to 1$ the long steps are dominant in the walk, and the pattern approaches the ballistic motion. As we increase μ, the long steps become less frequent and when $\mu = 3$ the walk resembles Brownian motion. In Fig. 2.2 we show samples of the trajectories changing the μ exponent.

The targets are randomly distributed in the space and the walker moves according to the following rules:

1. If a target lies within the visual perception r_v of the walker, then it will move on a straight line towards the nearest target site.

2. In the absence of a target site within a distance r_v, the walker chooses a direction uniformly in the interval $[0, 2\pi)$ and a flight distance ℓ_j according to Eq. (2.46).

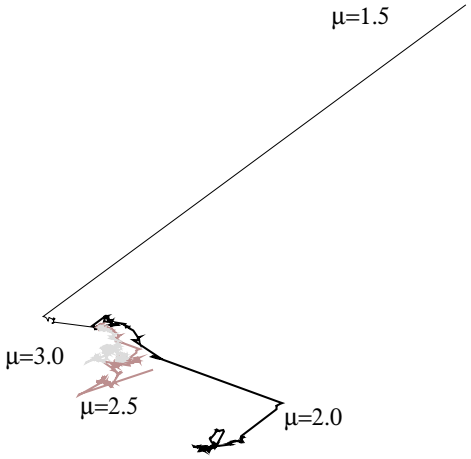

Figure 2.2 Stretches of a trajectory obtained from Eq. (2.46) for distinct search strategies, that is, distinct μ's. The same distance $L = 10^3$ was covered for every μ. As $\mu \to 1$ the walk becomes more and more superdiffusive, approaching the ballistic limit. When $\mu = 1.1$ the long steps are dominant, and the walker departs from the origin very fast. As we increase μ the frequency of long steps decreases. For $\mu = 2.0$ there is a combination of clusters of small steps interspaced by long jumps that corresponds to the optimal search strategy. Finally, when $\mu = 3.0$ the short steps are dominant in the distribution, and the normal diffusion regime is achieved.

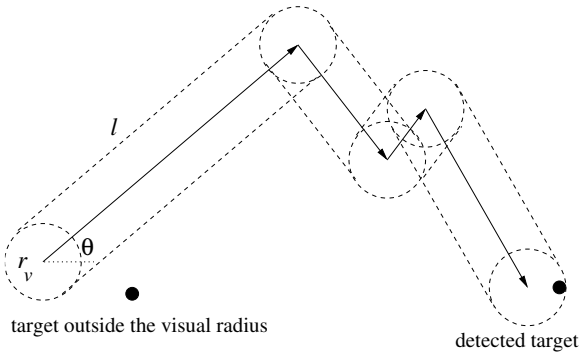

Figure 2.3 The random search heuristics. A step length is chosen according to Eq. (2.46) altogether with an isotropic direction θ. If a target enters the visual perception of the searcher along the step it is detected, otherwise the step is finished and a new choice of ℓ and θ is made. In the case of a detection, the step is truncated and the choice is repeated. The process is repeated until a pre-defined number of encounters is registered.

Then, the forager will cover the distance ℓ_j constantly looking for targets within its perception radius r_v. If a target is detected, the forager proceeds as in rule 1. Otherwise, it finishes the step and a new distance and flight length will be chosen and the process repeated.

The rules are condensed in Fig. 2.3.

Two types of targets are considered: *non-destructive*, that remain available to the forager during the search (even if they have been detected), and *destructive*, that once detected are eliminated from the environment. As we will see, the type of target in the environment will determine which search strategy is more efficient in the problem.

Let λ be the *mean free path* of the forager between two targets successively detected, that is, the average distance covered between two detections. For a two dimensional distribution, one has:

$$\lambda = \frac{1}{2r_v\rho}, \tag{2.47}$$

with ρ the target site area density. The average step length of a single flight distributed as Eq. (2.46) is, using a mean-field approximation [35]:

$$\langle \ell \rangle \approx \frac{\int_{r_v}^{\lambda} x^{1-\mu}\,\mathrm{d}x + \lambda \int_{\lambda}^{\infty} x^{-\mu}\,\mathrm{d}x}{\int_{r_v}^{\infty} x^{-\mu}\mathrm{d}x} = \left(\frac{\mu-1}{2-\mu}\right)\left(\frac{\lambda^{2-\mu} - r_v^{2-\mu}}{r_v^{1-\mu}}\right) + \frac{\lambda^{2-\mu}}{r_v^{1-\mu}}, \tag{2.48}$$

and in the second term it is assumed that a new target is always detected at a maximum distance λ away from the previously visited target. This approximation will truncate the steps in λ, which is important to avoid divergence in the step length.

The *search efficiency* η is defined as the ratio of the number of target sites visited to the total distance traversed by the forager. The total distance is the product of the number of detected targets and the average distance covered between two targets $\langle L \rangle$. Thus, we define η as:

$$\eta = \frac{1}{\langle L \rangle}. \tag{2.49}$$

Consider now that $\langle L \rangle$ is the product of the average length of a given step, Eq. (2.48), and the average number of steps between two detections N:

$$\eta = \frac{1}{N\langle \ell \rangle}. \tag{2.50}$$

We can estimate the number of steps between successive detections in two separate cases, for destructive foraging N_d and the non-destructive N_n. In the destructive environment, one has:

$$N_d \approx \left(\frac{\lambda}{r_v}\right)^{\mu-1}, \tag{2.51}$$

with $1 < \mu \leq 3$. If the forager has the opportunity to revisit a target, the number of visited targets in Eq. (2.51) overestimates it. Let r_0 be the small distance between the last detected target and the location after the next successive step. For a Brownian walker ($\mu \geq 3$), Eq. (2.51) scales with $N_d \sim \lambda^2$. The time required by a Brownian walker initially in the center of a one-dimensional container of radius λ to achieve the boundary is $N_d = \lambda^2/2D$, where D is the diffusion constant. Nevertheless, for the non-destructive case, one has $N_n = (\lambda - r_0)r_0/2D$, because the previous site (a distance r_0 away) can be revisited. Thus, the scaling is quadratic for destructive foraging and linear in the non-destructive one. It follows that

$$N_n \approx \left(\frac{\lambda}{r_v}\right)^{(\mu-1)/2}, \tag{2.52}$$

for $1 < \mu \leq 3$. The approximation in Eq. (2.52) becomes better as λ/r_v increases (that is, in more sparse targets distributions). The results in Eq. (2.51) and (2.52) can be analytically proven [36, 37].

Now, we will study the behavior of Eq. (2.50) using the expression of N for the non-destructive foraging. Considering $\lambda \gg r_v$ and substituting Eq. (2.52) and (2.48) in Eq. (2.50) and maximizing μ one gets:

$$\mu_{opt} = 2 - \delta, \tag{2.53}$$

with $\delta \sim 1/[\ln(\lambda/r_v)^2]$. Thus, the bigger the ratio λ/r_v (the sparser the environment), the optimal strategy becomes closer to $\mu = 2$. When $\lambda \leq r_v$ (for a high density of targets), we have $\langle \ell \rangle \sim \lambda$, and most of the steps, irrespective of μ, will finish upon encounters. Then, an optimal strategy is not demanded for an environment plentiful of targets. In the destructive foraging, using Eq. (2.51) it is not possible to maximize the efficiency function, however, η achieves bigger values when $\mu \to 1$. As $\mu \to 1$ the number of steps with $\ell < \lambda$ decreases, thus most steps are finished when a target is detected.

Chapter 3

Emergent vs Evolutive Lévy Flights

In this chapter we address the nature of Lévy flights: is it an innate strategy that evolved in the organisms or the resulting pattern from the interaction between a simplistic strategy and a complex environment? We present a collection of numerical results supporting the robustness of Lévy flights across different heterogeneous landscapes. Further, we explore the effects of a very high (and very low) targets density in the step length distributions. We find out that a Brownian-like pattern emerges when a Lévy flight is performed in a very dense environment. Our results reinforce the innate character of Lévy flights.

3.1 Introduction

In nature, most animals are constantly foraging for food. This is a vital activity: the life or death of an organism depends on its foraging success. In the absence of food, animals experience starvation and a long period of starvation can lead to death. If organisms survive and die depending on their foraging strategy, then *natural selection* has run its course. Surviving animals will supply its genes to the future generations, while the genetic characteristics of unqualified animals will be eliminated, and along with it less effective search strategies.

Given the importance of successful foraging strategies, understanding the rules that guide the foraging behavior has been an important subject in behavioral ecology [38, 39]. Mathematical models have been employed in the description of foraging behavior, and an important consideration is made in most of the models: the *optimization* of a fitness function. The fitness of a foraging animal is a function of the foraging efficiency, that is

usually measured in terms of "energy"[1]. Thus, it is expected that natural selection has resulted in animals that forage so as to maximize their fitness – in other words, they optimize its fitness function. Models that assume the optimization of a fitness function are the focus of *optimal foraging theory*.

Lévy flights are non-oriented random walks whose step lengths follow a power law $P(\ell) \sim \ell^{-\mu}$ with $1 < \mu \leq 3$. They have been successfully employed in the modeling of animal foraging since 1996, when a study about the movement patterns of albatrosses gathered evidences of a $\mu \sim 2$ Lévy walk strategy [3]. Nevertheless, this random walk model has been recognized as an efficient search strategy since 1986, when it was shown that a Lévy flight reduces the oversampling of a previously inspected region [40]. Another convenience of Lévy flights is the fact that N random walkers performing Lévy walks will visit more distinct sites than N Brownian walkers, a consequence of the enhanced diffusivity in Lévy flights [41]. Following the 1996 work, an analytical formulation of the random search problem for targets with unknown locations found out that a Lévy walk with a $\mu \sim 2$ index optimizes the search efficiency (ratio between the number of detected targets and the covered distance in the search process) [35]. The same strategy that optimizes the analytical problem leads to the higher efficiency in numerical simulations of random searches in homogeneous, sparse and non-destructive targets distributions.

Especially in circumstances where the resources are scarce in the environment, strong empirical evidences indicate the presence of Lévy flights in a wide range of animal species (for a compilation of works see [5]). Since this particular search behavior can be optimal in numerical simulations and is observed in several animal species, an hypothesis that the mechanisms behind the Lévy walk search behavior have an evolutionary origin was raised. The Lévy flight foraging hypothesis can be synthesized as [42]:

> Since Lévy flights and walks can optimize search efficiencies, therefore natural selection should have led to adaptations for Lévy flight foraging.

The hypothesis requires that no information about the targets locations is available to the walker, and no learning is possible. Also, the targets are randomly distributed and the overall density of resources is small. The visual radius of the forager is small and the targets do not provide "clues", like odor plumes, that can be used by the walker to follow the target. Further, another simplification assumed is that the only task during the foraging is the localization of resources, so activities like the return of the forager to its nest are not included. Finally, predator-prey dynamics are ignored in the model.

[1] Here energy accounts for the caloric reserves of an animal: it will gain energy by food ingestion and loose it during the locomotion in the search process.

On the other side, another class of works claim that the Lévy pattern observed in empirical works is an emergent property, and the interaction between the animal and its complex landscape is responsible for the Lévy pattern observed [43]. A study on spider-monkeys, animals with high cognitive skills, outlined that the emergent scale-free motion pattern (previously identified as Lévy flights [30]) results from the mental maps used by the animals in a heterogeneous distribution of trees [44]. In an empirical study involving bumblebees [45], the authors argue that since a bumblebee will avoid a given flower that was previously visited by several other bees, this will make their flights occasionally very long, resulting in a Lévy flight distribution.

Recently, a study with mud snails foraging in spatially different landscapes (homogeneous and heterogeneous food distributions) revealed the presence of Lévy flights irrespective of the spatial distribution of food [46]. Another evidence of the evolutive feature of Lévy flights was observed in jellyfishes, where the optimal superdiffusive strategy is dynamically tuned to forage efficiently in scenarios where the food density fluctuates [47]. Further, experiments with mussels support the hypothesis that the Brownian motion observed in arrangements with a high food density is emergent, a consequence of the high frequency of food encounters [48].

Using our experience in numerical simulations of random searches in a series of heterogeneous landscapes, we reinforce that the mechanisms behind the observed Lévy patterns have an evolutive signature. In this chapter we will present a set of simulations that explored the robustness of $\mu = 2$ in complex targets distributions, as well as an analysis of the truncation effects in the steps distribution.

3.2 Lévy Flights in Complex Landscapes

We have designed different heterogeneous landscapes to study the targets distribution impact in the search dynamics. More complex landscapes are closer to natural habitats: the distribution of zooplankton (a very important food resource in the oceans) has a fractal structure [33, 49], and forests are fragmented in heterogeneous disconnected patches [50]. In this section we will describe the construction of a heterogeneous distribution of circular patches and the implementation of a fractal landscape. The random search simulations will be made using this set of complex landscapes. Then, we will discuss the impact of the landscape in the optimal search strategy.

3.2.1 Heterogeneous patchy configuration

The homogeneous patchy configuration is characterized by a given number of patches (N_p) that have the same radius (R) and the same targets density (ρ_t) inside each patch. These patches are located inside a squared environment with side M. The fact that now the targets are constrained inside patches means that we have a more realistic counterpart of the distribution of resources in nature [51]. A statistical analysis of the homogeneous patchy configuration was made in a recent work [52].

Here we address with more details configurations where the patches have some degree of heterogeneity, like different target densities and different sizes. We designed three configurations to explore heterogeneous patches:

1. **Random sizes:** The radius of each patch p is chosen from an uniform distribution in the interval $0.03M < R^{(p)} < 0.3M$. Inside each patch the targets distribution is uniform, with a fixed average distance between targets l_t.

2. **Random targets density:** Now the size of each patch is fixed, but the average distance between targets for a given patch p is uniformly picked in the interval $5 < l_t^{(p)} < 350$, resulting in a landscape with dense and sparse patches.

3. **Random size and targets density:** We fixed a given amount of targets N_t to be uniformly distributed inside patches with different sizes ($0.03M < R^{(p)} < 0.3M$). In this way, the targets density in small (large) patches is high (low).

In Fig. 3.1 we have the results obtained from simulations of the search process in the three landscapes described above. Each simulation lasted until the detection of $Q = 10^4$ targets, and was performed over $\overline{N} = 2.5 \times 10^3$ runs. Every new simulation has a different spatial configuration of patches that are characterized with the same set of parameters. Also, the walker starts the search always outside the patches.

In Fig. 3.1(a)–(c) we have stretches of the trajectory performed by three search strategies: $\mu = 1.1$ (ballistic), $\mu = 2.0$ (optimal super-diffusive) and $\mu = 3.0$ (normal diffusion) in the heterogeneous landscapes. We have the patches with different sizes in (a); patches with different targets density in (b) and different sizes and densities in (c). The resulting search efficiency for each configuration is shown in Fig. 3.1(d)–(f) for landscapes with $N_p = 10$ and $N_p = 5$ patches. The patch heterogeneity explored here does not affect the classical result $\mu_{opt} \approx 2$ for the optimal strategy, the same result obtained in the homogeneous patchy configuration [51].

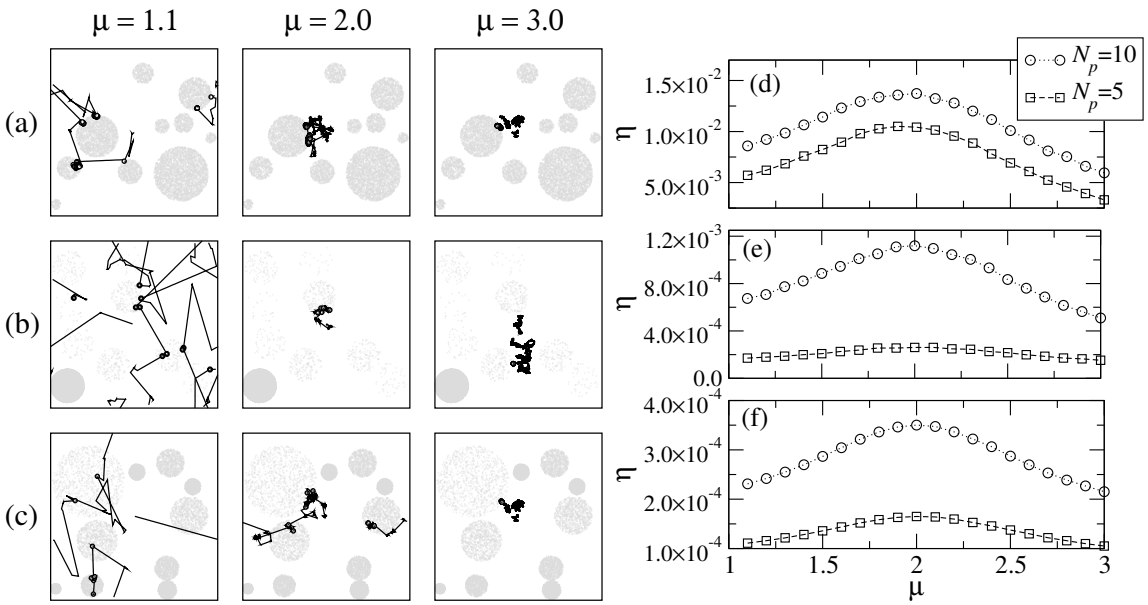

Figure 3.1 In (a)–(c), a fragmented landscape with heterogeneous patches is explored by super-diffusive random searches with strategies $\mu = 1.1$, $\mu = 2.0$ and $\mu = 3.0$. In (a), the patches have distinct sizes with the radii uniformly distributed in the range $0.03M \leq R \leq 0.3M$ and a constant targets density $l_t = 100$. In (b), the sizes remain fixed in $R = 0.1M$ and now the average distance between targets is uniformly distributed in the interval $5 \leq l_t \leq 350$. A landscape of patches with different sizes and densities, but with fixed number of targets inside is shown in (c), where the radii range in the same interval of (a) but the densities vary uniformly in the interval $17 \leq l_t \leq 170$. In (d)–(f) we have the statistical search efficiency η for the corresponding (a)–(c) configurations with 10 (circles) and 5 (squares) patches. Each simulation was performed 2.5×10^3 times.

3.2.2 Fractal patches

We used a *Lévy Dust* distribution for the resources [53], that is, the collection of points in the space visited by a Lévy walker whose steps are given by a power law:

$$P(d) = \begin{cases} 0, & d < d_0 \quad \text{or} \quad d > d_{max}, \\ Ad^{-\beta}, & d_0 \leq d \leq d_{max}. \end{cases} \tag{3.1}$$

The direction ϕ between two steps is uniformly distributed in the interval $[0, 2\pi)$. The d_0 (d_{max}) corresponds to the smallest (largest) step allowed and A stands for a normalization constant. The power law exponent β is connected to the fractal dimension d_F of the set of points by $d_F = \beta - 1$. In order to have N targets in the environment, we need a Lévy Dust of N steps.

Since our simulations are realized in a finite environment, we have to consider the effects of the borders during the targets creation. As $\beta \to 1$ the frequency of the long steps increases, and a situation where the final coordinates of a given jump achieve a

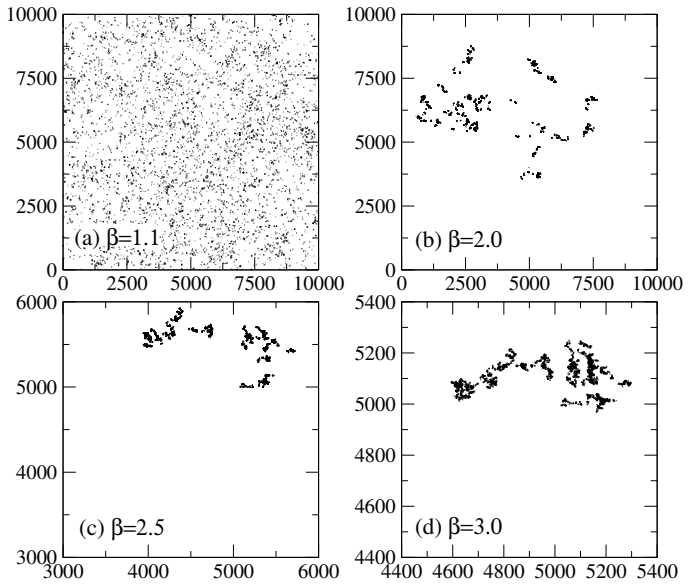

Figure 3.2 The fractal landscapes obtained using the Lévy Dust distribution of targets from Eq. (3.1) with $d_0 = 1$ and $d_{max} = M$ (side of environment). In (a) we have $\beta = 1.1$ and the resulting pattern looks like the homogeneous targets distribution. In (b) some small clusters of targets are observed, since $\beta = 2.0$ produces both long and small steps in Eq. (3.1). As we increase β, the targets become closer as the small steps are dominant. In (c), $\beta = 2.5$ and the area occupied by the targets is small (compare the scales with (a) and (b)). Finally, in (d) $\beta = 3.0$ corresponds to a very small area of targets.

region beyond the border of the environment may be observed. To prevent this problem, we adopted the mechanism known as *bouncing of coordinates* presented in [53]. The mechanism will detect when a given combination of step length d and turning angle ϕ will achieve the forbidden region, and then eliminate this attempt choosing a new combination of d and ϕ from Eq. (3.1). The resulting fractal environments obtained from the process described are shown in Fig. 3.2 for some particular configurations.

We also explored the effect of controlling the distribution of fractal patches in the environment using the Lévy Dust distribution to determine the average distance between each patch. In empirical works it is common practice to employ two spatial scales in the study of resources distributions [54]. The following distribution will describe the average distance r between the patches:

$$P(r) = \begin{cases} 0, & r < r_0 \quad \text{or} \quad r > r_{max}, \\ Ar^{-\gamma}, & r_0 \leq r \leq r_{max}. \end{cases} \tag{3.2}$$

A schematic figure is shown in Fig. 3.3 for three fractal patches with the average distance between them given by Eq. (3.2). A careful choice of convenient parameters is necessary during the patches construction to avoid overlaps between them. The inferior limit (r_0) should be larger than the average size of the fractal patch, and the superior limit (r_{max}) should be smaller than the size of the environment. We studied the configuration of patches characterized by N_t, β, d_0 and d_{max} before the construction of the landscapes with several patches. During the simulation we make tests to detect a possible overlap

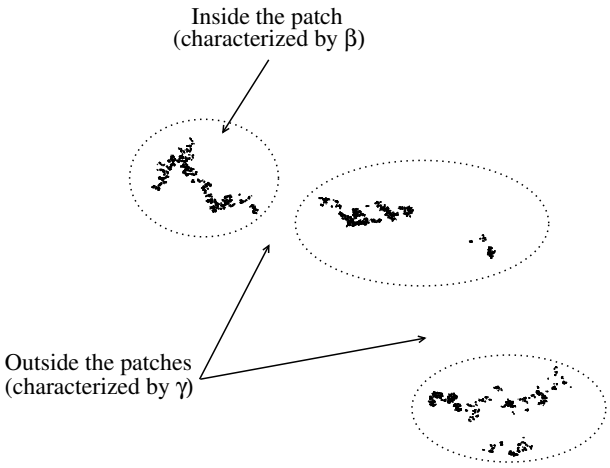

Figure 3.3 In this landscape each patch has $N_t = 5000$ targets whose distribution is given by the Lévy Dust of Eq. (3.1) with $\beta = 2.5$, $d_0 = 2$ and $d_{max} = M/10$. The average distance between the patches is now sorted from Eq. (3.2) with $\gamma = 2.0$, $r_0 = 500$ and $r_{max} = M$. The ranges for d and r are chosen so that the the patches do not overlap in the landscape.

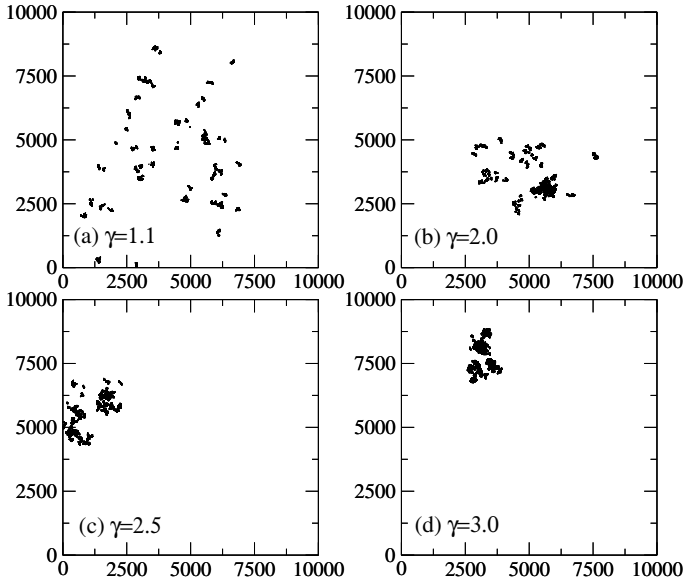

Figure 3.4 Landscapes with fractal patches whose distribution is given by a Lévy Dust with $r_0 = 100$, $r_{max} = M$ and four different exponents γ. Each patch (amounting to $N_p = 50$) has $N_t = 1000$ targets characterized by $\beta = 3.0$, $d_0 = 2$ and $d_{max} = M/10$. In (a) we have $\gamma = 1.1$ and the patches are scattered throughout the landscape. The patches become more closer in (b) with $\gamma = 2.0$, since the distances from the Lévy Dust are smaller as the exponent increases. In (c) $\gamma = 2.5$ and the patches are grouped together in a small region of the landscape. Finally, for $\gamma = 3.0$ in (d) the patches are so close that one cannot identify them individually.

with other patches or with the borders of the environment, using the same *bouncing of coordinates* mechanism described for the single patchy configuration.

In Fig. 3.4 the fractal patches have the same number of targets and are characterized by the same Lévy Dust distribution, but their spatial arrangement in the landscape follows a Lévy Dust with different exponent γ. In Fig. 3.4(a) the exponent used was $\gamma = 1.1$ and the average distance between patches is large, resulting in a large area occupied by patches. For $\gamma = 2.0$ in Fig. 3.4(b) the patches become more closer, because smaller distances are provided by the distribution. The patches will become more and more closer as we increase γ: in Fig. 3.4(c) and Fig. 3.4(d) we have $\gamma = 2.5$ and $\gamma = 3.0$ respectively, and the patches are grouped in a small area of the landscape, resulting in a small and very dense region.

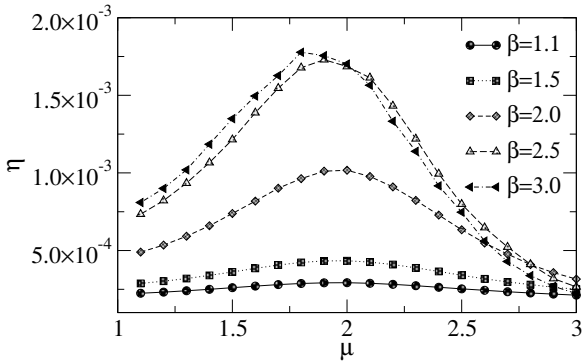

Figure 3.5 Search efficiency as a function of the strategy μ for different configurations β of $N = 10^4$ targets. The optimal strategy remains as $\mu = 2.0$ for $\beta = 1.1, 1.5$ and 2.0. When the targets are clustered in a very small region, more diffusive strategies have a better performance. Thus, $\mu = 1.9$ is optimal when $\beta = 2.5$ and $\mu = 1.8$ when $\beta = 3.0$ Each simulation was averaged over 2500 runs.

Once the spatial distribution of targets has been implemented in the model, we evaluate the performance of the search strategies in the new environment. In Fig. 3.5 the search efficiency η is shown for distinct β. The targets configuration that lead to a higher efficiency are $\beta = 3.0$ and $\beta = 2.5$, corresponding to Fig. 3.2(c) and (d). It implies that a small area with a high density of targets is better than a large area with a low resources density. This is in agreement with a previous result for circular patches [51] that the fragmentation of targets in more clusters decreases the overall search efficiency. The robustness of $\mu = 2$ as the optimal search strategy is verified in Fig. 3.5 for $\beta < 2.5$. A strategy with enhanced diffusivity ($\mu = 1.8$ for $\beta = 3.0$ and $\mu = 1.9$ for $\beta = 2.5$) is better when the targets are concentrated in a very small and dense area. The detection of a patch is a task optimized by the ballistic strategy $\mu = 1.1$ (see [52]), but the balance between an efficient patch detection and the localization of targets inside it is achieved when $\mu \approx 2$. When the patch is very small (like $\beta = 3.0$ or $\beta = 2.5$) its detection becomes more difficult for less diffusive strategies, and then a slightly small μ optimal strategy is observed.

When the patches have a fractal distribution in the space, the search efficiency in Fig. 3.6 shows a clear optimal strategy in $\mu = 2.0$ in all the configurations tested. The best distribution of patches in the environment now depends on the strategy adopted by the searcher. For $\mu < 2.5$, $\gamma = 3.0$ (corresponding to Fig. 3.4(d)) leads to the highest efficiency. On the other side, when $\mu \geq 2.5$ the best configuration changes to $\gamma = 1.1$, that is, a more homogeneous distribution of patches in the environment (Fig. 3.4(a)). When the patches are distributed in a larger area, it is easier for less diffusive strategies ($\mu \geq 2.5$) to detect a resource, and since the searcher continues close to the detected patch, it will continue to find targets in the region.

The results in Figs. 3.1, 3.5 and 3.6 show that the optimal Lévy strategy $\mu \approx 2$ performs better in a wide range of heterogeneous environments. The high number of empirical works that report the presence of Lévy flights in nature in different animal species – with

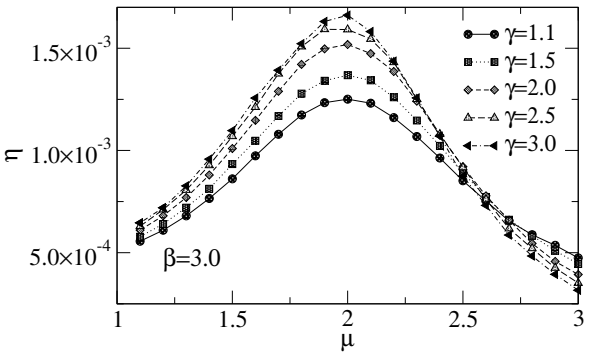

Figure 3.6 We distributed $N_r = 1000$ targets in $N_p = 50$ patches with the same parameters as in Fig. 3.4. Each efficiency curve represents the spatial arrangement of patches with a given γ parameter. Each patch was built with the same $\beta = 3$ parameter. When $\mu < 2.5$ the optimal configuration of resources uses $\gamma = 3.0$. As the strategy becomes less diffusive $\mu \geq 2.5$ the optimal configuration uses $\gamma = 1.1$. Each simulation was performed over 2.5×10^3 runs.

distinct cognition features – foraging in different environments increases the evidence about the universality of Lévy flight. Our findings support the idea that Lévy flights are optimal in a wide range of spatial configurations.

3.3 The Super-Dense and the Super-Scarce limits

Now we will present a set of simulations where the density of the homogeneous targets distribution is very high and very low. It is a well-known feature that Lévy flights will optimize searches in scarce environments, and in high density scenarios there is no pressure for an evolved search strategy since the resources are plentiful.

First, we tested for evidences that $\mu \approx 2$ is the best strategy for the search process when the landscape has a very high targets density, with the average distance between targets $l_t = 5$. In such a high density scenario the search strategy does not have a strong influence in the search efficiency, since most of the steps will be truncated due to encounters with targets.

Due to the construction of the extremely dense environment, the simulations consumed a very long computational time to be executed. The environment was carefully built to avoid dynamical traps: the distance between two targets X_a and X_b is such that $d(X_a, X_b) \geq 1.1 r_v$. This prevents the walker from being trapped between two targets during the search. However, the method used to avoid these dynamical traps demands a lot of computations during the environment construction. In order to finish the results, we reduced the number of averages in the simulations. Thus, the efficiency curve in Fig. 3.7 shows a considerable amount of fluctuations, but the overall optimization around $\mu = 2$ is robust. The differences in the search efficiency are very low, but we have a concrete higher η value for $\mu = 2.0$. That is, despite the very high density, the Lévy flight optimal strategy remains the best choice.

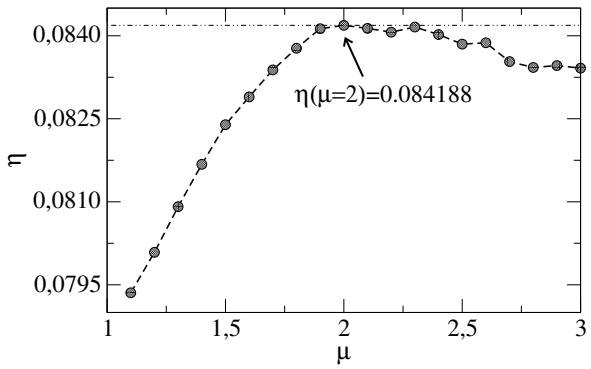

Figure 3.7 The search efficiency for a very dense targets distribution ($l_t = 5$). For $1.9 \leq \mu \leq 2.3$ the corresponding η values remain very close, but $\eta(\mu = 2)$ remains the optimal strategy. The auxiliary horizontal line was drawn to indicate the maximum value reached by η. The fluctuations are noticeable in this figure (especially for $\mu > 2$) because the number of averages, usually set to thousands, was reduced to 200. This artifact was necessary in order to finish the simulations, because the construction of a very dense environment has a high computational cost.

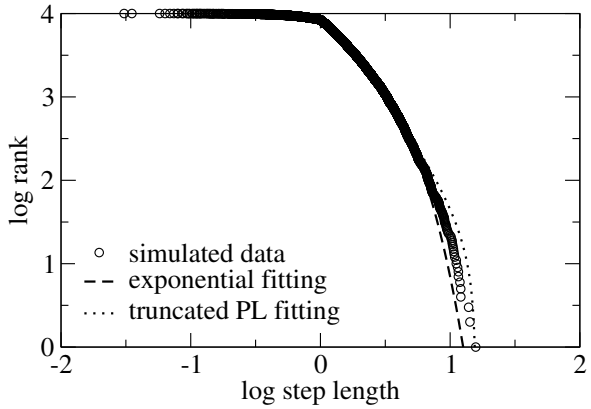

Figure 3.8 The truncated step size distribution of a Lévy walk with $\mu = 2.0$ in an environment with a very high targets density ($l_t = 2.5$). In the analysis we used the first 10^4 steps from the distribution, irrespective of them being truncated or non-truncated. The best adjustment for the tail of the distribution is an exponential fitting, the signature of a Brownian walker.

Now, we will show that the high frequency of steps truncation of an innate Lévy walk strategy ($\mu = 2$) results in a Brownian output steps distribution. We simulated a random walk in a very dense environment, where the average distance between two targets was $l_t = 2.5$. Again, the environment is such that the minimal distance between two targets is $d \geq 1.1 r_v$. During the simulations we saved the emergent distribution of steps, that is, the size of each step after the truncations. In Fig. 3.8 we have the rank plot of the distribution of steps that are emergent from the search process. We focused on the tail of the distribution, and compared a truncated power law fitting to an exponential fitting (that supports a Brownian-like motion). In this situation, we have that the likelihood of an exponential distribution is higher than that of a truncated power law. The log-likelihood of the truncated power law hypothesis is -2947, larger than the one for the exponential (-2938). The Akaike weight, used to compare models that describe the data, is 1 for the exponential distribution, and 0 for the power law. Thus, the statistical tests support that the output steps distribution has the signature of a Brownian motion. Further, even the best adjusted exponent for the truncated power law hypothesis ($\overline{\mu} = 3.3$) reflects a Brownian motion.

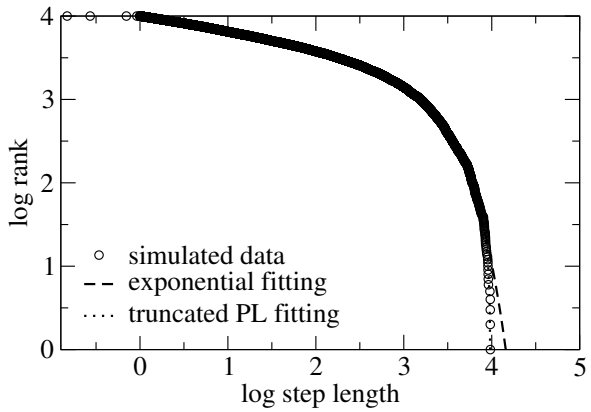

Figure 3.9 Similar to Fig. 3.8 but in a scarce environment ($l_t = 100$). Again the 10^4 first steps from the output distribution were analyzed, irrespective of their truncation. Now, the emergent distribution is very close to the original one: a truncated power law with $\overline{\mu} = 2.19$ represents the best fitting.

Finally, we show that in an environment with a low density of targets the truncations do not interfere so drastically in the step length distribution. In Fig. 3.9 the distribution of steps in a sparse environment ($l_t = 100$) is better adjusted by a truncated power law. The log likelihood is -5571 for the power law hypothesis and -5593 for the exponential. Also, the Akaike weight criteria now is 1 for the power law model and 0 for the alternative exponential hypothesis. Yet, the best adjusted exponent ($\overline{\mu} = 2.19$) is very close to the exponent of the original power law ($\mu = 2$).

3.4 Conclusion

The ongoing discussion in the literature about whether Lévy flights are an innate strategy developed by the organisms or is just an emergent pattern due to the complex distribution of resources has drawn attention to the field recently [55]. Empirical works with locomotion data that shows a truncated power law with exponents around $\mu = 2$ have been scrutinized about the statistical analysis employed or the data acquisition methods.

In this chapter we provided a broad collection of numerical results supporting the *innate* feature of Lévy flights. We showed that the $\mu = 2$ strategy optimizes the search in heterogeneous target distributions: circular patches with different sizes and target densities and fractal environments. Thus, numerically the robustness of $\mu = 2$ has been verified in complex targets distributions, in configurations that are close to the distribution of resources in nature.

We also investigated the effect of a very high density of targets in the emergent distribution of step lengths. In this situation, the steps are truncated frequently and the difference in the search efficiency between the worst strategy ($\mu = 1.1$) and the optimal ($\mu = 2.0$) is less than 6%. In fact, the convenience of adopting $\mu = 2.0$ is highlighted

when the targets are sparsely distributed in the environment [35]. Nevertheless, we showed that $\mu = 2$ still affords a better search performance in a very high targets density.

The truncation of steps can modify the emergent step length distribution, and we showed that a Brownian-like pattern is obtained from a Lévy walk distribution in a very dense environment. Otherwise, when the influence of the environment is not so drastic, as in the sparse distribution of targets, the Lévy walk pattern remains undisturbed.

Chapter 4

The Dynamic Search Environment

In this chapter we explored a dynamical distribution of targets in the environment. The density of resources increases over time until the stationary limit is reached, when the walker detects targets to the same extent in which they are created in the environment. We studied the influence of the search strategy in the stationary environment and compared it with the efficiency in the static targets distribution.

4.1 Introduction

In random search models, the search space is often a landscape where the number of targets (randomly distributed) remains constant [35]. In these models, several realizations of the same search parameters are performed with different randomly generated landscapes, to obtain the sufficient number of averages for the statistical analysis. The total number of targets remains constant, although its distribution in the space (the targets coordinates) changes at every new simulation. Spatial modifications in the same simulation are made in the destructive routine, when a detected target is removed from the current position and re-created somewhere else to conserve the total amount of targets [35]. Another class of works eliminates temporarily the detected target for a time interval τ, and the target site is re-created at the same coordinates after a time τ from its detection [56]. There are works with heterogeneous targets distributions (e.g. fractal structures [57], circular patches [51]), but so far a dynamic targets distribution is not present in foraging computational models.

In nature, the availability of resources is not static. In large time scales, one has, for example, the seasonal influence in the food quantity and distribution [58, 59]. Even in a short time scale, sometimes the distribution is dynamic, like the zooplankton (a very

import food source for marine species) being carried in oceanic waves [60, 61]. Also, there is the diel influence that makes some species adopt a diurnal or nocturnal foraging period [62]. Among the methods to infer the temporal availability of food, one tracks the seabirds distributions in the ocean to predict the density of fishes in a given time and region [63]. Empirical studies show evidence that animals will develop different strategies when its search space is dynamic [64]. For example, jellyfishes will tune their foraging strategy according to the current density of food [32, 65]. The migration of species, for example, is observed when the resources have a temporal availability induced by periodic events like rain fall, season, etc. Thus, in models that intend to investigate dynamic foraging problems, it is essential to consider temporal variations in the environment [66].

In this chapter we will present a model for a random search process in an environment with a variable targets density. The search will be performed by a random walker and the number of targets will increase periodically in the landscape. Every time the random walker covers a characteristic distance λ, a new target will be created in a random location of the environment. The search is destructive: once a target is detected, it will be removed from the list. In order to achieve the stationarity in the targets distribution, the average distance the forager covers between two targets has to be close to the characteristic distance λ. In our simulations with the dynamic environment, we want to verify if there is a stationary limit in this problem and then characterize the statistical quantities involved in the process.

4.2 The Model

We consider a squared region (side L) with periodic boundary conditions applied. When the random walker starts the search, there is only one available target in the environment. Every time the searcher covers a characteristic length λ, the environment will receive one new target at a random position. Also, the search is destructive and the visited targets are eliminated from the environment. Since our random walker has a constant speed, the time spent in the search will be proportional to the traveled distance. This characteristic distance λ and the search strategy μ will determine how fast the system will achieve the stationary limit. The process is illustrated in Fig. 4.1.

Throughout the search, the targets density increases, as shown in the panel of Fig. 4.2. In the beginning of the walk, the density increases in a higher rate because the targets are created faster than the searcher eliminates them. This becomes more evident calculating the ratio T/Q, that is, the ratio between the number of available targets and the number

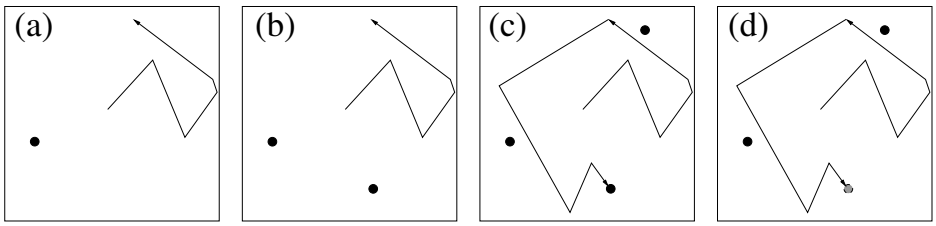

Figure 4.1 In the beginning of the walk (a) only one target is available. Another target will be created when the searcher covers the characteristic length λ in (b). More targets will be added every time a distance equal to λ is covered. When a target is detected (c), it will be removed from the environment (d).

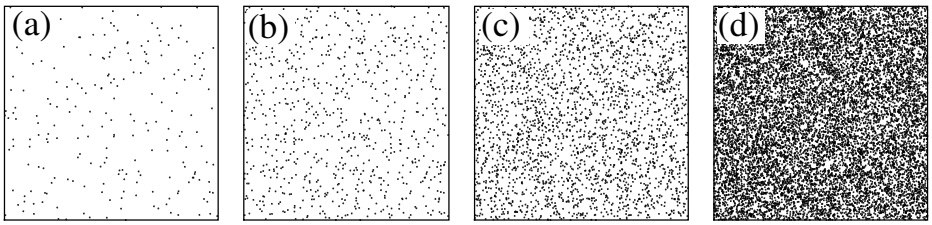

Figure 4.2 The increase in the targets density during the simulation. In (a) we have the environment in the beginning of the search process: $Q = 10$ targets were found from a total of $T = 221$ available targets. Then, in (b) $Q = 100$ targets were detected, and $T = 763$ targets are composing the environment. After $Q = 1000$ targets detected, in (c) we have $T = 2651$ targets in the environment. Finally in (d) $Q = 10000$ targets were found and $T = 12543$ targets are available in the environment. The characteristic length used to construct the targets was fixed in $\lambda = 20000$ and the search strategy was set to $\mu = 1.1$.

of detected targets. In Fig. 4.2(a), the environment in the beginning of the walk has $T/Q \approx 20$. This ratio decreases to $T/Q \approx 8$ in Fig. 4.2(b), $T/Q \approx 3$ in Fig. 4.2(c) and finally to $T/Q \approx 1$ in Fig. 4.2(d). The decrease in the T/Q ratio may indicate that the environment can achieve a stationary limit, when the creation of new targets balances the elimination of old ones.

As the targets density increases, the average distance between them decreases and so the mean free path of the landscape. In a very high density of targets, the frequency of flights that are truncated is high and hence the flights are shorter. In Fig. 4.3, we have a simple representation of the time evolution of the flight lengths. The flights are longer in the beginning of the search and become shorter and shorter as the targets density increases.

4.3 Results

We are interested in the stationary configurations of the problem, and the relation between the stationarity, the characteristic length λ and the search strategy μ. The model has five parameters: the visual radius $r_v = 1$ (fixed), the size of the grid $L = 10^4$ (fixed), the

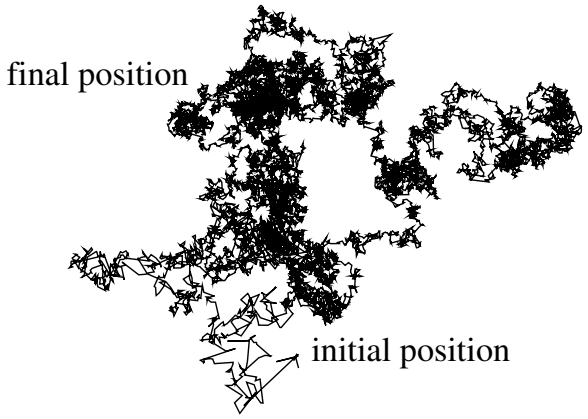

Figure 4.3 The increase in the targets density during the walk changes the length of the steps due to truncations. In the beginning of the search process, the targets density is very low and the steps are often completed without truncations. As the density increases, the steps now will truncate with a higher frequency, so the length of the flights decreases. There is a visual distinction between the region where the walk starts and where it ends. The characteristic length used was $\lambda = 5$ and the walker detected $Q = 2 \times 10^4$ targets with $\mu = 3.0$.

characteristic length λ (variable), the search strategy μ (variable) and the stop condition for the simulation Q (variable). We can identify the stationarity in the environment when the total amount of available targets remains nearly constant, indicating that the average distance covered between two targets is equal to the characteristic length λ.

Fig. 4.4 shows the temporal evolution of the number of available targets for a fixed search strategy $\mu = 1.1$ and distinct characteristic distances. The density of available targets achieves the stationarity first for the largest values of λ. The final number of targets in the stationary regime N_s is smaller for large λ. The $\mu = 1.1$ walker adjusts the average distance that it travels between two targets to coincide with λ faster when few targets are available. Since in the stationarity one has $\lambda = N\langle\ell\rangle$, the number of targets in the stationary regime depends on λ. Further, λ has an inverse relationship to N_s, thus for large λ one will have few targets in the stationarity. In Fig. 4.4 we have $N_s \approx 2500$ when $\lambda = 20000$, but $N_s \approx 18000$ for $\lambda = 2500$. Hence, the environment achieves the stationary limit faster when a few targets have to be created, and it is the case for large λ.

In Fig. 4.5 we show the amount of targets available for a fixed characteristic length $\lambda = 2500$ and distinct search strategies μ. The stationary configuration is achieved faster for lower μ exponents, and the number of available targets is smaller in the stationary regime for low μ. Here we stress that in the stationary limit the distance covered between two targets approaches the characteristic length λ. Thus, for $\mu = 1.1$ the walker adjusts its steps faster than the less diffusive strategies, reaching the stationary configuration before. For $\mu = 3.0$, the stationarity takes a longer time to be established, therefore more targets are present when the system approaches the equilibrium (it takes a long time to achieve the stationarity for $\mu = 3.0$, and it is not observed in Fig. 4.5). One feature of this dynamic environment is that in the stationary limit all the strategies will have the

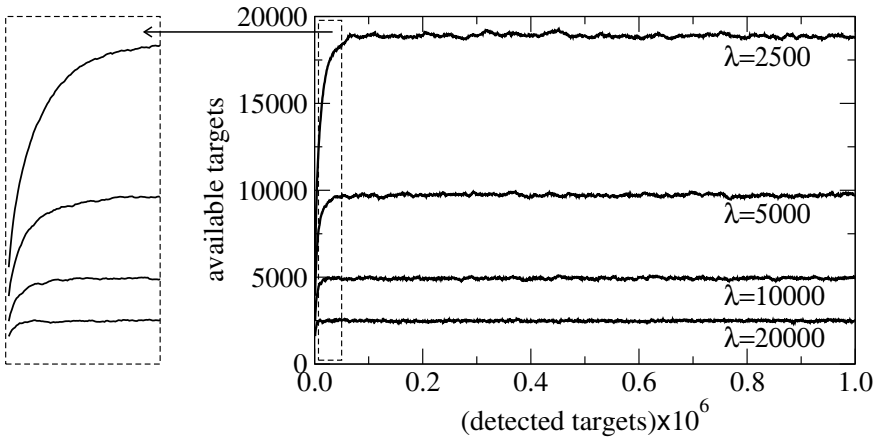

Figure 4.4 The number of available targets in the environment as a function of the number of detected targets with $\mu = 1.1$. This can be interpreted as the amount y of available targets when the target number x was detected, in a temporal order. The characteristic distance λ will determine how fast the stationary environment will be achieved: the configurations with large λ achieve the stationarity sooner than small λ. The final amount of targets is larger when the characteristic length is small: since it takes more time to achieve the stationarity, more targets are added in the environment. The inset on the right shows the stationarity being achieved in the beginning of the simulation.

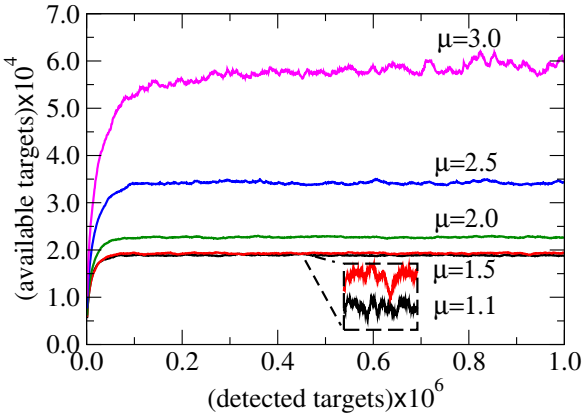

Figure 4.5 Same as Fig. 4.4 but for a fixed characteristic length ($\lambda = 2500$) and different search strategies. The search strategies close to the ballistic walk ($\mu \to 1$) will achieve the stationary configuration faster than the strategies near the Brownian limit ($\mu \to 3$). Similarly to Fig. 4.4, the amount of available targets is smaller in configurations that achieve the stationarity early.

same average step between two targets (coinciding with λ), thus all the strategies will have the same search efficiency η, roughly given by $1/\lambda$ in this case.

The search efficiency, given by the ratio between the number of targets detected and the traveled distance is shown in Fig. 4.6 for different strategies μ. Irrespective of μ, the search efficiency increases very fast in the beginning of the search and then the increase rate becomes nearly constant. It is a consequence of the density of targets, that increases in the onset of the search and then becomes stationary (see Fig. 4.4). The optimal strategy (highest η) changes with the simulation time: until the detection of the target number $T = 1.5 \times 10^3$ the best strategy is $\mu = 1.1$. The inset (i) in Fig. 4.6 shows the transition of the highest efficiency from $\mu = 1.1$ to $\mu = 1.5$. Then, $\mu = 1.5$ follows as the best strategy until the target number $T = 1.5 \times 10^5$ is detected, as shown in the

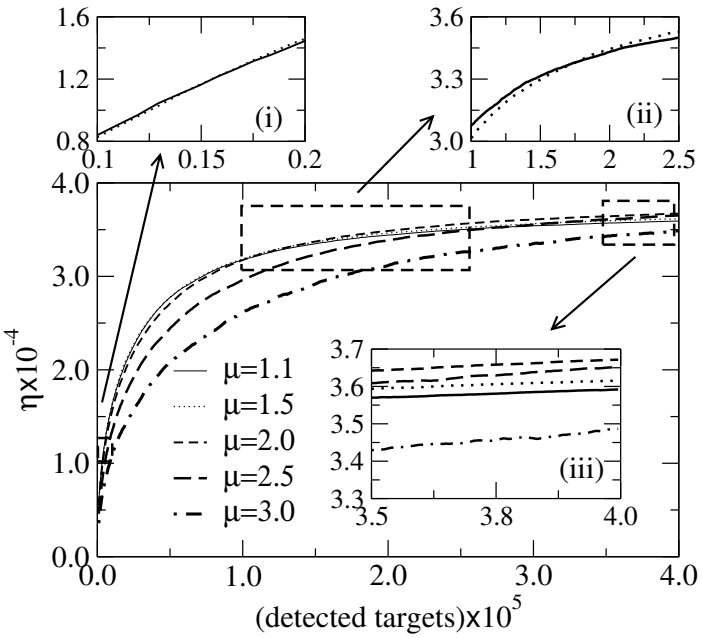

Figure 4.6 The statistical efficiency η for different search strategies μ as a function of the detected target in a temporal order. The inset (i) shows the transition from $\mu = 1.1$ to $\mu = 1.5$ as the higher efficiency. The η values become closer as the system evolves. The transition from $\mu = 1.5$ to $\mu = 2.0$ is shown in the inset (ii). Finally, inset (iii) shows that the efficiency values, irrespective of μ, converge to the same result. The characteristic length used was $\lambda = 2500$ and every walk finished when $Q = 4 \times 10^5$ targets were detected.

inset (ii) in Fig. 4.6. Finally, $\mu = 2.0$ reaches the highest efficiency values until the end of the simulation, as the inset (iii) in Fig. 4.6 shows. Still, the differences in the search efficiency values are very small when the stationarity is achieved.

Finally, in Fig. 4.7 a very long simulation shows the convergence of the search efficiency for all the strategies. Now all the strategies assume efficiency values very close, and in the inset of Fig. 4.7 we show that the exponent $\mu = 2.5$ assumes a slightly higher η value in the end of the simulation. The convergence in the efficiency is achieved because all the strategies share the same traveled distance between two targets (coinciding with λ) in the stationary regime. Thus, since $\eta = 1/\lambda$, the efficiency is nearly the same for all the strategies.

In order to verify that the search efficiency coincides for all strategies in the stationary limit, we implemented random search simulations in the static destructive distribution of targets. In these simulations, the number of targets (destructive) remains constant and matches the number of available targets in the stationary configurations. A comparison between the search efficiency values η_s for the static environment and η_d for the dynamic one is made on table 4.1. The number of targets in the stationary limit N_t is a function of the search strategy, as discussed in Fig. 4.5. All the combinations in table 4.1 lead to

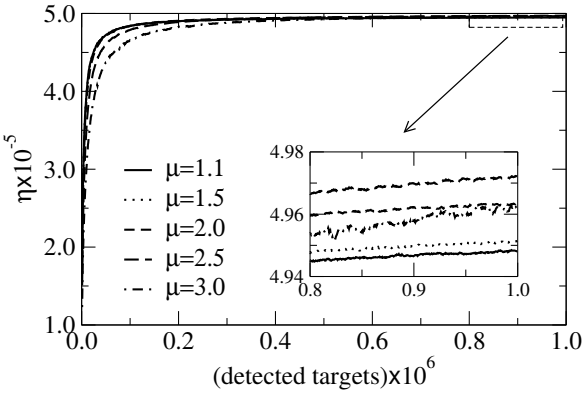

Figure 4.7 Same as Fig. 4.6 but for a longer characteristic length $\lambda = 2\times10^4$. In this longer simulation, the random walker detected $Q = 10^6$ targets. Now each strategy will assume numerical values for the efficiency that are very close during the stationary phase, as expected by the relationship $\eta = 1/\lambda$.

the same average traveled distance between two targets, and thus, to the same search efficiency, despite fluctuations.

Strategy	$\eta_d \times 10^{-5}$	$\eta_s \times 10^{-5}$	N_t
$\mu = 1.1$	4.95	4.93	2470
$\mu = 1.5$	4.95	4.92	2500
$\mu = 2.0$	4.96	4.98	2870
$\mu = 2.5$	4.97	4.96	4220
$\mu = 3.0$	4.96	4.92	7170

Table 4.1 A comparison between η_d (dynamic environment) and η_s (static) for $\lambda = 2\times10^4$. The number of targets in the stationary limit was used in the simulations for the static targets distributions. The same search efficiency is achieved for all the strategies μ.

4.4 Conclusion

In the random search model using a dynamic search environment we characterized the interaction between the search strategy and the density of targets. We showed that the stationary distribution of targets is achieved first for strategies that have enhanced diffusivity, that is, $\mu \to 1$. The condition for the stationary regime is the adjustment between the characteristic distance λ and the average traveled distance between two targets. In a static targets distribution, each search strategy will cover a different distance in the detection of a target. Thus, for a same λ, the time spent in the process to achieve the stationarity depends on the search strategy μ.

When μ is fixed, then the configuration with large λ values will reach the stationary limit faster. Since the number of targets in the stationarity N_s shows an inverse relation to λ, configurations with smaller N_s will become stationary faster.

We showed that all the search strategies can adjust the distance traveled between two targets to coincide with λ. Thus, the stationarity is achieved for all μ, but in different times. As a future collaboration, we are preparing an analytical formulation to this problem, to compare the numerical results with theoretical predictions. Further, the dynamic environment is spatially homogeneous in this work, and we are considering to extend the model to heterogeneous configurations. In a homogeneous distribution of targets, one has a well defined mean free path length. However, this quantity cannot be defined in more complex landscapes, like fractal ones. Studying the stationarity in heterogeneous spaces thus can provide a numerical value for the mean free path that does not have an analytical formula so far.

Chapter 5

Parallel Random Search

In this chapter we propose a method to parallelize random search processes and reduce the computational time demanded by the simulations. First, we characterized the spatial distribution of detected targets in the sequential random search. Then, the same sequential pattern of detections is introduced in the parallel random search, adjusting the initial coordinates of each parallel random walker. The parallel random search reduced the computational time demanded in sequential simulations.

5.1 Introduction

The use of computational models to understand a problem is a keystone tool in science nowadays [67]. However, several complex problems have a computational approach that is of difficult implementation [68], and the viability of the model depends on its optimization [69].

The parallel computing strategies [70] are a very important tool to reduce the computation time of simulations. However, to achieve a parallel code that shows a significant performance is often a difficult task. Usually, the algorithms that rely on sequential decisions are not easily parallelizable, like P-complete problems [71, 72]. However, some problems thought to be inherently sequential, like edge coloring [73] and the maximal independent set [74] also have found a parallel solution. The parallel algorithms can be constructed in a very different way from its sequential counterparts, like parallel genetic algorithms that have a super-linear performance when its computational efficiency is compared to their sequential versions [75]. A collection of multidisciplinary problems allowing parallel approaches can be found in Ref. [76].

The general random search problem consists of finding the best strategy for the encounter of randomly located target sites that can be detected in the limited spatial vicinity of the searcher [5]. From our experience on random search simulations, we have been facing difficulties concerning the long time it takes to have meaningful results, a consequence of the large number of averages required. In this area of research, the computational protocols are traditionally sequential: the random walker moves from target to target until some halt criterion is achieved. An alternative for the problem of one random walker looking for Q targets could be Q random walkers looking for only one target. In fact, our solution to the problem is based on this idea, but with some extra information to reach the same results that we have on the sequential version. The extra information that we are interested concerns the pattern that is built with the detected targets on the environment, like a footprint of the walker. This can be used on practical applications, especially in animal foraging, when it is useful to understand how the resources are exploited during the search.

The parallelization was made using OPENMP directives in the original C code [77]. We are able to specify that each thread will access the environment, stored on the shared memory, and proceed with its own random walk according to its private variables. The OPENMP approach was chosen because its directives have a simple implementation and it also provides a native solution for the memory consistency problem that appears in the parallelization.

5.1.1 Parallelization of random walks

The parallelization of random walks has been an important tool in Monte Carlo Simulations. In order to achieve the flat histograms to calculate the density of states, the Wang-Landau method employs independent random walkers for different energies [78, 79]. This method allowed the numerical solution for larger systems, and the independent random walkers are a crucial part of this. One possible parallelization of the method assigns one random walk for each available thread [80] using thousands of threads from the GPU. However, the sampling over the energy landscape is not sufficiently homogeneous, so it is necessary to specify more random walkers to the lower energy regions. An OPENMP approach [81] was made for the Ising model using the Wang-Landau method. The parallelism can be explored in the solution of partial differential equations that use the Monte Carlo method [82] with multiple random walkers.

In graph theory, one important application of parallel random walks is the study of the cover time of a graph (the necessary time to visit all the nodes). It is known that for some graphs of size n the implementation of k random walkers (since $k \leq \log(n)$) can decrease

the cover time by a k factor [83]. However, the choice of the initial coordinates for the walkers will influentiate in both the cover time and the hitting time of random regular graphs [84, 85]. There is an optimal initial coordinates choice that depends on the topology of the graph and minimizes the cover and hitting times. The $s-t$ connectivity problem, where one has to determine if the vertices s and t are connected to a same component, also gains efficiency when several random walkers are initialized. In wireless networks, the use of multiple random walkers on a search for a target reduces both the computing time and the network overhead [86].

In model-checking algorithms, the bug detection is faster when using parallel random walkers [87]. These independent random walks can explore more sites of the network [88] in a fraction of the sequential time, since the revisitations to the same node are decreased in this arrangement. Parallel random walkers can be used to simulate the behavior of a honeybee colony foraging [89] applied to a random search for errors in a network. This algorithm allocates parallel foragers that will search for resources in a given patch based on simple instructions about the quality of the patch. Another model with biological inspiration uses ant robots that work in a parallel decentralized fashion to explore an expanding landscape [90].

5.2 Sequential Search Properties

In order to construct a parallel version for the random search problem, we explored some properties of the sequential version of the code that will be necessary for our parallel implementation.

The search environment is a square grid (size D) with periodic boundary conditions applied. In this environment a given amount of targets will be distributed in a homogeneous way, with an average distance l_t between each other. The l_t characterizes the density of targets: the larger (smaller) l_t, the lower (higher) the density. The targets are non-destructive and can be detected more than once during the search. The searcher is a random walker whose steps ℓ_j are taken independently from a probability density distribution $P(\ell) \sim \ell^{-\mu}$ $(1 < \mu \leq 3)$ for $r_v < \ell_j < D$ and 0 otherwise. The directions are uniformly distributed in $0 \leq \phi < 2\pi$.

One feature of the random search that does not have much attention in the literature is the spatial pattern formed from the detected targets. An analytical approach was made [91] but considering several random walkers with a common starting position, not the resulting pattern of one random walker. In the foraging of different animal species, each one will explore the resources in a different spatial scale: some of them have a dispersal

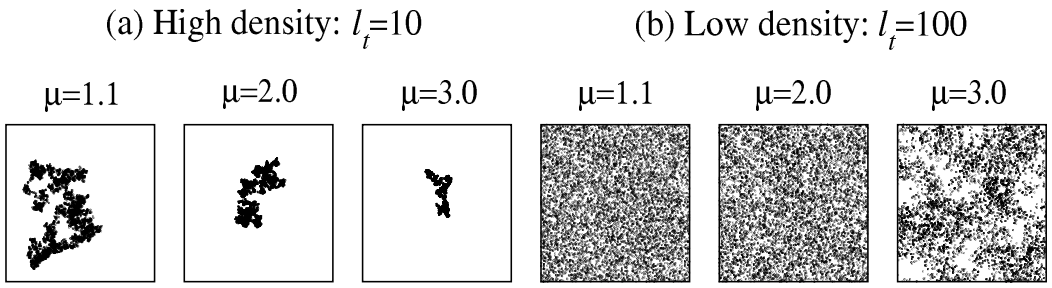

Figure 5.1 Spatial pattern obtained from the detected targets as the random walker (strategy μ) searched in a dense (a) and in a sparse (b) configuration. In the high density regime, the presence of long steps in the ballistic walk ($\mu = 1.1$) results in a large area covered with targets, contrasting with the narrower region of the Brownian walker ($\mu = 3.0$). On the other hand, in the low density of targets the distribution of the detected ones is almost homogeneous over the entire landscape for $\mu = 1.1$ and $\mu = 2.0$. Even for the Brownian searcher the visited area is larger in the sparse distribution of targets. Each search detected 10^4 targets.

rate higher than the others [92]. In our model, each search strategy μ leaves a particular footprint on the environment: ballistic searches will explore a larger region of the space than the Brownian searchers, a consequence of the step lengths. Also, as we modify the density of targets, the spatial pattern changes. These properties are summarized on Fig. 5.1, that shows the distribution of detected targets for distinct search strategies in dense (a) and sparse (b) configurations. Our intention in this section is to characterize the interaction between the searcher and the environment using the spatial pattern of the detected targets.

To characterize the particular spatial pattern associated with each search strategy, we study the behavior of the distribution of distances between two sequentially detected targets. We record the distance as a straight line that connects the two targets. As our environment has periodic boundary conditions, for each couple of points we have two possible values for the distance between them. For convenience, we will always use the shortest distance in our records. If the same target is detected in a sequence, the distance is zero and this is not accounted on the distances record to simplify the distribution. We will keep the information about the number of revisited targets for a later analysis. Also, we will work with the logarithm of the distances because this quantity seems to follow a normal distribution under certain conditions, as can be seen in Fig. 5.2.

The set of histograms displayed in Fig. 5.2 has the same parameters used in the patterns of Fig. 5.1. Except for Fig. 5.2(a), the data seem to follow a normal-shaped distribution with definite parameters mean m and standard deviation σ. Even though the fitting is not accurate, working with an approximate distribution is sufficient in our method. Since superdiffusive search strategies have a steps distribution with both short and long components that depends on its search exponent μ, the resulting interaction between the

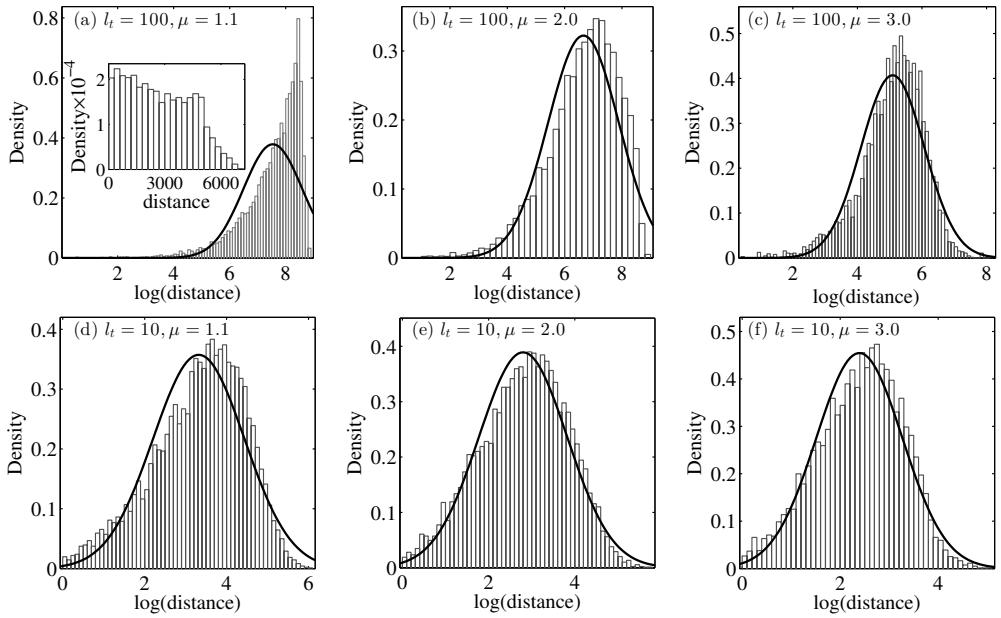

Figure 5.2 Histograms of the logarithm of the distances between successively detected targets for different μ's and l_t's. Each set of data was recorded from a single simulation of a search for 10^4 targets. The original sets are reasonably well fitted by lognormal distributions (seen as Gaussians (continuous curves) because of the logarithm rescaling), except in a sparse environment for a ballistic walker, case (a). In the inset of (a) we have the histogram of the original distances, showing a fairly uniform distribution. One can "artificially" generate the same patterns of Fig. 5.2 using this analysis.

walker and the targets is not uniform. The searcher will accomplish detections both close to its last visited target and far away from it. However, when $\mu = 1.1$, the frequency of long steps is very high, and in a low density scenario (say, $l_t = 100$) the detected targets are usually very distant from each other. The histogram in the inset of Fig. 5.2(a) shows the (original) distribution of distances prior to the logarithm transformation. It does not display the typical heavy tail of lognormal distributions, presenting instead a low decay (specially for distances up to $D/2 = 5 \times 10^3$, being almost uniform in such region). This contrast with Figs. 5.2(b)–5.2(f), where both distant and close targets are found (but at different proportions) and the lognormal behavior is observed. When the targets density increases, even the ballistic searcher will tend to detect targets in the neighborhood of its last detection, and the distances distribution shows a lognormal shape. But we should emphasizes that to represent this a bit harder $\mu = 1.1$, $l_t = 100$ case (given rise to a homogeneous distribution of detected targets, see Fig. 5.1(b)) by a normal-shaped distribution with a large mean – thus consistent with Fig. 5.2 – already turns out be good enough for our latter purposes.

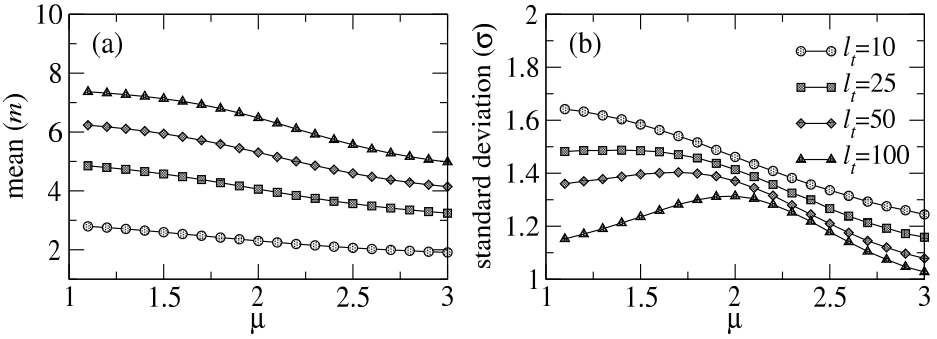

Figure 5.3 The mean (a) and standard deviation (b) that will be necessary to characterize the virtual environment for the parallel random searches. Each curve is the result of $N = 2.5 \times 10^3$ averages over the values of m and σ. The values of l_t range from a dense to a sparse configuration, $l_t = 10$ (circles), $l_t = 25$ (squares), $l_t = 50$ (diamonds) and $l_t = 100$ (triangles). The mean distance decreases with μ and increases with l_t, while the standard deviation has a more complex dependence on these variables.

From simulations of the sequential code, we get the parameters that provide the characterization of the normal-shaped distribution showed in Fig. 5.2. Working with the logarithm of the distances, we take advantage on the additive properties of the normal distribution and thus can perform averages on different spatial configurations. Thus, each sequential search was averaged over $N = 2.5 \times 10^3$ simulations consisting in the detection of 10^4 targets. In Fig. 5.3 we display the behavior of the mean m (a) and the standard deviation σ (b) of the logarithm of the distances between targets consecutively found as a function of the search strategy μ and for different configurations of the search space. As expected, Fig. 5.3(a) shows that the targets detected by the ballistic searcher are much distant than those visited by the Brownian searcher. Furthermore, the values for the mean of the distances increase as we take sparser configurations.

The standard deviation, Fig. 5.3(b), has a more complex behavior: it reaches the higher values in the dense configuration, indicating that larger fluctuations around the mean are present for smaller average distance between targets. This is a consequence of the numerous empty corridors in the environment. These corridors are long paths (like holes) where the searcher cannot detect targets within the r_v distance. This will have a more drastic impact when the longer jumps are more frequent ($1 < \mu \leq 2$), because a longer step will result in a longer path in the corridor. Even though the average distance between two targets is small, sometimes the searcher will travel a longer path in order to make a detection. As we will have a wider range of values for the distances, the standard deviation will increase. In the sparse configuration, the targets are always very distant from each other, so we do not have much variation on the distances.

Another peculiarity in Fig. 5.3(b) is the curve for $l_t = 100$: it is maximized around $\mu = 2.0$, in contrast with the other l_t values. This effect is a consequence of a feature of

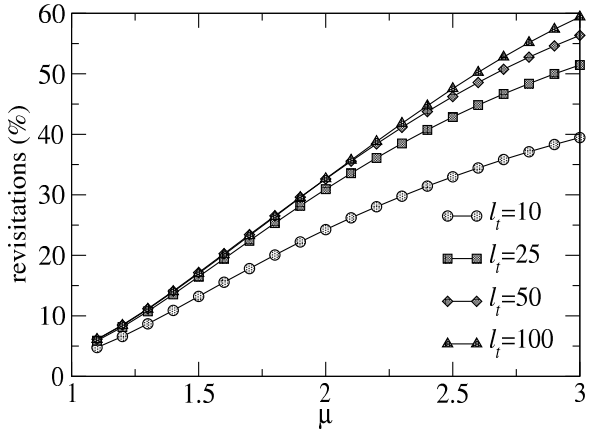

Figure 5.4 The percentage of targets that are revisited at least once during the search for $T = 10^4$ targets as a function of the search strategy μ, in environments with distinct average distances between targets l_t. Revisits to the last detected target are more frequent on the sparse configuration $l_t = 100$ for $\mu = 3.0$. As a consequence of the normal diffusion, the Brownian searcher has a higher probability to return to its starting position. On the other hand, ballistic strategies ($\mu \to 1$) tend to access faraway regions of the search space, leading to a small number of revisits.

the $\mu = 2.0$ strategy within a sparse environment: it will detect both distant and nearby targets, a signature of its super-diffusive behavior [93]. This increases the range for the distance values, resulting in a larger standard deviation for this particular configuration. The strategy that is able to minimize both the mean and the standard deviation is $\mu = 3.0$, because of its normal diffusion properties: it will always detect targets on its close neighborhood, decreasing both m and σ.

Finally, the last quantity used to characterize the spatial distribution of the detected targets is the fraction of targets that are revisited during the search. We consider that the target is revisited when the searcher leaves the current target and then finds it again at some subsequent step, without the detection of distinct targets in between. These are the zero distances that were temporarily ignored in the analysis of Fig. 5.3. In Fig. 5.4 we show the percentage of revisits during the search for $T = 10^4$ targets as a function of the average distance between targets l_t and search strategy μ. The highest number of revisitations occurs for $\mu = 3.0$, as expected for the normal diffusion regime. The density of targets also plays a role on this behavior: the sparser the environment (large l_t) the higher the probability to return to the same target. As it is going to be clear next, to know the number of revisitations in each random search configuration is fundamental to implement the parallelization procedure.

5.2.1 The construction of the virtual environment

The spatial pattern of detected targets (Fig. 5.1) is an important feature because it provides the information about how a single walker looking for a total of T targets progressively interacts with the environment. This pattern will be used to assign the initial coordinates for the parallel searchers. We call this construction the *virtual environment*. In the parallel version, we assume many independent random walkers (N_{rw}), each

looking for Q targets (with $Q \ll T$), so that $N_{rw} \times Q = T$. In order to reproduce the successive neighborhoods that a single walker experiences along the search, we use the parameters from Fig. 5.2 to generate the initial coordinates (i.e., *the starting positions* $\{(x,y)_{sp}\} = \{(x_1,y_1)_{sp},\ldots,(x_{N_{rw}},y_{N_{rw}})_{sp}\}$) of the N_{rw} parallel random walkers. According to our definition of $\{(x,y)_{sp}\}$ (see below), any parallel walker n, starting from a point $(x_n,y_n)_{sp}$, while finding just few targets effectively will experience a stretch of the full trajectory traveled by a single walker. Thus, collectively the parallel random walkers properly sample the long term characteristic of the sequential search.

To construct a correct set $\{(x,y)_{sp}\}$ for each strategy and environment parameters μ and l_t, we first generate a lognormal distribution of corresponding m and σ, Fig. 5.3. Thus, we follow the standard protocol [94] of initially creating (with a random number generator) a list of normal distributed numbers $\{u\} = \{u_1,u_2,\ldots,u_{N_{rw}}\}$ with mean 0 and standard deviation 1. Next, we obtain another list of also normally distributed numbers $\{v\}$, with mean m and standard deviation σ, simply writing $v = u\sigma + m$. Then, we apply the mapping $z = \exp[v]$, getting a lognormal distribution $\{z\}$ similar to those displayed in Fig. 5.2. Second, for a given m and σ, we simulate a usual simple random walk (i.e., with no search), for which the turning angles are drawn from an uniform distribution and the j-th step length is given by the element z_j of $\{z\}$. This walker takes in total N_{rw} steps and the coordinate positions of the successive steps end points form the set $\{(x,y)\} = \{(x_1,y_1),(x_2,y_2),\ldots,(x_{N_{rw}},y_{N_{rw}})\}$.

Third, and lastly, two extra transformations are performed to the above $\{(x,y)\}$:

(i) The number of revisited targets during the sequential search, which can be inferred from Fig. 5.4, determines how many starting positions of the parallel walkers should coincide (a necessary restriction if the parallel implementation is going to reproduce patterns similar to those in Fig. 5.2). Thus, if for a certain μ and l_t the revisitation fraction is P_{rev}, we take the last $N_{rw} \times P_{rev}$ distinct coordinates in $\{(x,y)\}$ and randomly set them equal to the first $N_{rw} \times (1 - P_{rev})$ coordinate values. We notice this straightforward procedure (seeking to obtain the final $\{(x,y)_{sp}\}$) can work well for Q not too big. However, there is no reason to make Q very large since then we may start loosing the advantages of the parallelization. Notice that in the parallel construction the walker can revisit its starting position and also detect a target in another walker's initial location, this last event corresponding to the sequential walker revisiting a target after detecting new ones.

(ii) In the sequential case, immediately after collecting a target located at, say (x_t,y_t), the walker initial position to look for the next target is obviously (x_t,y_t). Therefore,

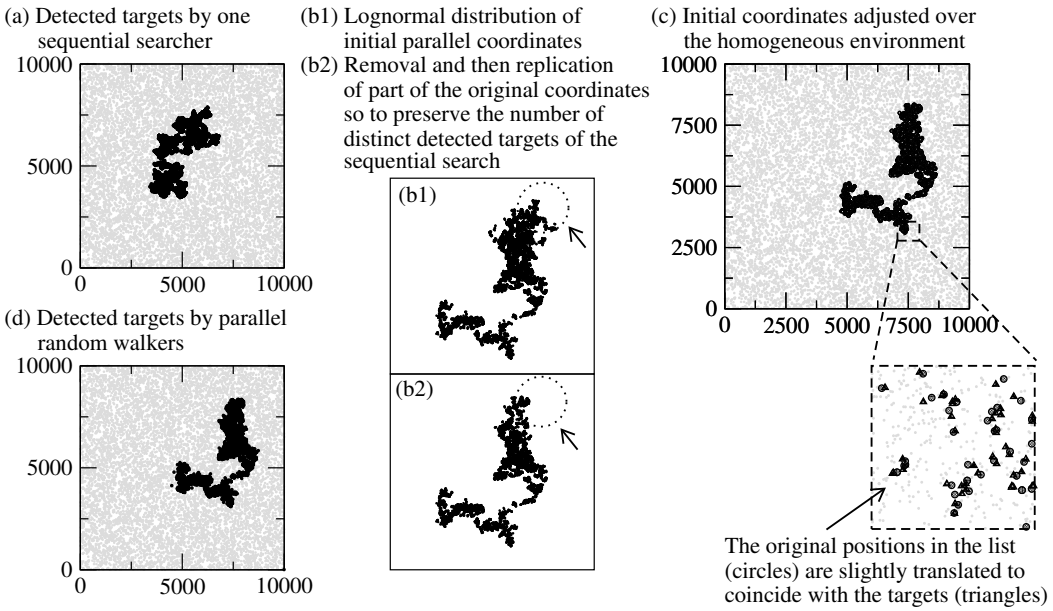

Figure 5.5 Illustration of the initial conditions construction for the independent parallel walkers. The parameters here are $T = 10^4$, $\mu = 2.0$ and $l_t = 10$ (the two latters associated to lognormal mean and standard deviation $m = 2.71$ and $\sigma = 1.07$, see Fig. 5.3). (a) The complete environment and the detected targets (black dots) by a sequential searcher. (b1) As explained in the main text, the lognormal distribution of distances is used to generate the shown set of positions $\{(x,y)\}$. (b2) The set in (b1) goes through the procedure (i): the last $N_{rw} \times P_{rev}$ positions coordinates (indicated by arrows) are randomly substituted by the first $N_{rw} \times (1 - P_{rev})$ coordinate values. Hence, the number of distinct points displayed in (b2) matches the number of distinct detected targets in the pattern in (a). (c) The transformation (ii): the set of positions in (b2) are translated so to coincide with the locations of the corresponding closest targets. (d) The found targets by all the random parallel searchers (which initiate their searches at the locations resulting from (c)). The patterns in (a) and (d) are very similar, e.g., notice their sizes, border shapes, and degree of compactness.

> we substitute each location $j \equiv (x_j, y_j)$ of the set $\{(x,y)\}$ resulting from (i) by the coordinates of the closest target to j. In doing so, we end up with lists $\{(x,y)\}$ of positions which have exactly the motifs shown in Fig. 5.2. Finally, we take these sets as ours $\{(x,y)_{sp}\}$'s.

Fig. 5.5 summarizes the above described scheme for the initial conditions attainment. The transformations (i) and (ii) are illustrated in Figs. 5.5(b)–(c). Furthermore, we can see that the pattern of detected targets using the sequential, Fig. 5.5(a), and parallel, Fig. 5.5(d), algorithms are indeed very similar.

Finally, we mention the localization of the targets nearest to the coordinates in the list $\{(x,y)\}$ – procedure (ii) above – also should be optimized, otherwise the computational time gain with the parallelization process would be less effective. With such an aim, we first divide the environment into M quadrants. Then, we determine to which quadrant q ($q = 1,2,\ldots,M$) a given (x_j, y_j) belongs to. Lastly, we look for the closest target to

this point (x_j, y_j) by inspecting only q and its first neighbor quadrants. This operation also has been parallelized to increase the efficiency of the code: each thread receives a pair (x_j, y_j) of starting coordinates, identifies to which quadrant q this pair pertains, searches in q and in the adjacent quadrants for the closest target, calculating the distances coordinate-targets, and then selects the target with the shortest distance. The task is completed by the proper change of (x_j, y_j) by the closest target location.

5.3 The Parallel Algorithm

Some part of the original code was kept sequential, consisting in the initialization of all the variables, creation of the environment and the construction of the list with the initial coordinates of the searchers without the correction. The first parallel construction generates the virtual environment. At this step, the list of initial coordinates is mapped into the search environment. Each thread will do the search for the closest target independently, looking in the vicinity of the coordinate it received.

The next parallelization was made in the routine that realizes the search, performing flights until one target is found. Each thread now receives the initial coordinate for its search and the list of available targets in the environment. In order to enhance the optimization, one could think about a smaller list, concerning the targets in the close neighborhood of the initial position. This is not the case here because searchers with $\mu \to 1$ tend to localize targets distant from its initial coordinate (recall the exploitation pattern in Fig. 5.1).

Each thread will perform its decisions regarding the length of the flights and the turning directions independently. For the records it will save the total traveled distance for the detection of one target. This will provide the search efficiency (the inverse of the average distance to find one target), and the averages will be made with the results of all the threads. In Fig. 5.6 we show the statistical search efficiency for both the sequential and parallel algorithms in a dense ($l_t = 10$) and a sparse ($l_t = 100$) configurations. The effiency curves are practically the same, and the optimal search strategy coincides ($\mu \sim 2$) as expected [35].

In our sequential simulations of the random search, the total time spent by each strategy is different: when $\mu \to 3$ the simulation time increases substantially. This is a consequence of the number of steps required to perform a detection, that is shown in Fig. 5.7. The searchers with $\mu \to 3$ demand more than a thousand steps to detect a single target in a low density configuration, while the ones with $\mu \to 1$ need a dozen steps to do the same task. As the search for the target in the list is done at every step, it

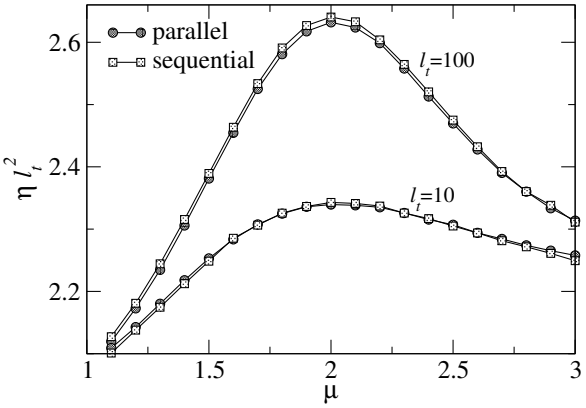

Figure 5.6 Search efficiency (normalized by l_t^2) obtained from the parallel (circles) and sequential (triangles) implementations. It is clear that the sequential and parallel codes present practically the same numerical results. The stop condition is the detection of $T = 10^4$ targets in both dense ($l_t = 10$) and sparse ($l_t = 100$) environments. In the parallel code example here, each of the $N_{rw} = 10^4$ walkers looks for just a single target ($Q = 1$). The averages are performed over $N = 2.5 \times 10^3$ simulation runs.

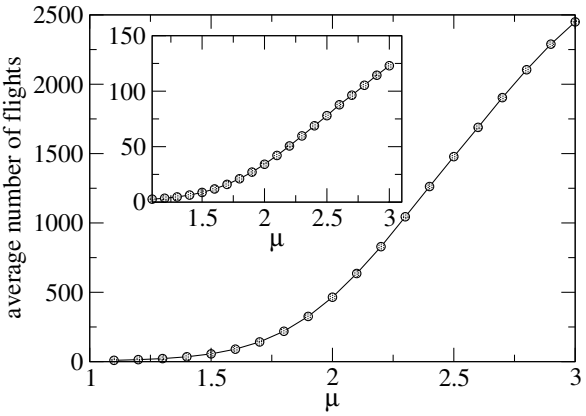

Figure 5.7 A comparison between the average number of flights required to detect a target in a sparse (average distance between targets fixed in $l_t = 100 r_v$) and a dense (inset, $l_t = 10 r_v$) environment. In a low density scenario, searchers with $2.5 \leq \mu \leq 3$ will realize more than a thousand steps to detect one single target. If we consider the dense environment, the amount of steps for the same task drops to a hundred for $2.5 \leq \mu \leq 3$. On the other hand, for strategies between $1.1 \leq \mu \leq 1.5$ the number of steps to make a detection are less than 10 for the high density and less than 60 in the low density conditions.

is natural that the verification for some strategies will take a longer simulation time. For an environment with a higher targets density, the required number of steps for $\mu \to 1.1$ and $\mu \to 3$ is from less than a dozen to a few hundreds, respectively.

The Fig. 5.8 shows the comparison between the parallel and sequential simulations, with a different number of targets for each thread. The simulation time increases with μ: the shorter simulations are realized when $\mu \to 1^+$ and the time increases until $\mu = 3$. This feature is present in the sequential and parallel measured times, and is a consequence of the behavior discussed in Fig. 5.7. We can anticipate that our parallel routine does not have the perfect scale on the number of processors (namely, the simulation in k processors demands (sequential time)/k time units to finish). We analyzed the effect of taking longer parallel searches, with each thread detecting q targets ($q > 1$). This will decrease the computational time as we compare with the sequential results, but the division in 1, 10, 100 or 1000 targets for each thread does not interfere substantially in the duration of the search.

The difference on the average number of steps realized between two targets in the dense and sparse arrangements will also affect the resulting speedup of the simulations.

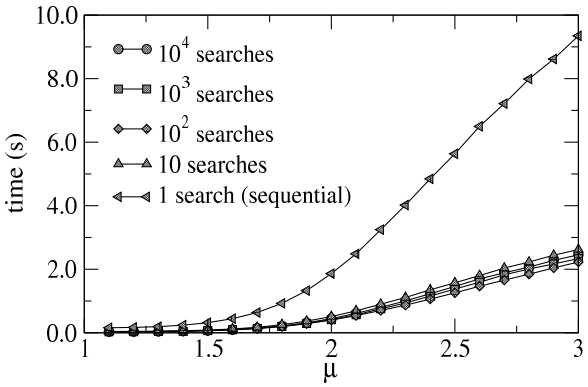

Figure 5.8 Simulation time (in seconds) required to search for 10^4 targets in a low density configuration ($l_t = 100r_v$) for n independent searches. The slowest simulation was performed by a single thread ($n = 1$) looking for all the targets, that is, the sequential limit. For $n = 10$, each searcher will detect 10^3 targets independently. For $n = 10^2$ ($n = 10^4$) each thread detects 10^2 (10) targets concurrently. Finally, we have the maximal parallelization, with 10^4 threads detecting one target. The simulation was realized in a CPU with 16 cores (32 threads).

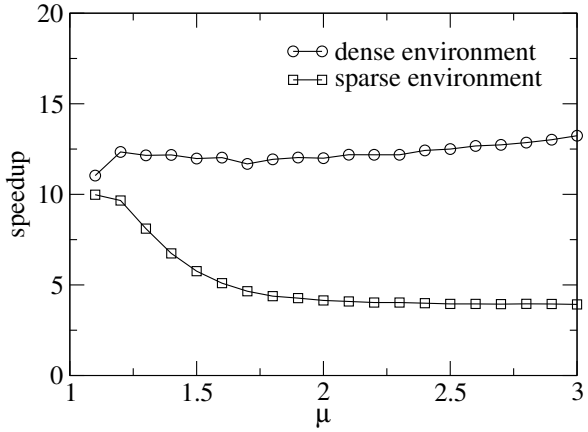

Figure 5.9 The speedup (ratio between sequential and parallel time cost) for dense and sparse configurations is not constant. For a high density environment, the resulting speedup is almost constant. However, the performance does not shows the same improvement in the sparse configuration. The difference is due to the overhead created when the threads are realizing a lot of steps - then acessing the targets list a lot of times - simultaneously.

The speedup is the ratio between the sequential and the parallel elapsed times. In a quick analysis, this speedup should not depend on the particular strategy adopted by the searcher, being approximately constant in all of them. However, Fig. 5.9 shows that this is verified only for a dense targets distribution. In this situation, the parallel search is around 10 times faster than the sequential one for the range of strategies analyzed. The computational gains in the sparse arrangement are higher when μ is very close to the ballistic limit (speedup is about 10), but quickly decrease when $\mu > 1.2$, becoming constant (speedup now is about 4) when $\mu > 1.7$. This is a side effect of the higher flux of access to the targets list realized in the sparse configuration: each thread that demands a thousand of jumps to detect a target will try to read the list a thousand of times. As the amount of steps is lower in the dense scenario, the number of times the list will be read by the thread is lower, allowing the approximately constant speedup.

5.4 Conclusion

The method that we presented to address the parallelization of the random search is efficient in reducing the computational efforts required in the sequential simulations. We analyzed the interaction between a particular search strategy and the spatial pattern of their detected targets, identifying the distribution that generates the pattern. The study that characterizes the region composed by the detected targets is a new contribution in the random search literature. The implementation of the virtual environment is very simple and does not increase substantially the computational cost of the algorithm. In the literature there is an alternative method for generating parallel random walks using *Brownian bridges* [95, 96]. However, the method currently does not work for super-diffusive models and requires the assignment of an initial and a final coordinate for each parallel random walker, while in our method we specify a region.

The parallel architecture chosen (OPENMP) has a pre-existent solution to the problem of several threads accessing the same data, and is of easy implementation. Even though an extra work is done by the parallel code (regarding the construction of the virtual environment) we obtained a better performance in the parallel version of our code. The cases where the computational gains were lower can be justified by the fact that several threads try to access the same vector structure at the same time concurrently, causing a thread overhead.

We recognize that this method works only for a homogeneous targets distribution. When the resources are fragmented in the space, the identification of a pattern of detected targets is more difficult. The results present in this chapter were recently published in the journal *Computer Physics Communications* [97].

Chapter 6

Composite Search Strategies in Patchy Landscapes

In this chapter we address the use of a composite search strategy instead of Lévy flights in patchy landscapes. The motivation of this work is the dual foraging strategy of *Drosophila* larvae: in the same species, a fraction of its population forages using a composite search strategy and the remaining part performs what looks like Lévy flights. We modeled the problem numerically and then show that the best search strategy depends on the availability of resources. Finally, we tracked the motion of the two types of larvae experimentally, and compare the results with the literature.

6.1 Introduction

What is the best strategy to explore resources that are fragmented in the landscape? This is a very important question in animal foraging, and a vast literature of empirical, mathematical and numerical works has been dedicated to this problem. As an example, we have the marginal value theorem [34] that determines how long a forager should stay inside a patch. There is also a series of works that discusses the necessity of a dual search strategy that behaves differently in regions with or without food. Models with a dual strategy are known as *composite random searches* [43]. In composite search models, the organism is assumed to switch between two (or more) simple random walk models [55]. The trajectory pattern of a composite random walk can be mistaken as a Lévy flight because it shows clusters of small steps interspersed with less frequent longer steps. The

trigger that switches between the search modes can be internal to the organism [98] or an external stimulus from the environment [43].

In a composite search, the behavior prior to the detection of a food patch is more dispersive, with a low turn frequency and long steps. Once inside the patch, the behavior changes to a more tortuous movement with short step lengths. This mechanism is supposed to increase the search efficiency, and has been documented in species like beetles [99], honeybees [100], fishes [101] and birds [102]. This composite strategy relies on the animal's ability to differentiate the two regions as inside or outside food patches. Lévy flights, on the other side, do not account for the distinction between regions with or without food, and can be used in animals that show a weak interaction with the environment.

The *Drosophila melagonaster* larvae show a dual foraging behavior in nature: a fraction of their population will change its movement pattern inside food patches (a composite search) while the other part does not seem to change the current search strategy in the presence of food [103]. The proportion of individuals in each group changes according to the density of resources, and it is assumed that this mechanism benefits the species as a whole, as an adaptation to the unpredictable distribution of resources in nature.

In this chapter we will study two random search models. One based in a composite search strategy and another as a classical Lévy flight. Using two distinct search environments, we want to characterize when the advantage of using one or another search strategy leads to a more drastic increase in the search efficiency. The numerical results will then be compared with the predictions from the literature that describes the *Drosophila* foraging.

Furthermore, we were able to test both foraging behaviors in an experimental work. It is a very difficult task to capture the movements of a free-ranging animal in the laboratory, but the *Drosophila* larvae are very small and simple organisms that are appropriate for this type of study. In the experiments, we tracked the larvae in an environment free from most external stimuli, capturing the foraging process in details. The experimental data are then compared to the current literature on *Drosophila* foraging.

6.1.1 Foraging polymorphism in *Drosophila* larvae

The genetic diversity observed inside a population can produce differences in the morphology and behavior of the individuals [104]. When two or more distinct phenotypes co-exist in the same population of a species (living in the same habitat at the same time), this species is said to be *polymorphic*. The polymorphism can be observed, for example, in the different foraging strategies adopted inside the same population [103]. For example,

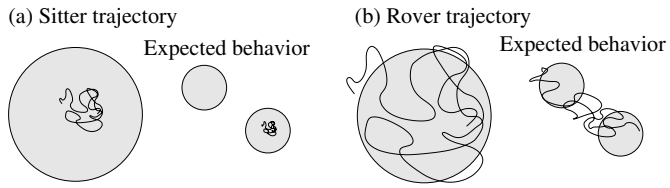

Figure 6.1 Expected differences in the behavior of *Drosophila* larvae. When more patches are available, the rover strain is likely to have an advantage in the localization of new resources.

the *bluegill sunfish* has part of its population adapted to forage at the open water and another part adapted to explore the litoral zone, with both morphological and behavioral adaptations [105]. Another dual behavior is observed in *Caenorhabditis elegans* worms foraging in fragmented food distributions [106]. One variant is the *solitary* strain, where the individuals forage alone and over the entire surface of the food patch. Animals belonging to the *gregarious* strain will forage in groups and explore only the border of the food patch.

It is known that the *Drosophila melanogaster* larvae exhibit two distinct behaviors concerning the foraging task, labeled as *rover* and *sitter* [103]. It was observed that when foraging in a yeast paste, the sitter larvae covered shorter distances when compared to rovers. Then, it was predicted that in the presence of fragmented food resources, a sitter larva tends to remain in the visited food patch for a long time, while a rover larva will easily leave the current patch and then explore other patches. Their behavior changes only in the presence of food patches, and both strains have the same behavior in the absence of food. In Fig. 6.1 we illustrate the hypothesized locomotion pattern of each larva in the presence of food patches.

Studies indicate that the presence of foraging polymorphism in *Drosophila* larvae is maintained by density-dependent selection [107]. Basically, density-dependent selection processes are observed when the population growth rate is regulated by the density of population. It can be a positive density-dependent process, when the increase in the population density implies in (a higher) population growth. On the other hand, negative density-dependent selection will curtail the population growth when the density increases. In *Drosophila* larvae scenario, the rover variant is selected in a high density rearing condition, whereas the sitter phenotype is selected under low density conditions [107]. In a high density rearing condition, the longer foraging path covered by rovers will benefit them. The food density decreases locally and the discovery of new patches will allow access to high quality food. When the rearing condition is in a low density population, it is not necessary to move away from the food patch because there is plenty of food. In this situation, sitter larvae are at more advantage over the rovers as they spend less energy executing a shorter foraging path.

Foraging also depends on food density and the internal state of the animal. When foraging in low density patches, both rover and sitter larvae cover shorter distances [108]. If the larvae are starved before allowed to feed in patch, both strains will also cover smaller distances. This plastic behavior showed by the *Drosophila* larvae illustrates their adaptation in different environments and has also been documented in adult flies [109, 110]. When subjected to malnutrition during the larval stage, the sitter exploratory behavior in adult *Drosophila melanogaster* increases [111]. Also, the survival of the sitter strain is higher than the rover, indicating that the sitter strategy is advantageous under food deprivation [112].

The food acquisition in rovers and sitters is also distinct: rovers will have a lower food intake and higher glucose absorption than sitters [113]. As a consequence, rover larvae show a higher survival rate when foraging in low quality food patches. This feature explains the result that rovers are selected when reared in high larval density [107].

In the following, we will focus on the search performance of rover and sitter larvae employing two random search models in a patchy environment. Using two different densities of targets, we want to characterize the situations where both models produce similar fitness, and when one strategy will be drastically better than the other. This simple comparison between the models can help us to understand the environmental pressure for the selection of one strain or another.

6.2 Simulations of Composite Random Searches

Now, we investigate the impacts of using a composite random search strategy with distinct behaviors inside and outside of the patches. Essentially, we will change the power law exponent of the step lengths distribution based on the searcher current localization. The foraging strategy of rovers and sitters will be modeled according to the description in the literature [107]. In our model, we will ignore the ability of the larvae to smell the food locations (chemotaxis [114, 115]), since in our heuristics the interaction between the searcher and possible clues is not included.

6.2.1 The composite random search model

The targets are clustered inside of the patches of fixed radii R, and the average distance between targets l_t is kept constant so the density is the same in all patches. The forager is able to detect a change in its neighborhood when it enters the patch or leaves it, and do not has any clues about the patch localization until it is detected.

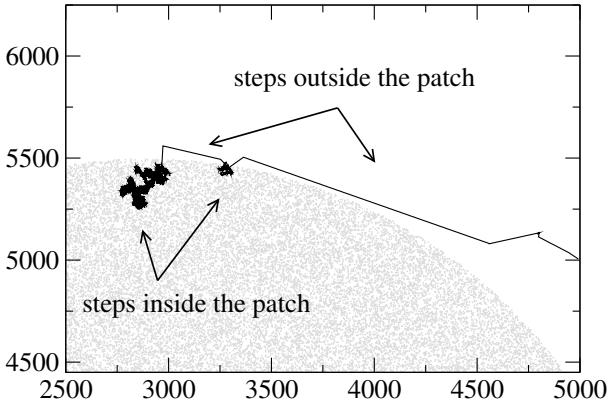

Figure 6.2 Illustration of the composite search strategy detecting targets in the border of the patch. The patch has a radius $R = 2500$ (environment with size $M = 10^4$) and the average distance between targets is $l_t = 10$. The forager walks with $\mu_{out} = 1.1$ outside the patch and changes it to $\mu_{in} = 3.0$ once it is inside the patch.

The walk is governed by the usual truncated power law steps distribution, but now the current position of the searcher is analyzed in order to choose the strategy μ. During the step, we check if its coordinates are inside a patch every fraction of covered distance ρ ($\rho = 10$). If the forager leaves the patch during the step, the step is truncated when the position outside is detected and a new step will be chosen with the appropriate new exponent. The same process is applied when a step towards a patch occurs.

The step lengths distribution is given by the following expression, where r_v is the visual radius of the searcher and $\ell_{max} = M$ is the size of the (squared) environment:

$$P(\ell) = \frac{(\mu-1)}{r_v^{1-\mu} - \ell_{max}^{1-\mu}} \times \begin{cases} \ell^{-\mu}, \text{ if } r_v < \ell < \ell_{max}, \\ 0, \text{ otherwise.} \end{cases} \tag{6.1}$$

Now the μ exponent ($1.1 \leq \mu \leq 3$) changes according to the current coordinates of the searcher (f_x, f_y):

$$\mu = \begin{cases} \mu_{in} & \text{if } (f_x, f_y) \text{ is inside a patch,} \\ \mu_{out} & \text{if } (f_x, f_y) \text{ is outside the patches.} \end{cases} \tag{6.2}$$

Figure 6.2 shows a stretch of a composite random searcher changing its step lengths when it enters (and leaves) a patch. In our simulations we changed both μ_{in} and μ_{out} values in the interval $1.1 \leq \mu \leq 3$.

We expect that the sitter strain of *Drosophila* larvae behave like a composite random searcher: once inside a food patch, it is supposed to remain inside it for a long period, thus executing small displacements. On the other side, rovers are more prone to leave the patch and detect another food resource. In Fig. 6.3 we show an illustration of the simulated strategies during the search. In the literature it is usual to employ a combination of $\mu = 1.1$ and $\mu = 3.0$ in the composite random search model, and we kept

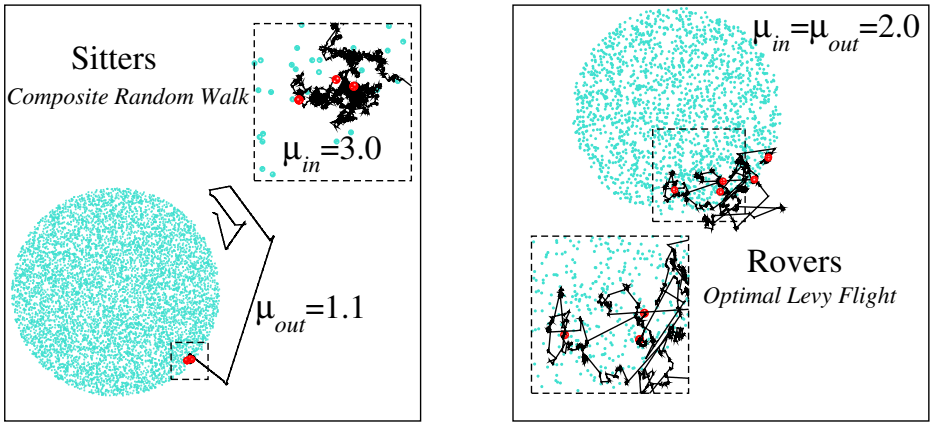

Figure 6.3 We assigned a composite search model to the sitter strain, with $\mu = 1.1$ as the strategy outside the patch and $\mu = 3.0$ inside it. For the rovers, we considered a single optimal search strategy $\mu = 2.0$ that is fixed during the search. Notice that the area explored by the rover is much larger than the one inspected by the sitter.

these parameters to compare the results with the ones already published. Surely our approach to the problem is very simple, but our aim is to explore numerically when one type of strategy is better than the other.

6.3 Numerical Results

We are interested in the numerical increase of the search efficiency when the forager is able to change its strategy based on its location. In the efficiency computation, we ignore the fact that the random searcher from the composite walk has information about the environment. We have in Fig. 6.4 the search efficiency for the composite random search and the single strategy search for both dense 6.4(a) and sparse 6.4(b) patch distributions. A composite strategy where the step lengths are adapted according to the differences in the environment has a better performance (for $\mu_{out} = 1.1$ and $\mu_{in} = 3.0$) when compared to the single strategy model. For the dense configuration in Fig. 6.4(a) the use of a fixed strategy outside the patches $\mu_{out} = 1.1$ resulted in an increase of the values of η for all μ_{in} strategies considered. The fact that we do not have exactly the same η values for $\mu = 1.1$ is a consequence of the additional truncations that are performed when entering and leaving a patch, that are not present in the single strategy search. However, the advantages of the composite search are not verified in the efficiency of the sparse case in Fig. 6.4(b) for strategies with $\mu_{in} \leq 2$. This is a consequence of the difficulty of remaining inside a (sparse) patch when long steps are made in the border, and then the efficiency decreases. The frequency of long steps for $\mu > 1.1$ is smaller than

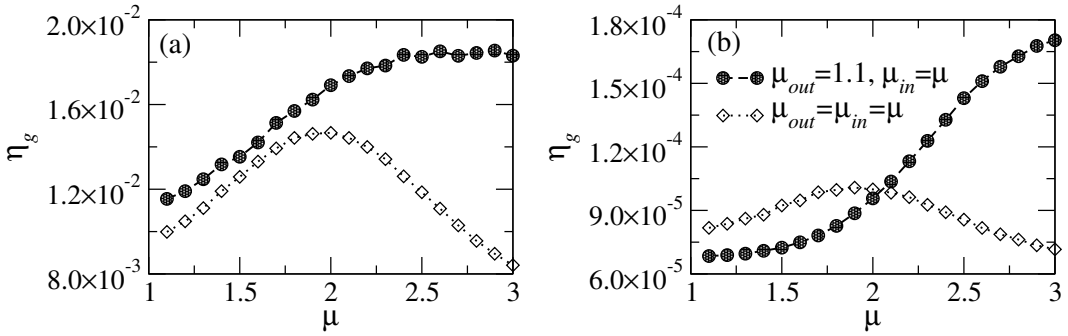

Figure 6.4 The search efficiency η as a function of the exponent μ for a configuration with dense (a) and sparse (b) patches. The composite strategy is represented by the dark circles, with a ballistic strategy ($\mu_{out} = 1.1$) fixed outside patches and μ_{in} ranging in the interval $1.1 \leq \mu_{in} \leq 3.0$ inside the fragments. The search with a single strategy (white diamonds) is maximized in $\mu \approx 2$ ([52]), but the composite strategy $\mu_{out} = 1.1$ and $\mu_{in} = 3.0$ achieves the highest efficiency in both (a) and (b). In the simulations $N_p = 10$ patches with radius $R = 0.1M$ were available in the environment. The dense configuration (a) corresponds to $l_t = 10$ and the sparse (b) $l_t = 100$. Each curve was averaged over 2.5×10^3 simulations run.

for $\mu = 1.1$, so this becomes a problem when the searcher is just in the border of the patch and leaves it without detections. However, when the inside strategy approaches the Brownian limit, the advantage of using $\mu_{out} = 1.1$ outside the patches is considerable, and then the efficiency for the composite strategy increases. This behavior is not observed in Fig. 6.4(a) because the high density of targets difficults the process of leaving the patch continuously (see [52] for a discussion about this effect).

According to the literature, the rover strain will show an enhanced foraging performance when the local density of resources is low [103]. In this situation, they can explore the nearby region and eventually discover new feeding areas, increasing their performance. However, in our simulations the overall patch density in the environment is kept constant. Thus, leaving one low density patch to find another equally bad is not an advantage for the rovers. In fact, in the efficiency curve Fig. 6.4(b) (low density patches) the composite strategy achieves almost twice the efficiency of a Lévy flight with $\mu = 2$. In this scenario the sitter strain is more efficient, since its search efforts are not wasted looking for a better resource that does not exist. The locomotion cost in *Drosophila* larvae is very high [116], and in situations where the overall food has a low density it is more efficient for the individuals to save energy avoiding unnecessary displacements.

When the overall patch density is high, both models achieve similar efficiency values. In Fig. 6.4(a) the composite model is 20% more efficient than the corresponding $\mu = 2$ optimal Lévy flight. In this situation the higher diffusivity of rovers is not penalized because more rich patches are available in the environment. Similarly, the sitters also show a high efficiency remaining inside a high quality patch. Thus, in this environment

composed of high density patches, we expect that both strains have a similar foraging fitness.

6.4 The Experimental Results

The experiments were realized with the two strains of *Drosophila melanogaster* larvae that show differences in the foraging strategy: the rovers and the sitters. The experimental methodology is described in Appendix B. Here we will present the results obtained tracking groups of 10 larvae in a patchy landscape. The food recipe used is a solution of 5ml of apple juice, 0.342g of sucrose, 0.8g of agar and 195ml of distilled H_2O.

First, we have to stress that our methodology is slightly different than the common one in the literature. Thus, we are not reproducing the same experiments, but investigating new properties. To our knowledge, so far the behavior of rovers and sitters was not studied in a composite landscape, with regions with and without food. The works addressed only the behavior inside food patches and, extrapolating the results, make predictions about the behavior in a multi-patch environment [103]. Further, the same food has been used in all the experiments (a yeast mixture), and the maximal duration of the observation was 6 minutes. Also, only the individual behavior of the larvae was analyzed, that is, only one animal was tracked per experiment in the previous works. In our experiments, we used landscapes with well-delimited circular patches with different sizes. The food is a mixture of sucrose and apple juice. Moreover, we have tracked 10 larvae simultaneously for 90 minutes, obtaining a collective long-term behavior (but only the first 50 minutes of the data are shown in the analysis).

We have measured the traveled distance of each larva inside and outside the food patches. In the following, the environment has only one big patch placed in the center of the tracking arena. According to the literature, we expected to see very distinct results, with the traveled distance of rovers much longer than the one covered by sitters. In Fig. 6.5(a) we show the trajectories of 10 rover larvae after 50 minutes of foraging activity. Each larva was initially placed in the center of the patch. We analyzed the trajectories using a software designed to this type of tracking experiment [117]. To compare with the literature data, we made two analysis: one that lasts only 6 minutes and a longer observation of 50 minutes. In Fig. 6.5(b) we show the covered distance inside and outside the food patch for the first 6 minutes and for 50 minutes. In the first 6 minutes, the rover larvae spent the time foraging mostly inside the patch, but eventually they left the food (as can be seen in the trajectories). Their foraging path inside the patch measured an average of 120mm (after 6 minutes), and 1000mm (50 minutes). The covered distance

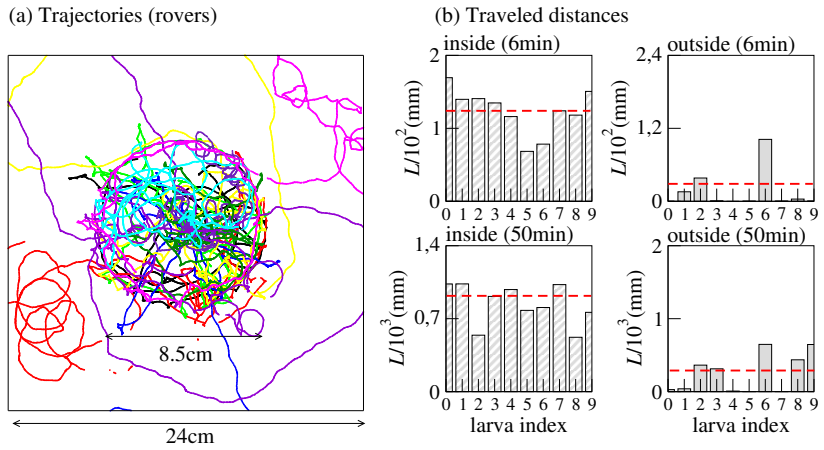

Figure 6.5 The trajectories of 10 larvae from the rover strain that were initially at the center of the patch are shown for 50 minutes of foraging in (a). The size of the patch and the arena are indicated. The covered distance inside and outside the patch were measured for the first 6 minutes and also for 50 minutes. The average distance inside the patch is larger than outside, indicating that most of the larvae remained in the food region.

outside the patch was consistently smaller: 30mm for 6 minutes of foraging and 300mm after 50 minutes.

The sitter behavior, shown in Fig. 6.6, is quite similar to the one of rovers in Fig. 6.5. Again, the traveled distance inside the patches is larger than the one outside them. However, according to the literature one expects that the distance covered by the sitters should be consistently smaller than the one covered by the rovers. And even though the traveled distance inside the patches is slightly larger for the rovers (1000mm after 50 minutes against 800mm for sitters), unexpectedly the sitters moved more outside the patch than the rovers (after 50 minutes they covered a distance almost twice the one by rovers). For the first 6 minutes, the rovers covered an average of 120mm while inside the patch, and the sitters only 90mm. In the literature, however, the differences in the traveled distance are much more drastic for the foraging in 6 minutes: in [103] the rovers covered on average 160mm and the sitters an average of 60mm. The food used in their experiments was a yeast solution, different of the sucrose and apple juice compound. Also, their foraging experiment was inside a petri dish (8.5cm diameter) filled with food, and our tracking was inside a squared arena with sides measuring 24cm.

When more than one food patch was available to the larvae, we expected that more rovers were able to travel between the food during the experiment. First because the patches are smaller and the larvae left it more frequently. Second because they can smell the other food source when reaching the border of the current patch. To our knowledge, the behavior of rovers and sitters in a controlled multi-patch environment was not studied so far. In the following experiment, 5 larvae were placed in the center of each patch. In

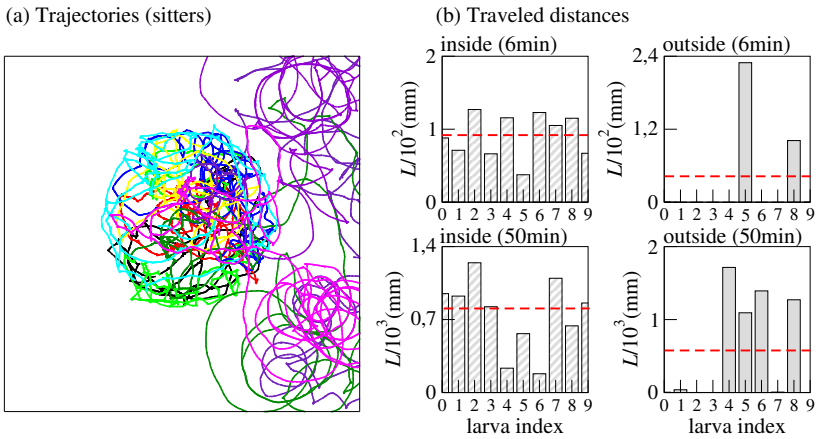

Figure 6.6 Same as Fig. 6.5 but for the sitter strain. The same scale for the distances was used for both strain to facilitate the comparison.

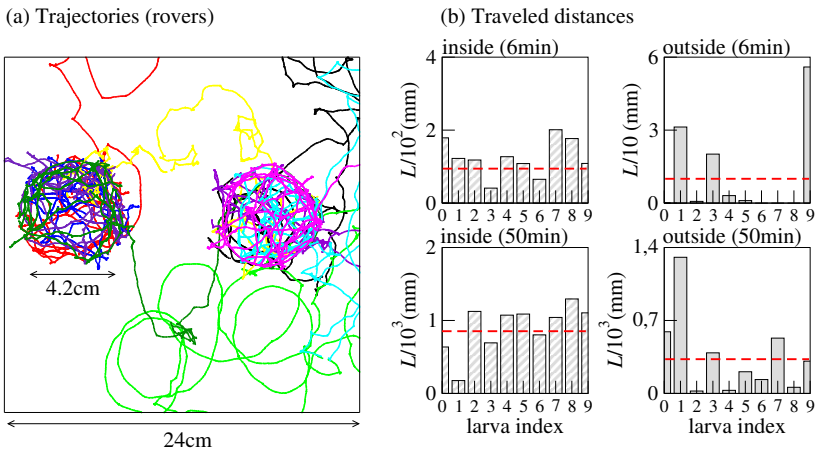

Figure 6.7 Trajectories of 10 larvae from the rover strain in a landscape with two food patches (a). In the beginning of the experiment, 5 larvae were placed in the center of each patch. The size of each patch is indicated in the figure. The covered distances (b) were separately measured inside and outside the patches, and again the proportion of time spent inside the food is larger than in the outside.

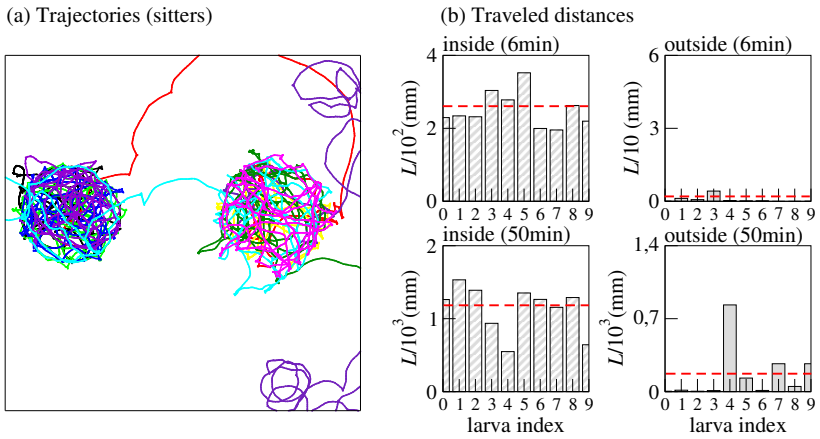

Figure 6.8 Same as Fig. 6.7 but now for the sitter strain. The covered distance inside the patch is substantially larger for the sitters, and through the analysis of the trajectories one can verify that the number of larvae that left the food is smaller than in Fig. 6.7.

the trajectories of the rover larvae in Fig. 6.7(a) 6 out of 10 larvae left the current patch, and 2 of them changed one patch for the other. The visual identification of the food patches is easy since the trajectories inside them are much more dense than outside. The traveled distances in Fig. 6.7(b) show that the larvae remained mostly inside the patches. Similarly to Fig. 6.5(b), the average covered distance inside the patches was 120mm and 10mm outside for the first 6 minutes of foraging. After 50 minutes, the covered distances were 900mm inside and 350mm outside the food patches.

In Fig. 6.8(a) the trajectories of the sitter larvae are visually more constrained inside the patches than the rovers in Fig. 6.7(a). Only 4 out of 10 larvae left the patch during the experiment, and 2 of them changed one patch to another. The sitter larvae remained more inside the patches than the rovers: in Fig. 6.8(b) we see that the average traveled distance inside the patch for 6 minutes of observation was 250mm (compare with 120mm traveled by the rovers). The sitter larvae barely left the patch before 6 minutes of activity. After 50 minutes of experiment, the average covered distance inside the patch was 1200mm for the sitter strain (900mm for rovers). Outside the patches the traveled distance was 130mm after 50 minutes (350mm for rovers).

Even though the predictions from the literature were not verified in the experiment with a single patch, the rover and sitter expected behavior was observed in the multi-patch scenario. In the case of two patches, the sitter larvae remained mostly inside the food area, and covered a longer path inside the food than the rovers. Although the literature expects longer foraging paths for rovers, here we have a more complex situation where the rovers can explore the environment and detect other food patches. In fact, more rovers left the initial region in order to look for another patch during the observations.

In this situation the higher diffusivity of the rover strain was verified, for a collective behavior (closer to the behavior in nature) and for a long observation.

6.5 Conclusion

In this work we developed a numerical model to study composite search strategies in patchy landscapes and compare it to Lévy flights. The motivation for conducting this study was the dual foraging behavior documented for *Drosophila melanogaster* larvae, where part of the population forages using a composite search strategy and the remaining group employs what looks like a Lévy flight strategy.

Our numerical results are in agreement with the predictions of the rover and sitter behavior from the literature. Even though the Lévy flight strategy does not outperforms the efficiency of the composite strategy, in this model we do not account for the benefits of visiting more than one food source, that are very important for *Drosophila* larvae to avoid the over-exploitation of a food resource. Also, the patches are homogeneous and have the same targets density. A more realistic model, that is being developed, should adopt a heterogeneous distribution of patches.

In the experimental work, we have tried to quantify the behavioral differences between rovers and sitters measuring their foraging paths. We designed patchy landscapes to study the behavior inside and outside the food, something new in the current literature. In the configurations that we tested, the behavioral differences between rovers and sitters are not as clear as in the literature. We conducted more experiments with anosmic larvae to analyze the behavior in the absence of cues and tested environments with more patches. Currently, we are still analyzing the data.

Chapter 7

Observable Representation and the Random Search

In this chapter we present the random search as a stochastic process. The transition matrix **R** of the search process stores the information concerning the locations visited by the random walker. Then, we applied the observable representation method to infer the geometrical properties of the search environment, using the eigenvectors from **R**. Finally, we show that the slowest eigenvectors from **R** preserve the information about the distribution of targets.

7.1 Introduction

The observable representation (OR) is a method that allows the visual inference of relevant statistical properties of a stochastic process [118, 119]. The OR is an embedding of a space, usually discrete, in $\mathbb{R}^n$, for some n. The space is the set of states of a Markov process, from which one can write a transition matrix with the transition probabilities between the states of the process. Then, through the analysis of the slowest eigenvectors of that matrix, one can recover information about the dynamics of the process.

The method is successfully applied in stochastic processes that satisfy the detailed balance condition [118]. However, it was shown that even systems that do not satisfy the condition are suitable to the method as well [120]. The observable representation has been used in the study of non-equilibrium phase transitions [121, 122], spin glasses [123], coarse-graining models [118] and in the reconstruction of coordinate spaces [119].

The dynamics of the process manifests in the OR: states that are dynamically close in the process (e.g., they are in the same phase) will be geometrically close in the

OR. The OR method can split the different phases that a system experiences with a proportional quantity of points in each phase. For a simple random walk process, the OR can reconstruct the geometry of the environment, as shown in [118].

Our main purpose is to apply the OR analysis to a random search problem and extract, besides the search environment geometrical configuration, the targets spatial distribution. First, we will illustrate the method in a simple random walk process with fixed step lengths. Then, we will apply the same ideas to a random search problem, with a given geometry to the targets distribution.

7.2 Stochastic Processes and the OR

In many problems that concern modeling the behavior of some system, the information available is not sufficient to determine how the system behaves, or the exact description is not possible because the behavior is too complicated. For situations like these, a *probabilistic model* is very useful.

In a loose sense, we say that a *stochastic process* is simply a probability process, that is, any process whose evolution can be analyzed successfully in terms of probability. In other words, a time-dependent random variable $X(t)$ assuming the values $x_1, x_2, x_3, \ldots$, etc at times $t_1, t_2, t_3, \ldots$ will have a joint probability density,

$$p(x_1, t_1; x_2, t_2; x_3, t_3; \ldots) \tag{7.1}$$

that completely describes the stochastic process. In this section we will discuss a very important class of stochastic processes, known as the *Markov processes*. Then, a collection of mathematical properties from stochastic matrices is introduced to support the formulation of the observable representation.

7.2.1 Markov processes

Let $X(t)$ be a stochastic process whose states are taken from a countable space $\mathscr{X}$ with $t \in \mathscr{T}$. Then, the set $(X(t_1), X(t_2), \cdots, X(t_N))$ will have a known distribution for $t_1, t_2, \cdots, t_N \in \mathscr{T}$. If $t_i \in \mathbb{Z}$ ($t_i \in \mathbb{R}$) for all i we say that the process is discrete (continuous) in time.

The stochastic process $X(t)$ is a *Markov process* if for $t_1 < t_2 < \cdots < t_N < t_{N+1}$ the distribution of $(X(t_1),X(t_2),\cdots,X(t_N),X(t_{N+1})$ is such that:

$$P(X(t_{N+1}) = x_{n+1}|X(t_1) = x_1, X(t_2) = x_2, \cdots, X(t_N) = x_N) = \\ P(X(t_{N+1}) = x_{n+1}|X(t_N) = x_N). \quad (7.2)$$

For a Markov process, the state of the process at a given time has all the information about the previous evolution that is necessary to predict the future behavior. In a simplified notation, we can write:

$$P(x_{N+1}|x_1, x_2, \cdots, x_N) = P(x_{N+1}|x_N). \quad (7.3)$$

An alternative definition of a Markov process can be stated in the following way. The stochastic process $X(t)$ is a Markov process if for $t_1 < t_2 < \cdots < t_p < \cdots < t_m$, conditional on $X(t_p) = x_p$ (the present state), $(X(t_1),X(t_2),\ldots,X(t_{p-1}))$ (the past states) and $(X(t_{p+1}),X(t_{p+2}),\ldots,X(t_m))$ (the future) are independent.

We call a Markov process *time homogeneous* if the following expression

$$P(X(t+\tau) = x_k|X(t) = x_j) \quad (7.4)$$

does not depend upon t. If every state on $\mathscr{X}$ can be reached from every other state, the Markov process is said to be *irreducible*.

7.2.2 The transition matrix

For a discrete time Markov process, the probability that a state x makes a transition to a state y,

$$p(y,x) = P(X(t+1) = y|X(t) = x) \quad (7.5)$$

is called the *transition probability*. These transition probabilities are the matrix elements from the transition matrix $\mathbf{R}$, and the convention in this work is

$$\sum_{x\in\mathscr{X}} p(x,y) = 1 \quad y \in \mathscr{X}, \quad (7.6)$$

that is, the summation over a column of $\mathbf{R}$ is fixed. As we will see, the transition matrix $\mathbf{R}$ is a *stochastic matrix*. Stochastic matrices have important properties that are summarized in Appendix C.

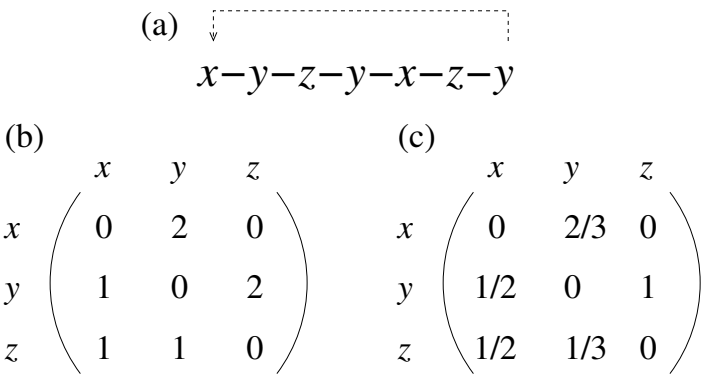

Figure 7.1 A simple process in (a) is written as a transition matrix **R** in (b). Every time a state x goes to y in the following time step a transition is recorded adding +1 to the $R(y,x)$ element. The process is repeated to all the remaining transitions, and the last state (here y) is connected to the first one (x) in the end. Finally, we normalize the **R** columns to make it a stochastic matrix (c).

The construction of a transition matrix

Suppose we have a Markov process, where the states are $x,y,z \in \mathscr{X}$. The system goes through these states in this particular order:

$$x \to y \to z \to y \to x \to z \to y. \tag{7.7}$$

We will record these transitions in a matrix, *the transition matrix* **R**, in the following way:

- If n is the size of the states space $\mathscr{X}$, then the **R** matrix has dimension $n \times n$ and is initialized with zeros.
- When the state x makes a transition to a state y ($x \to y$) we add +1 to the matrix element $R(y,x)$. This step is repeated through all the transitions in the process.
- The final state is artificially connected to the first one, so that every state goes to another one and the probability is conserved.
- To calculate the probabilities, we normalize the columns of the **R** matrix.

The process used in the construction of the matrix **R** is illustrated in Fig. 7.1 and further details can be consulted on [124]. The connection between the last and the first state is important to preserve the stochasticity of **R**.

7.2.3 The observable representation

In a stochastic process, we have an underlying coordinate space that is subjected to the dynamical rules. For example, in a Brownian motion process the walker interacts with the coordinate space through the dynamical transition rules. The main idea behind the observable representation is to recover the information about the underlying coordinate

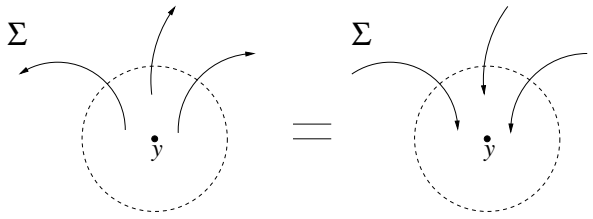

Figure 7.2 The detailed balance condition. The total flow entering the state y should be the same total flow that exits y in the detailed balance.

space using the "slowest" eigenvectors of the transition matrix. In this section we will introduce the *detailed balance* condition, and show that when a transition matrix $\mathbf{R}$ satisfies this requirement it will be possible to write $\mathbf{R}$ in terms of a symmetric real matrix and then establish a relationship between the eigenvectors from $\mathbf{R}$ and $\mathbf{S}$ (that are orthogonal, as shown in theorem C.2.2).

Stochastic Processes and the Detailed Balance

It is possible to connect the dynamical distance of a stochastic process (in the detailed balance) with its spectral counterpart in the observable representation [118].

The detailed balance condition is the requirement that the stochastic process is in equilibrium, that is, there is a stationary eigenvector $\mathbf{p}$ such that $\mathbf{Rp} = \mathbf{p}$. We can write this condition in the following way:

$$\sum_y R_{xy} p_y - p_x = 0, \tag{7.8}$$

and since $\sum_y R_{yx} = 1$ (from the conservation of probability), we can write:

$$\sum_y \left(R_{xy} p_y - R_{yx} p_x \right) = 0. \tag{7.9}$$

In the equation above, the sum must vanish for every term, so we can write the detailed balance condition as:

$$R_{xy} p_y = R_{yx} p_x. \tag{7.10}$$

This result can be stated as an equilibrium of the probability flow: the total flow that enters a particular state y is the same total flow that exits it, as outlined in Fig. 7.2.

One important property of a transition matrix that satisfies the detailed balance condition is the existence of a symmetric matrix $\mathbf{S}$ given by $\mathbf{S} = \boldsymbol{\sigma}^{-\frac{1}{2}} \mathbf{R} \boldsymbol{\sigma}^{\frac{1}{2}}$, where $\boldsymbol{\sigma}$ is a diagonal matrix with the eigenvalues λ_i from $\mathbf{R}$. This can be verified in the following

way [125, 126]:

$$\left(\boldsymbol{\sigma}^{-\frac{1}{2}}\mathbf{R}\boldsymbol{\sigma}^{\frac{1}{2}}\right)_{xy} = \left(\sigma_x^{-\frac{1}{2}} R_{xy}\sigma_y\sigma_y^{-\frac{1}{2}}\right) \tag{7.11}$$

$$= \left(\sigma_x^{-\frac{1}{2}}\sigma_x R_{yx}\sigma_y^{-\frac{1}{2}}\right) \tag{7.12}$$

$$= \left(\sigma_x^{\frac{1}{2}} R_{yx}\sigma_y^{-\frac{1}{2}}\right) = \left[\left(\boldsymbol{\sigma}^{-\frac{1}{2}}\mathbf{R}\boldsymbol{\sigma}^{\frac{1}{2}}\right)^{\top}\right]_{xy}, \tag{7.13}$$

where in the right hand side from the first to the second line the detailed balance condition was used. A real symmetric matrix $\mathbf{S}$ can be decomposed in the form:

$$\mathbf{S} = \mathbf{Q}\boldsymbol{\Lambda}\mathbf{Q}^{\top}, \tag{7.14}$$

where the columns of $\mathbf{Q}$ are the orthogonal and normalized eigenvectors of $\mathbf{S}$ and Λ is a diagonal matrix whose entries are the eigenvalues of $\mathbf{S}$. Besides this, all the entries of $\mathbf{Q}$ are real and $\mathbf{Q}^{\top} = \mathbf{Q}^{-1}$.

We will show now that $\mathbf{R}$ and its symmetric counterpart $\mathbf{S}$ share the same eigenvalues, preserving a close relationship between its eigenvectors. The connection between the matrix elements from $\mathbf{R}$ and $\mathbf{S}$ can be written as:

$$S_{xy} = \frac{1}{\sqrt{p_0(x)}} R_{xy}\sqrt{p_0(y)}, \tag{7.15}$$

with the eigenvalue equation for $\mathbf{S}$ given by:

$$\sum_y S_{xy}\psi(y) = \lambda\psi(x). \tag{7.16}$$

Using the expression from Eq. (7.15), we will write the eigenvalue equation using $\mathbf{R}$:

$$\sum_y \frac{1}{\sqrt{p_0(x)}} R_{xy}\sqrt{p_0(y)}\psi(y) = \lambda\psi(x) \Longrightarrow \sum_y R_{xy}\sqrt{p_0(y)}\psi(y) = \lambda\psi(x)\sqrt{p_0(x)}, \tag{7.17}$$

and the right eigenvectors from $\mathbf{R}$ are given by:

$$p(x) = \sqrt{p_0(x)}\psi(x). \tag{7.18}$$

Similarly, the left eigenvectors are given by:

$$A(x) = \frac{1}{\sqrt{p_0(x)}}\psi(x). \tag{7.19}$$

The observable representation

Now we will define the construction of the observable representation of a given Markov process that satisfies the detailed balance condition with a transition matrix **R**.

Since **R** satisfies the detailed balance, its eigenvalues are real and can be written as $1 = \lambda_0 > |\lambda_1| \geq |\lambda_2| \cdots \geq 0$. Associated to $\lambda_0 = 1$ there is a strictly stationary distribution p_0, which is a right eigenvector of **R** (since $\mathbf{R}p_0 = p_0$). The left eigenvector is $A_0 \equiv 1$ and $A_0 = A_0\mathbf{R}$ expresses the conservation of probability. In the detailed balance, **R** can be written using a symmetric matrix **S**. Consider $\sigma \equiv \text{diag}(\sqrt{p_0})$ a diagonal matrix with the squared root of the stationary distribution in its diagonal, then $\mathbf{S} = \sigma^{-1}\mathbf{R}\sigma$. Say that ψ_α are the eigenvectors from **S**. Then, for a particular eigenvalue λ_α we can relate the eigenvectors from **R** and **S** using:

$$p_\alpha(x) = \sqrt{p_0(x)}\psi_\alpha(x) \qquad \text{and} \qquad A_\alpha(x) = \psi_\alpha(x)/\sqrt{p_0(x)}. \tag{7.20}$$

The m-dimensional observable representation is the collection of points:

$$\mathscr{A} \equiv \{\mathbf{A} \in \mathbb{R}^m | \mathbf{A} = (A_1(x), A_2(x), \ldots, A_m(x)) \quad \text{for} \quad x \in \mathbf{X}\}. \tag{7.21}$$

To visualize the above relation, write the eigenvectors as row vectors. Take the first m eigenvectors one atop the other. The set of points of the observable representation are the columns obtained in the following array:

$$\begin{array}{cc} & \text{Points of the observable representation } (\downarrow) \\ & \begin{array}{ccccc} \mathbf{A}(x_1) & \mathbf{A}(x_2) & \mathbf{A}(x_3) & \ldots & \mathbf{A}(x_N) \\ \downarrow & \downarrow & \downarrow & & \downarrow \end{array} \\ \text{Eigenvectors } (\rightarrow) & \begin{array}{ccccc} A_1(x_1) & A_1(x_2) & A_1(x_3) & \cdots & A_1(x_N) \\ A_2(x_1) & A_2(x_2) & A_2(x_3) & \cdots & A_2(x_N) \\ \cdots & & & & \\ \cdots \quad \vdots & \vdots & \vdots & \vdots & \vdots \\ \cdots & & & & \\ A_m(x_1) & A_m(x_2) & A_m(x_3) & \cdots & A_m(x_N). \end{array} \end{array}$$

Distances in the OR

Let $p_x(u,t)$ be the probability distribution (at time t) of a system that was previously at $x \in \mathscr{X}$ for $t = 0$. We can write this as

$$p_x(u,t) = R^t_{ux}, \tag{7.22}$$

where R^t_{ux} is the probability of a transition from a state x to a state u after t steps. We can define a kind of distance between the states x and y as the variation of the distance between $p_x(u,t)$ and $p_y(u,t)$:

$$D(x,y;t) \equiv \sum_u \left| \frac{p_x(u,t) - p_y(u,t)}{\sqrt{p_0(u)}} \right|, \tag{7.23}$$

where $p_0(u)$ corresponds to the u component of the stationary eigenvector. The summation is realized over all the possible states u. The distance presented in Eq. (7.23) measures how far the trajectories that started at x and y will be at a given time t. We will write $\mathbf{R}$ in terms of the symmetric matrix $\mathbf{S}$ and the diagonal matrix $\boldsymbol{\sigma}$:

$$\begin{aligned} \frac{p_x(u,t)}{\sqrt{p_0(u)}} &= \frac{1}{\sqrt{p_0(u)}} R^t_{ux} \\ &= \frac{1}{\sqrt{p_0(u)}} (\boldsymbol{\sigma} \mathbf{S}^t \boldsymbol{\sigma}^{-1})_{ux}. \end{aligned} \tag{7.24}$$

From the definition of the symmetric matrix $\mathbf{S}$ we write its spectral decomposition:

$$(\boldsymbol{\sigma} \mathbf{S}^t \boldsymbol{\sigma}^{-1})_{ux} = \sum_a \sqrt{p_0(u)} \lambda_a \psi_a(u) \psi^\top(x) \frac{1}{\sqrt{p_0(x)}}. \tag{7.25}$$

Using the relationship between the eigenvectors from $\mathbf{R}$ and $\mathbf{S}$, Eq. (7.19) we have:

$$\begin{aligned} \frac{p_x(u,t)}{\sqrt{p_0(u)}} &= \sum_a \lambda_a^t \psi_a(u) \frac{\psi_a^\dagger(x)}{\sqrt{p_0(x)}} \\ &= \sum_a \lambda_a^t \psi_a(u) A_a(x). \end{aligned} \tag{7.26}$$

The definition for the distance presented in Eq. (7.23) is similar to the $L1$ norm, that is, the sum of the absolute value of the vector components. It is a well known result from the functional analysis that the $L1$ norm exceeds the $L2$ norm, that is given by the square root of the sum of the squared absolute values. Using the inequality between the norms

and the expression in Eq. (7.26), we can write:

$$D(x,y;t) \geq \sqrt{\sum_u \left(\frac{p_x(u,t) - p_y(u,t)}{\sqrt{p_0(u)}} \right)^2}$$
$$= \sqrt{\sum_u \left| \sum_a \psi_a(u) \lambda_a^t [A_a(x) - A_a(y)] \right|^2}. \tag{7.27}$$

The summation over a in Eq. (7.27) can be written in a more convenient way, using the fact that the eigenvectors $\psi_a(x)$ are orthonormal. Using the orthonormality, we can simplify the following expression,

$$\sqrt{\sum_u \sum_a \sum_b \psi_a(u) \psi_b^\dagger(u) c_a c_b^\dagger} = \sqrt{\sum_u \sum_a \sum_b \psi_a(u) \psi_b^\dagger(u) c_a c_b^\dagger \delta_{a,b}} \tag{7.28}$$
$$= \sqrt{\sum_a |c_a|^2}. \tag{7.29}$$

It follows that:

$$D(x,y;t) \geq \sqrt{\sum_a |\lambda_a|^{2t} |A_a(x) - A_a(y)|^2}. \tag{7.30}$$

We will truncate the sum at the mth component: since the magnitude of the eigenvalues are decreasing monotonically (with its index) the inequality is preserved,

$$\frac{D(x,y;t)}{|\lambda_m|^t} \geq \sqrt{\sum_{a=1}^{m} |A_a(x) - A_a(y)|^2}. \tag{7.31}$$

The right hand side of Eq. 7.31 is the distance in the observable representation space. The inequality implies that two points that are dynamically close, that is, there are transitions between them during the stochastic process, will be close in the observable representation too.

7.3 The OR for the Random Walk

The random walk can be recorded as the set of positions $\{(x_1,y_1),(x_2,y_2),\cdots,(x_n,y_n)\}$ that were visited by the walker. Consider each position as a state $\{X_1,X_2,\cdots,X_n\}$ with $X_1 = (x_1,y_1)$, etc., and $\mathscr{X}$ the set with all the possible states of the random walk process. The random walk is realized in a rectangular grid of size $P \times Q$, so the total number of possible states for the walker is PQ. The construction of the transition matrix for the

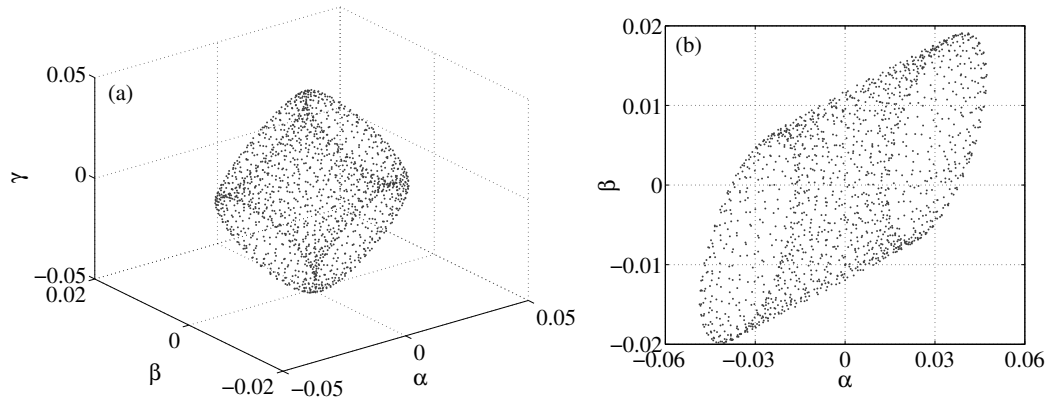

Figure 7.3 The resulting OR for the simple random walk with fixed step lengths $\ell = 2$ in a regular grid with size 40×40. Since we applied periodic boundary conditions, we recover the original space as a torus-like structure in the 3d OR (a). The walker realized 2×10^5 isotropic steps during the process, visiting all the 1.6×10^3 available positions in the grid. In (b), the 2d projection of the observable representation using the first two eigenvectors. Here we simplified the notation using $\alpha = \mathrm{Re}(V_2)$, $\beta = \mathrm{Im}(V_3)$ and $\gamma = \mathrm{Re}(V_4)$ (see text).

random walk is made according to the method discussed in Fig. 7.1, connecting the last state to the first one.

The normalization of the transition matrix **R** is made in its columns, so **R** is a stochastic matrix. Even though it is not an equilibrium process, we can still construct its observable representation using the first eigenvectors of the **R** matrix. We will use the second, third and fourth slowest eigenvectors to illustrate a random walk in a regular grid with periodic boundary conditions. The first eigenvector is constant and is not used in the representation. We expect that the OR will preserve the geometrical properties of the space where the walk tooks place.

First we analyzed the walk in a squared grid with dimension 40×40. The connection in the borders, consequence of the periodic boundary conditions, provides the torus pattern exhibited in Fig. 7.3(a), the three-dimensional (3d) OR. The choice of the real or imaginary parts of the first three eigenvectors (V_2, V_3, V_4) is made in a convenient way for each particular case and we abbreviate them α, β and γ. The dynamics of the system is mapped in its observable representation: states that are close in the process will be close in the OR. Fig. 7.3(b) shows the two-dimensional (2d) OR using the first two eigenvectors: in this situation one needs the 3d plot to clearly identify the spatial structure.

The set of eigenvectors used in Fig. 7.3 is analyzed in Fig. 7.4. The particular choices of real and imaginary part of the eigenvectors are made to access the torus pattern. The imaginary part of V_2 is the null vector, so we take $\mathrm{Re}(V_2)$ as the first

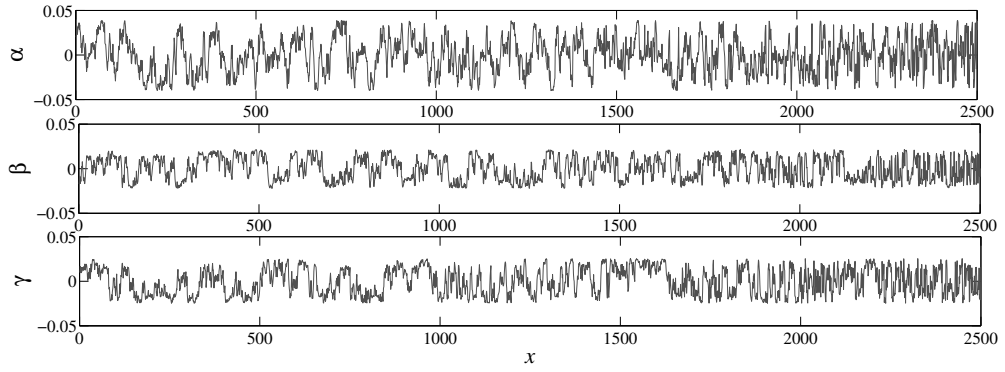

Figure 7.4 The corresponding eigenvectors used in Fig. 7.3. In this situation we took a convenient combination of real and imaginary parts of each eigenvector to visualize the torus structure.

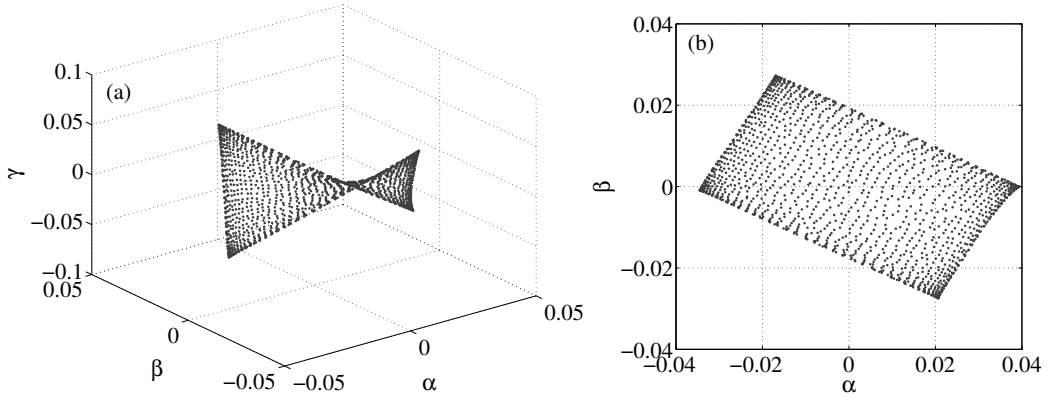

Figure 7.5 The same as Fig. 7.3 but for reflexive boundary conditions in the environment. In (a) the 3d observable representation has a rectangular shape, that is highlighted in the 2d figure in (b).

eigenvector. We have $\mathrm{Re}(V_3(x)) = \mathrm{Re}(V_4(x))$ for every $x \in \mathscr{X}$, so we choose $\mathrm{Im}(V_3)$ to get linear independence in the construction of the OR. The set $\{\mathrm{Re}(V_2), \mathrm{Im}(V_3), \mathrm{Re}(V_4)\}$ is particular to this example; we may choose a different arrangement for the OR of another process. The interpretation of a single eigenvector does not leads to insights about the spatial pattern. The combination of them is the source of information for the observable representation.

When we apply reflexive boundary conditions in the same squared space, the corresponding 3d OR, exhibited in Fig. 7.5(a) has a rectangular shape. Now the 2d representation in Fig. 7.5(b) is sufficient to identify the pattern in this process. The final picture is clearly influenced by the rules of the dynamical process.

We also investigate the impact in using different dimensions for the grid, decreasing one of the dimensions and increasing the other one. We used periodic boundary conditions in this set of simulations, and now the environment has dimension $P \times Q$. Specifically, we

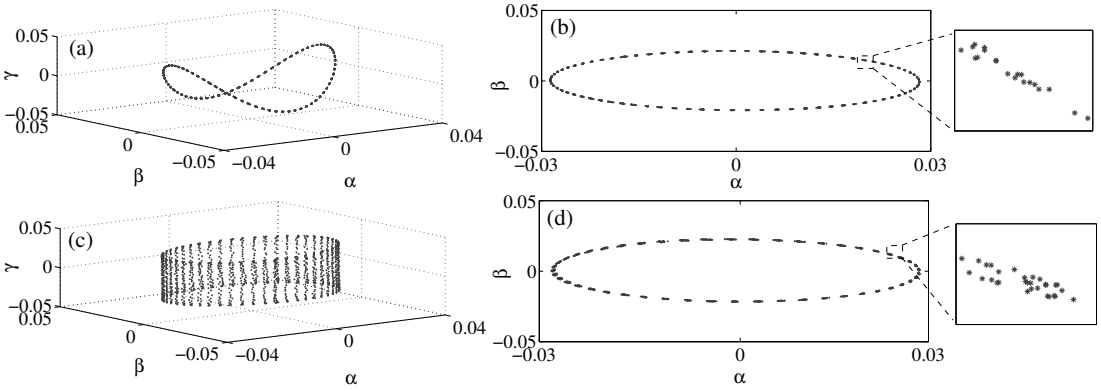

Figure 7.6 Observable representation for a random walk in rectangular environments. For a rectangle 80×20 the 3d OR in (a) has a structure similar to a ring with clusters of points equally spaced. In (b) the 2d representation with a zoom in one of the 80 cluster regions reveals that inside each cluster there are 20 points. For a rectangular configuration closer to a square, we analyzed a grid of length 50×30 in (c). The resulting OR approaches the torus pattern of Fig. 7.3. Inside each of its 50 clusters we can identify 30 points (d).

want to study the transition between the 1d random walk OR (a ring in the OR [119]) and the 2d random walk (a torus). In Fig. 7.6 we have both the 3d and 2d OR for two configurations of grid sizes: 80×20 (a),(b) and 50×30 (c),(d). For the 80×20 grid the 3d observable representation has a structure similar to the ring of the one-dimension random walk, except for the clusters of points that compose the ring (instead of a single point in the 1d case). In a close inspection, we can identify that inside each cluster the same amount of points is observed. For example, for the pattern in Fig. 7.6(a) we have 80 clusters with 20 points inside (recall that the environment's dimension is 80×20). Similarly, in Fig. 7.6(b) we have 50 clusters with 30 points inside (the dimension now is 50×30). The information about the spatial dimensions is stored in the OR.

To investigate further the role of the OR in the organization of the number of points in a given number of clusters, we mapped the OR points with its corresponding dynamical states. The larger dimension (lets say P) will dictate the number of clusters, and the smaller will correspond to the number of points inside each cluster (Q). The states inside a given cluster will share the same x coordinate, varying the y coordinate. For a simple configuration, in Fig. 7.7 we have 20 clusters of 10 points each. The clusters are ordered in the states x coordinates: $\{(1,y),(2,y),\cdots,(19,y),(20,y)\}$.

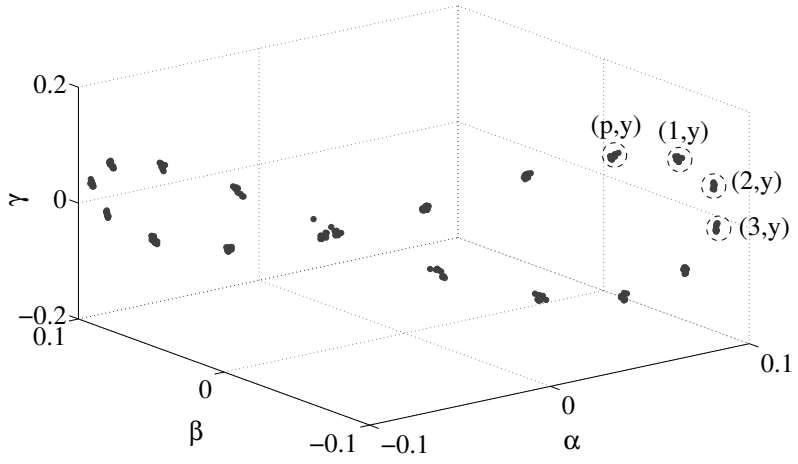

Figure 7.7 The OR for a random walk in a 20×10 grid. Inside each one of the 20 clusters, we found 10 points that represent the states of the process that share the same abscissa coordinate, as indicated in the figure. The clusters are ordered: the one with coordinates (P, y) $(y \in [1, 10])$ is followed by the one with $(1, y)$, followed by $(2, y)$ and so on. The states that are closer in the dynamics are mapped into close positions in the OR.

7.4 The OR and the Random Search

For the random search we consider a random walker with a fixed step length and uniform turning angle distribution, wandering in a grid of size $M \times M$. The grid is discrete, with m^2 cells of size M/m, and the walker has its initial and final positions matching the grid vertices. This is made using a small translation in the final coordinate of a jump, selecting the nearest vertex of the grid, ensuring that the position (x, y) is an integer number[1].

The targets are non-destructible, allowing the forager to visit the same target during the search process. At each step, the forager will perform a jump of length ℓ in a given direction θ that is uniformly distributed in $(0, 2\pi]$. Along the jump, the forager will constantly look for targets that are within a distance r_v (its visual radius) of its current position. If a target is detected, then the jump will be truncated and the final position of the step will be the coordinate of the target. Otherwise, the step will be completed in a vertex of the grid, with the final adjustment of coordinates. It is important to fix $\ell > r_v$, so the forager leaves the detectable region when a target is found. This process is illustrated in Fig. 7.8, where a stretch of an ordinary trajectory realized by the forager is exhibited. The walk is finished when a given amount of targets Q is found.

[1] We require that the positions are integers to decrease the size of the states space (this space comprises all the possible coordinates visited during the process). A series of mathematical operations will be realized using the transition matrix, and its size must be small enough to allow the computations.

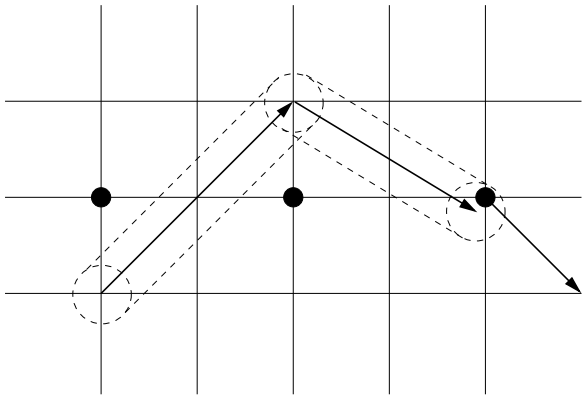

Figure 7.8 The search dynamics. The detectable targets have to be inside the visual radius r_v of the forager. The thick lines that have an arrow indicating its direction are the jumps. The dashed lines are a visual guide to the detectable region.

To investigate the impact of targets in the observable representation, we applied the random search rules discussed above in environments with a fixed targets distribution. The first environment is constructed with 9 targets, according to the distribution presented in Fig. 7.9(b). The coordinates of the targets are fixed in (21,29), (25,29), (29,29), (21,25), (25,25), (29,25), (21,21), (25,21) and (29,21). The searcher has a visual radius fixed in $r_v = 3$, so when it is in the vicinity (within a distance smaller than 3) of one target, it will detect it. The step sizes are fixed in $\ell = 4$, so that the searcher leaves the neighborhood of the current target after it detects it. The targets are indestructible, and can be detected several times during the search process.

The final OR for the random search preserves the same geometry of the original targets distribution. The points corresponding to the targets are the ones in the outside region of the (now distorted) torus in Fig. 7.9(a). For a given target, two points are assigned in the OR: one corresponding to the target's coordinate and another containing all the positions that can reach the target in a single jump. In fact, let (x_t, y_t) be the targets coordinate. For every position (x, y) such that $\sqrt{(x-x_t)^2+(y-y_t)^2} < r_v$ the next step will be the target detection. Then, all the points that satisfy this condition (for $r_v = 3$ there is a total of 24 points) will be mapped in the same position in the OR.

Looking at the 3d OR in Fig. 7.9(a), we can retrieve some information concerning the dynamics of the process. The distinction between the points that are the attractors to the targets and the regular points is clear: they are expelled from the interior of the torus. Also, there is no distinction between the positions that will reach the target in a single jump: their dynamical meaning is the same, and will occupy the same position in the OR. In Fig. 7.9(c) we have the 2d projection, preserving the same distance between targets showed in Fig. 7.9(b).

Now we have the same number of targets of the previous configuration, but with a slightly different distribution in Fig. 7.10. The coordinates of the targets now are (25,25), (20,20), (30,20), (30,30), (20,30) for the inside square and (5,5), (45,5), (5,45) and

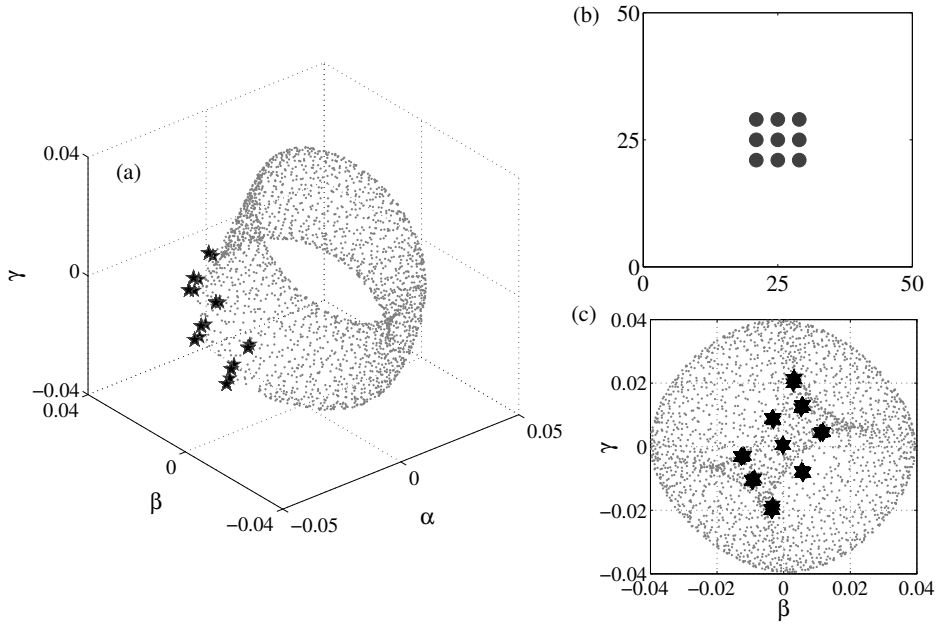

Figure 7.9 The resulting 3d observable representation (a) for the targets distribution showed in (b) and its 2d projection (c). The external points were marked with stars to help the visualization of the targets position in the OR. The targets are the points outside the torus in (a), and follow the same geometry as shown in (b).

(45,45) in the external square in Fig. 7.10(b). The 3d OR, in Fig. 7.9(a) shows the targets following the same structure but in two different regions. We used labels to connect the states to the environment, and their distribution is the same. The 2d projection, in Fig. 7.9(c) exhibits the distinction between the inner and outside squares in the OR.

7.5 Conclusion

In this chapter we used spectral tools to characterize the random search. Using the observable representation method, we first studied how the dynamical rules of a simple isotropic random walk influence the states space. We showed that the boundary conditions used in the random walk will determine the structure of the OR: periodic boundary conditions result in a torus states space and reflexive conditions lead to a rectangular OR.

Then, we studied how the one-dimensional random walk (a ring in the OR) transitions into a torus in the two dimensional problem. We considered rectangular spaces with dimension $P \times Q$, with $P > Q$ and showed that in the OR the pattern is a ring composed of P clusters with Q points inside each one. Further, there is an ordering in the coordinates of the OR: the points in a given cluster are $\{(p,1),(p,2),\ldots,(p,q)\}$. The organization of

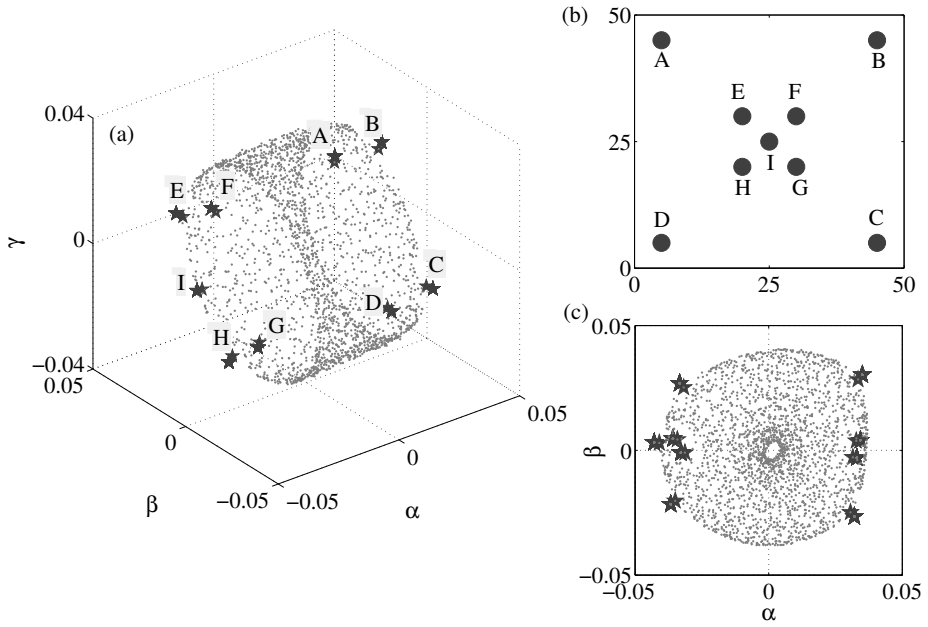

Figure 7.10 Same as Fig. 7.9 but with a different targets distribution. In (a) and (b) the targets have labels to highlight the same spatial distribution.

the information in the OR is very efficient, even for a simple random walk process we can extract the details of the system using the method.

Finally, we applied the method in a random search process. Our goal was to extract the geometry of the targets distribution in the OR. We successfully recovered the targets locations through the projections. For the two different geometries that we tested, we were able to identify the targets as the points expelled from the original torus. Also, the points preserved their distance in the OR. The original pattern of the targets distribution (a square arrangement) is perfectly recovered in the OR.

Chapter 8

A Statistical Mechanics Model for Species Evolution

In this chapter we address an evolutionary model (the Tangled Nature model) using statistical mechanics and thermodynamics tools. Our analysis studies the formation of stable configurations, and highlights the importance of cooperative interactions in the evolutionary process. We also explored the features of the interaction network, showing that a system with only weak interactions between its individuals does not survive. Further, increasing the number of connections will lead to a more instable pattern, less robust. We analyze the model using a set of thermodynamics quantities that fully characterize the states of the system, a difficult task in evolutionary models. Finally, we apply simulated annealing techniques that enhance the exploration of the genotype state, increasing the mutation rate.

8.1 Introduction

The evolution process is usually studied in two different time scales: *microevolution*, regarding the changes observed in the individual level, and emergent *macroevolution*, patterns observed at large time scales. At the individual level, the interactions between species, the resources available from the environment and the occasional mutations of the genetic code control microevolution [127]. Regarding macroevolution, we have data from fossil records showing the extinction patterns and diversification of species [128]. The connection between the macroevolution pattern and the microevolution is not totally understood. The fossil records do not support a smooth and gradual transition between

the species over time, something that would be expected by the natural selection rules in the individual scale [129–131].

According to the fossil records, the evolution is not steady, in the sense that the creation and annihilation of species is not stable over time. The data support the hypothesis that the process is characterized by bursts of high evolutionary activity followed by metastable configurations [132, 133]. This intermittent behavior is known as *punctuated equilibria* [134], where the punctuation corresponds to high activity phases followed by periods of stasis. The natural selection operating in the microevolution scale was supposed to generate only gradual transitions of species in the fossil records, and not the complex punctuated pattern observed. However, one does not need a very complex set of rules in a system to produce punctuated equilibria behavior: systems with self-organized criticality [135] can generate emergent punctuated patterns using simple rules [136, 137].

Statistical mechanics models are often concerned about systems with a very large number of interacting individuals. For example, the description of an emergent pattern through a set of rules governing its individual units has been very successful in spin glasses, a problem that has a great deal of applications [138]. The resemblance between the macroevolution pattern and statistical mechanics problems has inspired some physicists in developing models that try to connect micro and macroevolution, using simplified approaches. The Bak and Sneppen model [139] is very popular in the literature, because it produces an emergent self-organized state with avalanches of extinctions alternating with coevolution of species, the hallmark of punctuated equilibria. The NKC model [140] introduces the idea of a dynamically evolving fitness landscape that also results in an emergent punctuated equilibria pattern. Both the NKC and the Bak-Sneppen models use a Complex Systems approach to the evolution process, and are frequently used in the construction of new models in the literature. For a review with more models, see [141] and references therein.

Evolutionary models usually are conceived specifying the possible interactions between its elements and the environment, with a set of rules defining the time evolution of the system. The distribution of these interactions can determine the properties of the future emergent behavior, like its stability and survival. The interactions can be regarded as the ones observed in food chains, describing mutualistic, antagonist and neutral relationships. The interaction network in the evolutionary context is very important, since it accounts for the coevolution of species [142]. The characterization of these networks is a very complex task due to the high number of interacting elements and the difficulty to quantify its interaction strength. Indeed, analysis of extensive food webs data have

revealed that these networks have small world properties, like high clustering, and also a power-law scaling [143].

In this work we used a known evolutionary model, the Tangled Nature (TN) model [144–146] that shows some of the interesting properties of the actual evolution process, like the punctuated equilibria behavior. The interaction network in this model also provides asymmetrical relationships, and allows the coevolution of species selecting combinations of mutualistic individuals. We studied the long term behavior of the emergent pattern when one changes the interaction network properties, comparing the results with predictions from the current literature.

Finally, characterizing the evolution process using thermodynamics tools is a challenge, since it is not an equilibrium process [147]. We propose in this work adapted thermodynamical definitions to study the behavior of the energy, entropy and temperature in quasi-stable states and how they respond to the hectic periods. Also, we apply this thermodynamical formalism to special configurations of the interaction network to compare the results. Using the thermodynamics quantities one can analyze the process quantitatively, which is definitely a step forward in the statistical mechanics models of the evolutionary problem. The key component in the maintenance of quasi-static periods is the combination of mutualistic individuals. We calculate the number of possible combinations of mutualistic pairs in the TN interaction matrix and show that the system performs an exhaustive search for pairs when it is at a hectic period. We applied simulated annealing techniques [148] to the system, in order to speed up the formation of quasi-stable periods increasing the mutation rate. We conclude that a control of the mutation rate can make a more effective exploration of the genotype space in the TN model, finding cooperative pairs with high interaction strengths faster than a constant mutation rate system.

8.2 An Introduction to the Tangled Nature Model

The Tangled Nature model [144, 145] provides a description of an evolving system that is constructed via interactions at the individual level. In what follows, we use the model rules from Ref.[145]. The rules are defined at the level of microevolution, with reproduction, mutation and annihilation being applied to individuals. This theoretical model has an emerging macroevolutionary pattern, with features similar to those of punctuated equilibrium observed in fossil records. The existence of different interactions between the individuals allows a rich dynamics, with competition, mutualism and exploitation mechanisms. According to a study of the network properties of the Tangled Nature model

[149] the interaction strength between the elements increases with time, revealing that the species become more adapted at later stages of the evolution process [149]. Also, there is an interplay between interaction strengths: they cannot be too strong, resulting in a frozen system, nor too weak, leading to chaotic behavior. This interplay between different relationships provides the intermittent behavior emerging from the model: metastable periods and reconfiguration phases. The interactions can be characterized as a dynamic fitness landscape, where the probability of a species to reproduce depends on the other species that are present [146].

The individual types are represented by binary sequences: a type x is a string $\mathbf{S}^x = (S_1^x, S_2^x, \ldots, S_L^x)$ with $S_i^x \in \{0,1\}$, for all i. The length of the string L allows 2^L different individual types, and the space that contains these representations or types is called the genotype space $\mathscr{S}$. The population of the system at a time t is $N(t)$, and each individual $\mathbf{S}^x$ will have a population of $n_x(t)$ identical copies, with $0 \leq n_x(t) \leq N(t)$. The interaction between different individuals, say $\mathbf{S}^x$ and $\mathbf{S}^y$, is obtained from the matrix elements $J(x,y)$ and $J(y,x)$. The J matrix is non-symmetric and represents a simplified network of mutualistic, antagonistic and predatory interactions. The details of the construction of J are discussed in the Appendix D; now it is sufficient to say that only a fraction θ of the elements are non-zero and are uniformly distributed in the interval $(-1,1)$. If $J(x,y) \neq 0$, then $J(y,x) \neq 0$, and if one of them is zero, the other must also be zero. There are no interactions between individuals of the same genotype, so $J(x,x) = 0$ for every x. The non-symmetric nature of J allows situations where $J(x,y) > 0$ but $J(y,x) < 0$, where one individual takes advantage of the existence of other and at the same time decreases its fitness.

The interactions provided by J are necessary to calculate the probability that a given individual $\mathbf{S}^x$ will be able to reproduce. The following function, $H(\mathbf{S}^x, t)$, determines the ability of $\mathbf{S}^x$ to reproduce:

$$H(\mathbf{S}^x, t) = \frac{1}{cN(t)} \sum_{\mathbf{S} \in \mathscr{S}} J(\mathbf{S}^x, \mathbf{S}) n(\mathbf{S}, t) - \mu N(t), \tag{8.1}$$

where the sum is realized over all the living individuals in the system, c controls the inhomogeneity of the population and μ corresponds to a measure of the carrying capacity of the environment. The quantity $H(\mathbf{S}^x, t)$ is related to the probability of producing offspring, p_{off}, in the following way:

$$p_{\text{off}}(\mathbf{S}^x, t) = \frac{\exp[H(\mathbf{S}^x, t)]}{1 + \exp[H(\mathbf{S}^x, t)]} \in [0,1]. \tag{8.2}$$

At each time step, three processes are realized to induce the evolution. First, an individual is picked from the population and is annihilated with a probability p_{kill}. Then, another individual is chosen and a reproduction attempt is made, with probability p_{off}. If the last step was successful, two copies of the individual will be created, and the original one will be annihilated. Then, with probability p_{mut} per gene, a mutation attempt is implemented for the copies, changing S_i^x to $1-S_i^x$.

The average number of time steps necessary to kill all living individuals is $N(t)/p_{\text{kill}}$, and this is defined to be the number of time steps in one generation. The system is initialized with N_0 individuals of the same genotype. As time evolves, mutations provide a more diverse population. The system finds configurations where the interaction between the individuals is sufficiently large to maintain the co-evolution. As we will see, the combination of the principal species (the more populated ones) lasts until a mutant individual appears and breaks the actual combination.

In Fig. 8.1 we show the temporal evolution of a system with metastable periods that are separated by a reconfiguration phase. Note that for each genotype x a point is displayed on the line corresponding to that genotype if $n_x > 0$. Thus a solid line indicates that a particular genotype was abundant, but further details are not conveyed by the figure. We used a smaller genotype space than that presented in the original work ($L = 8$ instead of $L = 20$ in [145]), but this does not affect the aspects of the model on which we focus. The total population and diversity (number of distinct species) for the same temporal evolution is shown in Fig. 8.2. During the metastable periods, both quantities are fluctuating around a mean value, and decrease when a reconfiguration phase is triggered.

8.3 An Analysis of the Interaction Network

We start our investigation showing how important the organization of the interaction network is to the establishment of the quasi-static periods in the TN model. The interaction strengths between the individuals are provided by the (static) J matrix in the TN model [144]. For a pair of individuals x and y we have $J(x,y) \neq J(y,x)$, so the matrix is asymmetrical and provides distinct relationships between the individuals. Since the interactions are a very important feature of the model, we will study how the system reacts to changes in its interaction network.

First, we show that it is not possible even the survival of a system if the interactions between its elements are too weak. In Fig. 8.3 we have the representation of a particular system that endures less than 1000 generations, without the formation of quasi-static

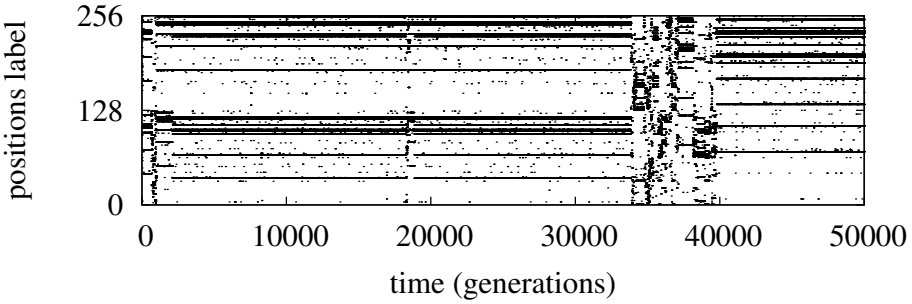

Figure 8.1 Occupation of genotype space as a function of time, given in units of generations. Here we used $L = 8$, so $2^8 = 256$ different individuals are available in the genotype space. At each time step, we place a dot to show that at least one individual with that genome is alive. When it is alive for several generations, a line is formed, with a cloud of sparse points representing the mutants frequently created. There is a visual distinction between the metastable and reconfiguration phases. The parameters here were set to $c = 0.1$, $\mu = 0.07$, $p_{\text{kill}} = 0.2$, $p_{mut} = 0.004$ and $N_0 = 100$. The simulation lasted for 5×10^4 generations.

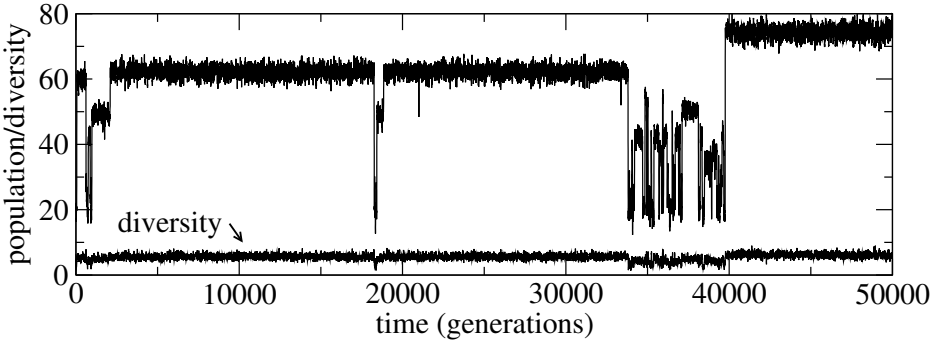

Figure 8.2 Population (total number of individuals alive) and diversity (number of different species) corresponding to the system in Fig. 8.1. Both the total population and the diversity decrease during the reconfiguration phases, and fluctuate around larger values during the metastable periods.

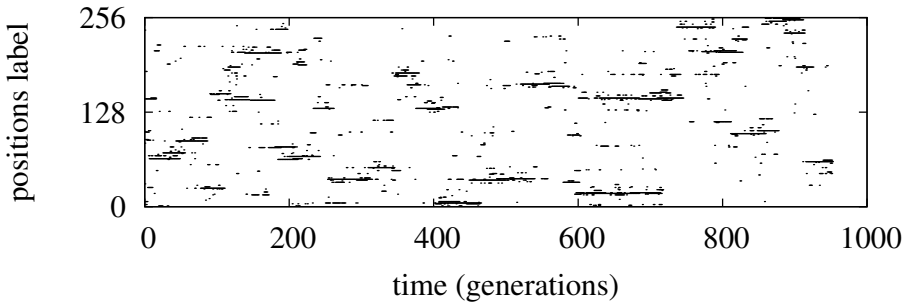

Figure 8.3 Same as Fig. 8.1 but for a network with weak interactions. The f and g vectors have its elements μ_i such that $-0.5 < \mu_i < 0.5$ for all $i = 1,\ldots,256$. The quasi-stable periods are not observed and the system vanishes just before the 1000th generation.

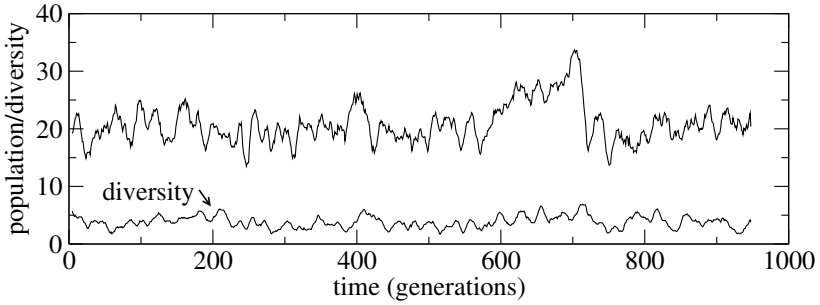

Figure 8.4 The average number of living individuals and the diversity for the same system shown in Fig. 8.3. The population is very small if compared with the data in Fig. 8.2.

periods (we repeated simulations with the same parameters but different random numbers and the results are consistent with Fig. 8.3). The set of parameters used were the same as in Fig. 8.1, but the vectors f and g used to build the matrix J (see Appendix D for more details) have its elements μ_i in the interval $-0.5 < \mu_i < 0.5$ (instead of $-1 \leq \mu_i \leq 1$ in Fig. 8.1) for $i = 1,\ldots,256$. The population in this system with weak interactions is very low, in Fig. 8.4 the number of individuals alive does not reach 40, in contrast with the higher populations in Fig. 8.2.

We also explored a system with a very high connectivity θ, where θ stands for the percentage of non-zero elements in J (see Appendix D). In this configuration $\theta = 0.75$ and each individual experiences 3 times more interactions than the one showed in Fig. 8.1. As we increase the number of links in the interaction network, the system experiences shorter stable periods, as can be seen in Fig. 8.5. The population and diversity in Fig. 8.6 now exhibit more fluctuations, because each quasi-static period has a distinct average number of individuals alive.

It is known that networks highly connected are more susceptible to instabilities and weakly interactive community networks do not persist in an ecosystem [150]. The

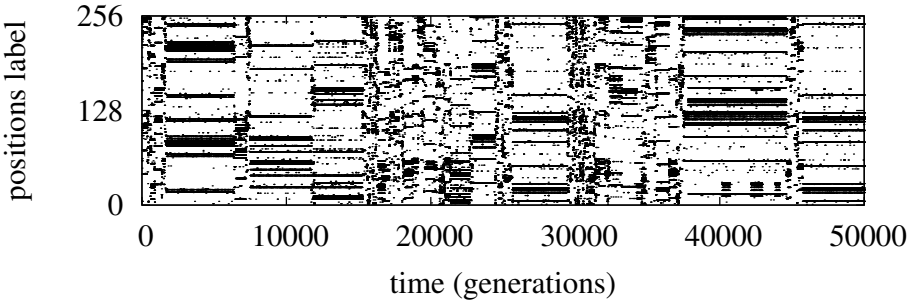

Figure 8.5 The genotype occupation for a system with a highly connected interaction network ($\theta = 0.75$). The quasi-static periods are shorter.

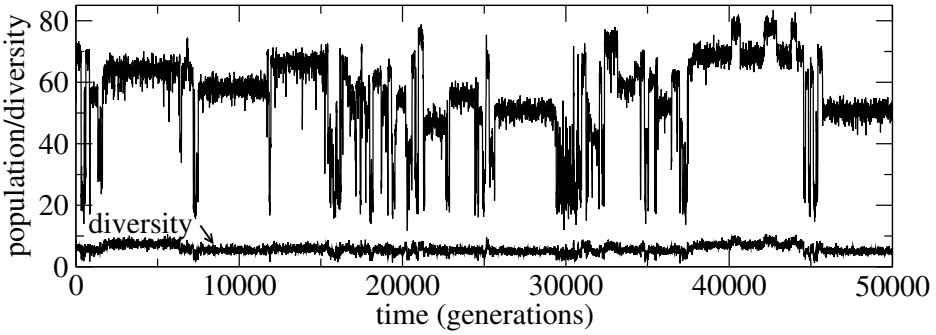

Figure 8.6 Number of individuals alive in a highly connected network (details in Fig. 8.5). The quantity fluctuates as the short quasi-static periods are quickly created and destroyed during the evolution.

distribution of strengths in the interaction network is very important to its overall stability, and the weak interactions are thought to work like dampers during disturbances in the network configuration [151, 152]. However, the presence of strong interactions is also crucial: as we showed in Fig. 8.3, the system does not experience quasi-static periods when only weak interactions are allowed. The population in Fig. 8.4 does not increase because the probability of reproduction of a given species in Eq. (8.2) depends on its overall interaction with the reamining living individuals from Eq. (8.1).

We investigate the response of the system by increasing the number of connections in the TN interaction network, and in Fig. 8.5 the lack of long quasi-stable periods is observed. When more species interact, a mutant can achieve the core of the structure more easily because more interactions are made. Once one individual is eliminated from the system, the elements connected to it will be affected as well, and when more interactions are active more individuals will be affected by the extinction of one. On the other hand, the system recovers from a hectic phase because more positive interactions are present as well. In scale free network models that are used in the description of real networks [153] one has that the distribution of links per node decays as a power-law. Individuals with several active links are not frequent in scale-free networks [154], and the robustness of this class of networks depends on the higher abundance of less connected nodes.

8.4 A Thermodynamics Approach

In this section we present an approach using thermodynamic definitions to describe the evolutionary process observed in the Tangled Nature model. We are working with a system that is out of equilibrium, so we make adaptations in our definitions.

In ordinary thermodynamics the temperature is defined as

$$\frac{1}{T} = \frac{\partial S}{\partial E}, \tag{8.3}$$

where E and S are the state functions, energy and entropy. We have to stress that our analogy of the TN model with conventional thermodynamics is flawed, because decisions for the reproduction of genome x are based on the non-homogeneous quantity $H(\mathbf{S}^x, t)$, defined in Eq. (8.1). Recall that the decision for asexual reproduction depends on p_{off}, defined in Eq. (8.2). The larger this quantity (the larger $H(\mathbf{S}^x, t)$) the greater the likelihood of reproduction. The quantity $H(\mathbf{S}^x, t)$ is not homogeneous because its first term is a ratio of populations, hence intensive (would not be doubled if system size

were doubled) while the second term is extensive. Despite the existence of what we have called a "flaw," we will show that some of these concepts can be applied to the TN model.

A state at a given moment of time is fully characterized by $\sigma \equiv \left(n_{x_1}, n_{x_2}, \ldots, n_{x_m}\right)$ with m the number of species (genomes) alive at that time and n_{ℓ_k} the number of individuals of genome ℓ_k that are alive. To emphasize the time dependence one could also write $\sigma(t)$.

The sum $\sum_y J_{xy} n_x n_y$ is a kind of global fitness. Summing over the "H_x" of all genomes, we call it the "energy," namely

$$E(\sigma) \equiv \sum_x H_x = \sum_{x,y} J_{xy} n_x n_y \,. \tag{8.4}$$

Depending on how much we know about a state, two kinds of entropy can be defined. If one knows nothing but the total population then the missing information in selecting an arbitrary individual is $I \equiv -\sum_x (n_x/N)\log(n_x/N)$. More realistic would be the logarithm of the multiplicity of a state, considering all individuals having the same genome to be identical. Calling this entropy, S, we have

$$S(\sigma) = \log \prod_x n_x! \,. \tag{8.5}$$

Since many of the population values $\{n_x\}$ will be small integers, it is better do not use Stirling's approximation here. Note that one usually introduces a constant in Eq. (8.5), the Boltzmann constant, equivalent to a choice of the base of logarithms. Since our temperature is not a priori defined anyway, it is simplest to use the natural logarithm in Eq. (8.5) and drop the constant.

Now suppose $n_x \to n_x + 1$. Then $(\Delta E)_x = \sum_y J_{xy} n_y$ and $(\Delta S)_x = \log(n_x + 1)$. There are choices in how to treat this, and we choose to evaluate the overall ΔE and ΔS by weighting the individual terms by occupation numbers. Thus

$$\langle \Delta E(\sigma) \rangle = \frac{1}{N} \sum_x n_x (\Delta E)_x = \frac{E(\sigma)}{N(\sigma)}, \tag{8.6}$$

$$\langle \Delta S(\sigma) \rangle = \frac{1}{N} \sum_x n_x \log(n_x + 1) \,. \tag{8.7}$$

By analogy with Eq. (8.3) we define the temperature of a state to be given by

$$T(\sigma) = \frac{\Delta E}{\Delta S} = \frac{E}{\sum_x n_x \log(n_x + 1)} \,. \tag{8.8}$$

Note that this expression is size dependent, i.e., T is not an intensive quantity. This feature is inherited from ΔS above, and is consistent with the reproduction decision being made on the basis of the non-homogeneous (neither intensive nor extensive) quantity $H_x = \sum_y J_{xy} n_y / cN - \mu N$. Using these quantities we can also, by analogy, define the "free energy" as $F \equiv E - TS$.

8.4.1 Thermodynamical quantities for specific configurations

We computed the energy E, entropy S, temperature T and free energy $E - TS$ according to the previous definitions. We stress one more time that the definitions are approximate and do not satisfy the requirements of classical thermodynamics of equilibrium systems.

We calculate the energy proposed in Eq. (8.4) for each generation in a simulation. As indicated, a generation consists of $N(t)/p_{\text{kill}}$ time steps, where $N(t)$ is the population at the beginning of the generation, and a time step is an attempt to annihilate, reproduce or mutate. As we pick an individual x to reproduce, we calculate $\sum_y J_{xy} n_x n_y$, that is, the energy associated with its interactions with the other living individuals. This calculation is repeated at each time step, and at the end of each generation we average these values.

Comparing Figs. 8.1 and 8.7, we note that the variation of these thermodynamic quantities is distinctly different during the hectic periods. In fact, it is possible to identify the regions where the current metastable configuration is broken, reflected in, among other criteria, lower energy values. But for all the definitions, the quantities fluctuate around a mean value during the quasi-static phases.

The thermodynamical quantities corresponding to the system with weak interactions is shown in Fig. 8.8. The numerical values for the energy (and the other variables) are very low compared to the ones of Fig. 8.7. Also, the values do not fluctuate around an average value like when a quasi-static phase is reached. This reflects the absence of stable periods in Fig. 8.3, the system does not have enough strength to develop stable configurations.

Finally, in Fig. 8.9 the higher connectivity of Fig. 8.5 reflects in more transitions for the thermodynamic quantities. The system alternates configurations with high and low energy values, and do not stabilizes for more than 10^4 generations in any of them. The higher connectivity implies in a weak system that is more vulnerable to mutants.

8.4.2 Using a "simulated annealing" strategy to speed up evolution

To understand the organization of the metastable phases, we tracked the interaction between the most populated species during such a period. The interaction is obtained

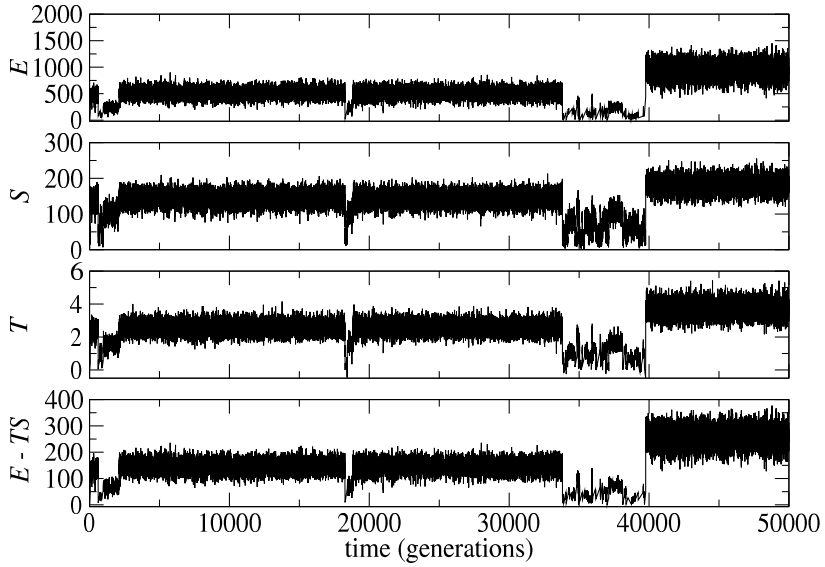

Figure 8.7 The statistical quantities defined in the text are displayed against the time for the same simulation shown in Fig. 8.1.

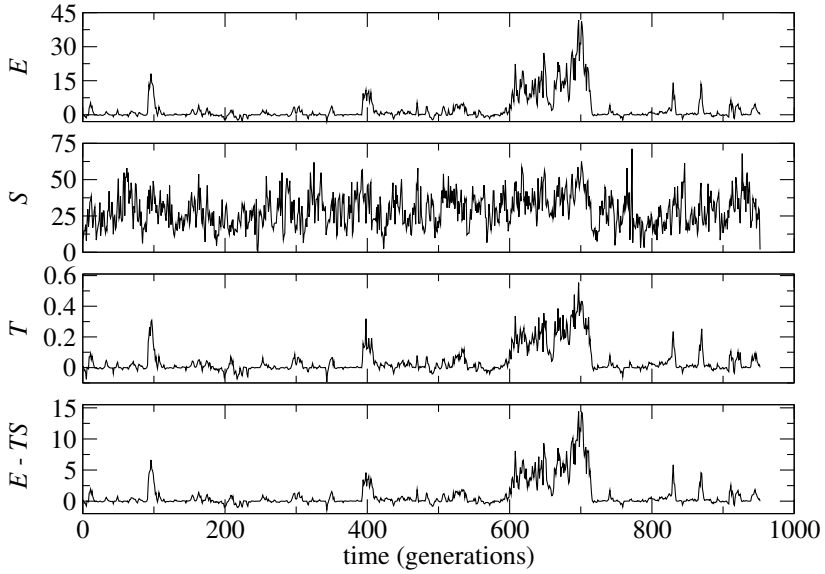

Figure 8.8 Same as Fig. 8.7 but for a weakly interacting system. The numerical values are very low, and reflect the absence of metastable configurations in Fig. 8.3.

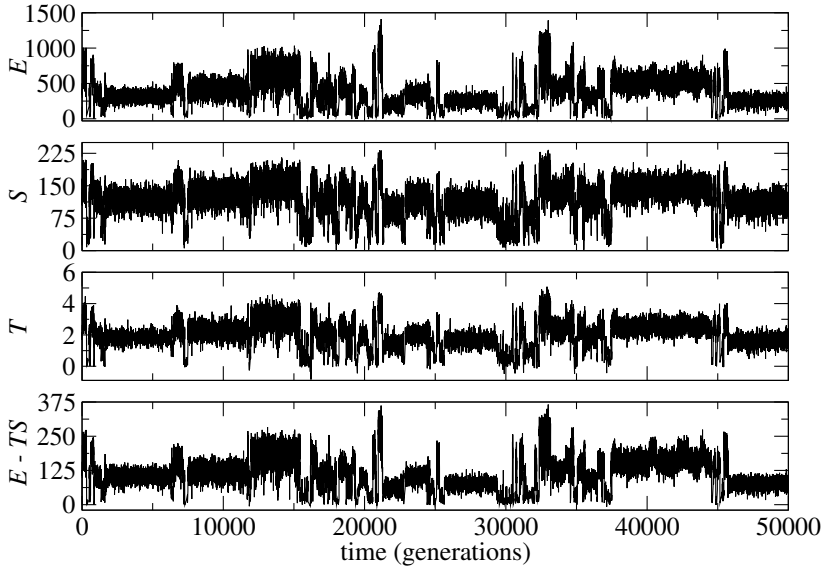

Figure 8.9 The thermodynamical quantities for the system with high connectivity. The oscillations observed in Fig. 8.5 are reproduced in the energy chart, and the transitions between hectic and quasi-static phases are clear.

from the J matrix elements (see Appendix D). As expected, the most populated species are cooperative, and the mutual interaction strength between them is high (e.g., above 0.4). A mutant can have a positive interaction with one member of the mutualistic pair and at the same time produce a negative impact on it (as in predator-prey dynamics). If such a mutation occurs, one of the principal species may be depleted (depending on the interaction strengths) and stability is lost. As a consequence of the mutations, the system then tries different solutions for the problem, and when a pair of cooperative species (with a mutual interaction above some threshold) is found, another stable period is observed.

To estimate the probabilities concerning the choice of cooperative pairs, we calculate the following quantities (the calculations are in the Appendix D):

$$p(\alpha) = \frac{\theta}{4}\left(1 + 2\alpha\log\alpha - \alpha^2\right), \tag{8.9}$$

and

$$p^{(3)}(\alpha) = \frac{3\theta^3}{16}\left\{\frac{1}{6}(1-\alpha)[1+\alpha(7+22\alpha)] + \alpha\log\alpha\Big[1+\alpha(3+\alpha)+\alpha\log\alpha\Big]\right\}. \tag{8.10}$$

Here, α is an interaction value $\alpha \in [-1,1]$ such that, for two species x and y one has $J(x,y) > \alpha$ and $J(y,x) > \alpha$. Similarly for three species x, y and z. So, $p(\alpha)$ is

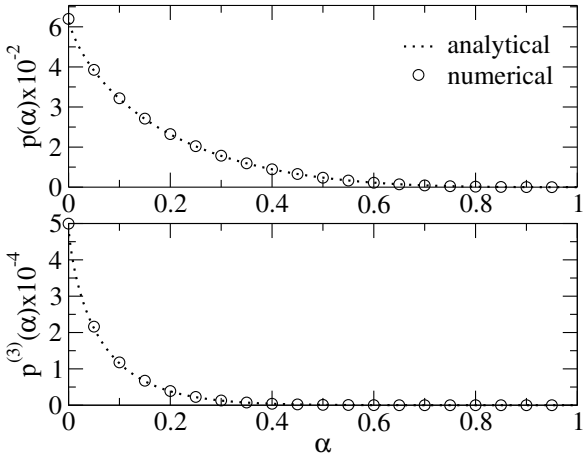

Figure 8.10 Analytical (dashed) and numerical (circles) results for the density of interactions above the α threshold.

the probability that two species have a mutual interaction larger than α, and $p^{(3)}(\alpha)$ corresponding to three species. The explicit calculations can be found in the Appendix D. In Fig. 8.10 we have the analytical and numerical curves of $p(\alpha)$ and $p^{(3)}(\alpha)$. The probabilities concerning a mutual pair with interaction above 0.9 are extremely low (even more drastic for finding a triplet satisfying this condition).

We point out that the total number of possible pairs is large (for $L = 8$ we have more than 3×10^4 different combinations for 2 species), so there are many configurations to test during the evolutionary process until finding a sufficiently good combination of cooperative species. The original TN model assumes a constant mutation rate during the time evolution [144]. A higher mutation rate can quickly produce more mutants during the evolution, and more combinations of individuals can be tested in order to find a mutualistic pair faster. Since the mutation rate is responsible for the rate of exploration in the configurations space, one can think that a higher mutation rate can scan the possible solutions faster, and the system could be "frozen" in the same configuration with a low mutation rate.

We define now a quantity that estimates the average interaction between the individuals inside a given generation. This average interaction is negative when the system is out of a stable phase, and can be used to identify the stable phases. Let $n'(t) = \frac{N(t)}{p_{\text{kill}}}$ be the number of steps inside a given generation, and at every time step (inside a generation) a species x will be selected to evaluate its interaction with all the other living individuals,

$$h(t) = \frac{1}{N(t)} \frac{1}{n'(t)} \sum_x \sum_{S \in \mathscr{S}} J(S^x, S) n(S, t). \tag{8.11}$$

The quantity $h(t)$ defined in Eq. (8.11) is higher when more positive couplings are observed in generation t. Our aim is to look for configurations with higher $h(t)$. Since

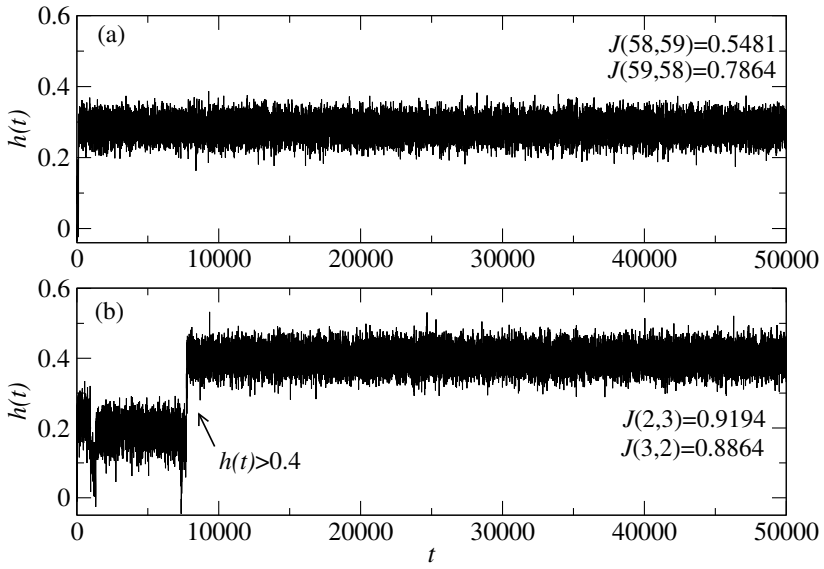

Figure 8.11 The average interaction in a system with the same interaction matrix J when a fixed mutation rate $p_{mut} = 0.004$ is set (a) and with a high mutation rate $p^*_{mut} = 0.01$ in the beginning (b). With the increase in the mutation rate the system is able to find a different configuration with a higher mutual interaction.

during the stable phases the configuration is made of two main species and a cloud of mutants, we have that $h(t)$ fluctuates around an average value. In order to explore the space faster, we increase the mutation rate in the beginning of the simulation, and when the system achieves a configuration with $h(t) \geq \tilde{h}$ we decrease the mutation rate. The threshold $\tilde{h}$ corresponds to a high interaction configuration, and we set $\tilde{h} = 0.4$. This approach follows a simulated annealing technique, very popular in optimization problems.

In Fig. 8.11(a) we have the average interaction for a system with a fixed mutation rate $p_{mut} = 0.004$, and the stable period is composed of a pair of species labeled 58 and 59 with $J(58,59) = 0.5481$ and $J(59,58) = 0.7864$. The combination of the pair of species can be optimized if one increases the mutation rate in the beginning of the simulation, as shown in Fig. 8.11(b). In this simulation, the initial high mutation $p^*_{mut} = 0.01$ decreases to $p_{mut} = 0.004$ when $h(t) \geq \tilde{h}$ and the system stabilizes with the main species 2 and 3 with $J(2,3) = 0.9194$ and $J(3,2) = 0.8864$.

We also calculated the thermodynamical quantities for the system with the simulated annealing implementation, shown in Fig. 8.12. The higher interaction between the dominant pair reflects in the higher energy obtained when the mutation rate is lowered after the threshold is achieved. Control of the mutation rate has been observed in bacteria [155], where a high mutation rate is maintained until a high fitness level is achieved, after which the mutation decreases.

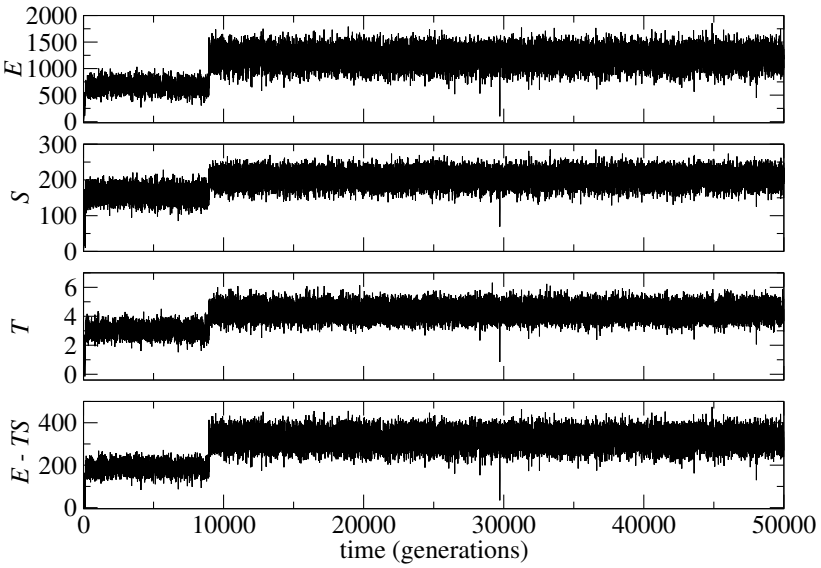

Figure 8.12 The thermodynamical results for the system with the simulated annealing implemented. When the interaction threshold is obtained and the higher mutation rate is switched to a lower one (shortly before the 10000th generation), a configuration with higher values for the energy is obtained.

8.5 Conclusion

In this work we explored distinct aspects of the evolutionary dynamics using a statistical mechanics model. One of the key aspects of the evolution is the coevolution of species, and we delve into this problem disturbing the interaction network of the TN model, looking at a weak and a high-connect network.

The coevolution is not possible if the interaction is insufficient, as shown in Fig. 8.3. This result was expected, since the fitness for reproduction accounts for the interaction of a species x and all the other alive individuals. Population survival was also lowered when the total interaction was reduced, as can be seen in Fig. 8.4.

If one increases the number of links in the interaction network, the system becomes more vulnerable. The faster transitions between quasi-static periods reflect the higher propensity of a mutant to invade the configuration. By increasing the number of connections for a given individual can result in both positive and negative relationships: the presence of more positive links makes the transitions to quasi-static periods faster, because more cooperative pairs exist in the network. On the other side, more negative interactions allow more mutants to invade the configuration and break the stability.

The overall behavior of the TN model was successfully translated in a set of thermodynamical quantities, allowing the identification of a quasi-static period. This approach was made using approximate quantities, and does not satisfy the traditional thermodynamics of equilibrium systems, mainly because the evolutionary process is out of equilibrium.

The energy, entropy, temperature and free energy assume values that fluctuate around a defined mean value during the quasi-static phases. When the configuration of the quasi-static phase is broken, all the thermodynamical quantities will immediately decrease, as shown in Fig. 8.7. For the low-interaction system, where no quasi-static period is obtained, the thermodynamical energy in Fig. 8.8 is very low and does not assume a mean value, reflecting the absence of quasi-static phases in Fig. 8.3. The highly connected network has a sequence of short quasi-static phases that overcome each other, and each of these phases show a defined average energy value in Fig. 8.9.

The quasi-static periods are maintained by couples of mutualistic species that have a positive mutual interaction. This structure resembles the one observed in nature, where the mutualistic species are very important in the stability of communities. In the TN model, the elimination of a species in the core of a mutualistic structure will often result in the end of a quasi-static phase. This is the result of a mutant x that gains benefits of the species y (increasing x population) and at the same time damages y, reducing its population. In nature, more effects have been related to the extinction of species and disturbances in a community equilibrium.

We quantified the amount of mutualistic combinations and showed that they are very rare in the TN model. The system has to discover the mutualistic pairs testing possible interactions and the new pairs are produced by mutations. If the mutation rate increases, more distinct mutants are produced and the exploration of the genotype space is faster. Our simulated annealing approach supports that a high mutation rate in the TN model will allow a faster detection of a mutualistic pair, with higher energy values as shown in Fig. 8.12.

Chapter 9

Conclusion

Truth is ever to be found in simplicity, and not in the multiplicity and confusion of things.

Isaac Newton

In this thesis different problems concerning *random searches* were studied by using different approaches. Given the diversity of applications of random searches, we looked for inter-disciplinary problems to study using simulations of a simple idealized model. In the development of this thesis distinct techniques were designed to each problem, like statistical mechanics, numerical simulations and data analysis.

In Chapter 3 we focused on a very important discussion in the literature, concerning the evolutive or emergent nature of Lévy flights. In this study we proposed a set of random search simulations in complex distributions of targets, and numerically we obtained evidences that Lévy flights ($\mu_{opt} \sim 2$) remain as the optimal search strategy. This contribution is important because it augments the range of scenarios where the optimality of Lévy flights has been numerically verified. This result supports the plasticity of Lévy flights across distinct distribution of resources, as an strategy that optimizes the animal foraging in a wide range of landscapes. Thus, based on our results we expect that the mechanisms behind Lévy flights share an evolutive (or innate) origin in the species where this movement pattern has been observed.

The problem studied in Chapter 4 is the random search in a dynamical distribution of targets. In this model, we were able to characterize how each search strategy copes with the changes in the environment. The result of the interaction between the searcher and the dynamical environment is an emerging stationarity in the distribution of targets. In the stationary regime, the searcher eliminates targets (approximately) at the same

rate that new ones are added to the environment. In our results we showed that the time required for the random search to achieve the stationarity depends on the search strategy and the rate used to create the targets. Ballistic walkers, with $\mu \to 1$ reach the stationarity first, and as we increase the μ exponent the time to obtain the stationary regime increases as well. Further, when the targets are added to the environment, the faster they are created the longer the time the system needs to reach the stationarity.

In Chapter 5, we discussed the development of a parallel algorithm to random searches. Given the inherently sequential nature of a random search algorithm, we designed a solution to the problem that recreates the trajectory of a single random walker in a group of parallel random walkers. Our goal in the parallelization method was to reduce the computation time of our simulations. After the parallelization was implemented, we were able to decrease the time of our simulations to a tenth of the sequential time in a configuration with a high density of targets, and to a fifth in the sparse environment. Our main contribution in this work was the development of a parallel protocol to random searches, and other tools, like GPU programming, can be used in the future to reduce the simulation time.

A new collaboration with an experimental group from the Zoology Department of the University of Cambridge was presented in Chapter 6. We studied a behavioral polymorphism in *Drosophila melanogaster* larvae that results in distinct foraging strategies. Since evolutionary pressures are responsible for this polymorphism, we investigated numerically the situations where one strategy performs better than the other. Our model reproduces the predictions from the literature, that a less diffusive strategy is better when the food density is low. In parallel with the numerical model, we tracked these larvae in a controlled experiment. Even though our observations are not in total agreement with the current literature, our work uses different experimental techniques and explores different questions.

In Chapter 7 we used a stochastic process approach to the random search problem. First we applied a spectral method, known as the observable representation, to a discrete random walk process. We wrote the transitions between the coordinates of the random walker in a transition matrix, and studied the projections of its slowest eigenvectors. This method allows the visual inference of the states space geometrical properties. We studied how the geometrical properties of the original space are recovered within the OR. Then, we applied the same method to the random search process, with two spatially distinct targets distributions. We showed that the full geometry of the targets configuration is recovered through the OR.

Finally, in Chapter 8 we explored a statistical mechanics model for species evolution. This model is known in the literature as the tangled nature model, and shows a punctuated equilibria pattern that coincides with the fossil records data. First we studied disturbances in the model's interaction network, and showed that neither a system with only weak interactions nor a highly connected population can produce a stable configuration. Further, we developed thermodynamic quantities to characterize the model, that allowed a quantitative approach to the problem. Finally, we applied a simulated annealing technique to optimize the search for stable configurations in the model.

Bibliography

[1] E. A. Codling, M. J. Plank, and S. Benhamou. Random walk models in biology. *Journal of the Royal Society Interface*, 5:813–834, 2008.

[2] P. M. Kareiva and N. Shigesada. Analyzing insect movement as a correlated random walk. *Oecologia*, 56:234–238, 1983.

[3] G. M. Viswanathan, V. Afanasyev, S. V. Buldyrev, E. J. Murphy, P. A. Prince, and H. E. Stanley. Lévy flight search patterns of wandering albatrosses. *Nature*, 381: 413–415, 1996.

[4] O. Bénichou, M. Coppey, M. Moreau, P.-H. Suet, and R. Voituriez. A stochastic theory for the intermittent behaviour of foraging animals. *Physica A*, 356:151–156, 2005.

[5] G. M. Viswanathan, M. G. E. da Luz, E. P. Raposo, and H. E. Stanley. *The Physics of Foraging: An Introduction to Random Searches and Biological Encounters*. Cambridge University Press, 2011.

[6] R. Brown. A brief account of microscopical observations made in the months of June, July and August, 1827, on the particles contained in the pollen of plants; and the general existence of active molecules in organic and inorganic bodies. *Philosophical Magazine*, 4:161–173, 1828.

[7] J. Bernoulli. *Ars conjectandi, opus posthumum. Accedit Tractatus de seriebus in nitis, et epistola gallicè scripta de ludo pilae reticularis*. Thurneysen Brothers, Basel, 1713.

[8] L. Bachelier. *Théorie de la spéculation*. Gauthier-Villars, 1900.

[9] K. Pearson. The problem of the random walk. *Nature*, 72:294, 1905.

[10] L. Rayleigh. XII. on the resultant of a large number of vibrations of the same pitch and of arbitrary phase. *Philosophical Magazine Series 5*, 10:73–78, 1880.

[11] A. Einstein. On the movement of small particules suspended in stationary liquids required by the molecular-kinetic theory of heat. *Annalen der Physik*, 17:549–560, 1905.

[12] M. von Smoluchowski. Zur kinetischen Theorie der Brownschen Molekularbewegung und der Suspensionen. *Annalen der Physik*, 21:757–779, 1906.

[13] J. Klafter and I. M. Sokolov. *First Steps in Random Walks: From Tools to Applications*. Oxford University Press, 2011.

[14] H. C. Berg. *Random Walks in Biology*. Princeton University Press, 1983.

[15] O. C. Ibe. *Elements of Random Walk and Diffusion Processes*. John Wiley & Sons, 2013.

[16] A. A. Borokvov and K. A. Borokvov. *Asymptotic Analysis of Random Walk: Heavy-Tailed Distributions*. Cambridge University Press, 2008.

[17] C. Gardiner. *Stochastic methods: a handbook for the natural and social sciences*. Springer, 4th edition, 2009.

[18] J. P. Nolan. *Stable Distributions - Models for Heavy Tailed Data*. Birkhauser, 2013.

[19] V. V. Uchaikin and V. M. Zolotarev. *Chance and Stability, Stable Distributions and Their Applications*. Utrecht, 1999.

[20] W. Feller. *An Introduction to Probability Theory and its Applications*, volume 2. John Wiley & Sons, Inc., 1966.

[21] R. N. Mantegna and H. E. Stanley. *An introduction to econophysics: correlations and complexity in finance*. Cambridge University Press, 2000.

[22] K. Falconer. *Fractal Geometry: Mathematical Foundations and Applications*. John Wiley & Sons Ltd., 1990.

[23] R. N. Mantegna and H. E. Stanley. Stochastic process with ultraslow convergence to a Gaussian: The truncated Lévy flight. *Physical Review Letters*, 73:2946–2949, 1994.

[24] B. V. Gnedenko and A. N. Kolmogorov. *Limit Distributions for Sums of Independent Random Variables*. Addison-Wesley, 1954.

[25] B. V. Gnedenko. *The Theory of Probability*. Chelsea Publisher Company, 1962.

[26] J. G. Skellam. Random dispersal in theoretical populations. *Biometrika*, 38: 196–218, 1951.

[27] J. G. Skellam. The formulation and interpretation of mathematical models of diffusionary processes in population biology. In M. S. Bartlett and R. W. Hiorns, editors, *The mathematical theory of the dynamics of biological populations*. Academic Press, 1973.

[28] A. Okubo and S. A. Levin. *Diffusion and Ecological Problems: Modern Perspectives*. Springer, 2nd edition, 2002.

[29] B. J. Cole. Fractal time in animal behaviour: the movement activity of *Drosophila*. *Animal Behaviour*, 50:1317–1324, 1995.

[30] G. Ramos-Fernandez, J. L. Mateos, O. Miramontes, G. Cocho, H. Larralde, and B. Ayala-Orozco. Lévy walk patterns in the foraging movments of spider monkeys (*Ateles geoffroyi*). *Behavioral Ecology Sociobiology*, 55:223–230, 2004.

[31] S. Bertrand, J. M. Burgos, F. Gerlotto, and J. Atiquipa. Lévy trajectories of Peruvian purse-seiners as an indicator of the spatial distribution of anchovy (*Engraulis ringens*). *Journal of Marine Science*, 62:477–482, 2005.

[32] G. C. Hays, T. Bastian, T. K. Doyle, S. Fossette, A. C. Gleiss, M. B. Gravenor, V. J. Hobson, N. E. Humphries, K. S. Lilley, N. G. Pade, and D. W. Sims. High activity and Lévy searches: Jellyfish can search the water column like fish. *Proceedings of the Royal Society B*, 279:465–473, 2012.

[33] D. W. Sims, E. J. Southall, N. E. Humphries, G. C. Hays, C. J. A. Bradshaw, J. W. Pitchford, A. James, M. Z. Ahmed, A. S. Brierley, M. A. Hindell, D. Morritt, M. K. Musyl, E. L. C. Shepard, V. J. Wearmouth, R. P. Wilson, M. J. Witt, and J. D. Metcalfe. Scaling laws of marine predator search behaviour. *Nature*, 451:1098–1102, 2008.

[34] E. L. Charnov. Optimal foraging, the Marginal Value Theorem. *Theoretical Population Biology*, 9:129–136, 1976.

[35] G. M. Viswanathan, S. V. Buldyrev, S. Havlin, M. G. E. da Luz, E. P. Raposo, and H. E. Stanley. Optimizing the success of random searches. *Nature*, 401:911–914, 1999.

[36] S. V. Buldyrev, M. Gitterman, S. Havlin, A. Ya. Kazakov, M. G. E. da Luz, E. P. Raposo, H. E. Stanley, and G. M. Viswanathan. Properties of Lévy flights on an interval with absorbing boundaries. *Physica A*, 302:148–161, 2001.

[37] S. V. Buldyrev, S. Havlin, A. Y. Kazakov, M. G. E. da Luz, E. P. Raposo, H. E. Stanley, and G. M. Viswanathan. Average time spent by Lévy flights and walks on an interval with absorbing boundaries. *Physical Review E*, 64:041108, 2001.

[38] R. H. MacArthur and E. R. Pianka. On optimal use of a patchy environment. *The American Naturalist*, 100:603–609, 1966.

[39] G. H. Pyke. Optimal foraging theory: A critical review. *Annual Review of Ecology, Evolution and Systematics*, 15:523–575, 1984.

[40] M. F. Shlesinger and J. Klafter. Lévy walks versus lévy flights. In H. E. Stanley and N. Ostrowsky, editors, *On growth and form: Fractal and non-fractal patterns in physics*, pages 279–283. Springer, 1986.

[41] G. Berkolaiko and S. Havlin. Number of distinct sites visited by lévy flights injected into a d-dimensional lattice. *Physical Review E*, 57:2549–2552, 1998.

[42] G. M. Viswanathan, E. P. Raposo, and M. G. E. da Luz. Lévy flights and superdiffusion in the context of biological encounters and random searches. *Physics of Life Reviews*, 5:133–150, 2008.

[43] S. Benhamou. How many animals really do the Lévy walk? *Ecology*, 88:1962–1969, 2007.

[44] D. Boyer, G. Ramos-Fernandez, O. Miramontes, J. L. Mateos, G. Cocho, H. Larralde, H. Ramos, and F. Rojas. Scale-free foraging by primates emerges from their interaction with a complex environment. *Proceedings of the Royal Society B: Biological Sciences*, 273:1743–1750, 2006.

[45] A. M. Reynolds. Lévy flight patterns are predicted to be an emergent property of a bumblebees's foraging strategy. *Behavioral Ecology Sociobiology*, 64:19–23, 2009.

[46] A. Kolzsch, A. Alzate, F. Bartumeus, M. de Jager, E. J. Weerman, G. M. Hengeveld, M. Naguib, B. A. Nolet, and J. van de Koppel. Experimental evidence for inherent lévy search behaviour in foraging animals. *Proceedings of the Royal Society B: Biological Sciences*, 282:20150424, 2015.

[47] A. M. Reynolds. Signatures of active and passive optimized lévy searching in jellyfish. *Journal of the Royal Society Interface*, 11:20140665, 2014.

[48] M. de Jager, F. Bartumeus, A. Kolzsch, F. J. Weissing, G. M. Hengeveld, B. A. Nolet, P. M. J. Herman, and J. van de Koppel. How superdiffusion gets arrested: ecological encounters explain shift from Lévy to Brownian movement. *Proceedings of the Royal Society B*, 281:20132605, 2013.

[49] P. A. Burrough. Fractal dimension of landscapes and other environmental data. *Nature*, 294:240–242, 1981.

[50] N. M. Haddad, Brudvig. L. A., J. Clobert, K. F. Davies, A. Gonzalez, R. D. Holt, T. E. Lovejoy, J. O. Sexton, M. P. Austin, C. D. Collins, W. M. Cook, E. I. Damschen, R. M. Ewers, B. L. Foster, C. N. Jenkins, A. J. King, W. F. Laurance, D. J. Levey, C. R. Margules, B. A. Melbourne, A. O. Nicholls, J. L. Orrock, D. X. Song, and J. R. Townshend. Habitat fragmentation and its lasting impact on Earth's ecosystems. *Science Advances*, 1:e1500052, 2015.

[51] M. E. Wosniack, M. C. Santos, M. R. Pie, M. C. M. Marques, E. P. Raposo, G. M. Viswanathan, and M. G. E. da Luz. Unveiling a mechanism for species decline in fragmented habitats: fragmentation induced reduction in encounter rates. *Journal of the Royal Society Interface*, 11:20130887, 2013.

[52] M. E. Wosniack, M. C. Santos, E. P. Raposo, G. M. Viswanathan, and M. G. E. da Luz. Robustness of optimal random searches in fragmented environments. *Physical Review E*, 91:052119, 2015.

[53] O. Miramontes, D. Boyer, and F. Bartumeus. The effects of spatially heterogeneous prey distributions on detection patterns in foraging seabirds. *PLoS ONE*, 7:e34317, 2012.

[54] M. E. Ritchie. Scale-dependent foraging and patch choice in fractal environments. *Evolutionary Ecology*, 12:309–330, 1998.

[55] A. M. Reynolds. Liberating lévy walk research from the shackles of optimal foraging. *Physics of Life Reviews*, 14:59–83, 2015.

[56] M. C. Santos, E. P. Raposo, G. M. Viswanathan, and M. G. E. da Luz. Optimal random searches of revisitable targets: crossover from superdiffusive to ballistic random walks. *Europhysics Letters*, 67:734–740, 2004.

[57] A. S. Ferreira, E. P. Raposo, G. M. Viswanathan, and M. G. E. da Luz. The influence of the environment on Lévy random search efficiency: Fractality and memory effects. *Physica A*, 391:3234–3246, 2012.

[58] H. Wolda. Seasonal fluctuations in rainfall, food and abundance of tropical insects. *Journal of Animal Ecology*, 47:369–381, 1978.

[59] R. H. Russel. The food habits of polar bears of james bay and southwest hudson bay in summer and autumn. *Arctic*, 28:117–129, 1975.

[60] E. R. Abraham. The generation of plankton patchiness by turbulent stirring. *Nature*, 391:577–580, 1998.

[61] L. R. Haury, H. Yamakazi, and E. C. Itsweire. Effects of turbulent shear flow on zooplankton distribution. *Deep-Sea Research*, 37:447–461, 1990.

[62] N. B. Metcalfe, N. H. C. Fraser, and M. D. Burns. Food availability and the nocturnal vs. diurnal foraging trade-off in juvenille salmon. *Journal of Animal Ecology*, 68: 371–381, 1999.

[63] D. K. Cairns. Seabirds as indicator of marine food supplies. *Biological Oceanography*, 5:261–271, 1987.

[64] H. Weimerskirch, M. Le Corre, S. Jaquemet, and F. Marsac. Foraging strategy of a tropical seabird, the red-footed booby, in a dynamic marine environment. *Marine Ecology Progress Series*, 288:251–261, 2005.

[65] G. C. Hays, T. K. Doyle, J. D. R. Houghton, M. K. S. Lilley, J. D. Metcalfe, and D. Righton. Diving behaviour of jellyfish equipped with electronic tags. *Journal of Plankton Research*, 30:325–331, 2008.

[66] T. Mueller and W. F. Fagan. Search and navigation in dynamic environments - from individual behaviors to population distributions. *Oikos*, 117:654–664, 2008.

[67] A. B. Shiflet and G. W. Shiflet. *Introduction to Computational Science: Modeling and Simulation for the Sciences*. Princeton University Press, 2nd edition, 2014.

[68] S. Arora and B. Barak. *Computational Complexity: A Modern Approach*. Cambridge University Press, 2009.

[69] C. H. Papadimitrou. *Computational Complexity*. Addison-Wesley, 1993.

[70] Raimondas Ciegis, David Henty, Bo Kågström, and Julius Žilinskas. *Parallel scientific computing and optimization: Advances and Applications*, volume 27. Springer Science & Business Media, 2008.

[71] Raymond Greenlaw, H James Hoover, and Walter L Ruzzo. *Limits to parallel computation: P-completeness theory*, volume 200. Oxford university press Oxford, 1995.

[72] JM Robson. Parallel algorithms for NP-complete problems. In *Computer science*, pages 379–382. Springer, 1992.

[73] H. J. Karloff and D. B. Shmoys. Efficient parallel algorithms for edge coloring problems. *Journal of Algorithms*, 8:39–52, 1987.

[74] R. M. Karp and A. Wigderson. Parallel algorithm for maximal independent set problem. *Journal of the ACM*, 32:762–773, 1985.

[75] Enrique Alba and José M Troya. A survey of parallel distributed genetic algorithms. *Complexity*, 4(4):31–52, 1999.

[76] Christian Bischof. *Parallel Computing: Architectures, Algorithms, and Applications*, volume 15. IOS Press, 2008.

[77] B. Chapman, G. Jost, and R. van der Paas. *Using OpenMP*. MIT Press, 2007.

[78] F. Wang and D. P. Landau. Efficient, multiple-range random walk algorithm to calculate the density of states. *Physical Review Letters*, 86:2050–2053, 2001.

[79] F. Wang and D. P. Landau. Determining the density of states for classical statistical models: A random walk algorithm to produce a flat histogram. *Physical Review E*, 64:056101, 2001.

[80] J. Yin and D. P. Landau. Massively parallel Wang-Landau sampling on multiple GPUs. *Computer Physics Communications*, 183:1568–1573, 2012.

[81] L. Zhan. A parallel implementation of the Wang-Landau algorithm. *Computer Physics Communications*, 179:339–344, 2008.

[82] A. Youssef. A parallel algorithm for random walk construction with application to the Monte Carlo solution of partial differential equations. *IEE Transactions on Parallel and Distributed Systems*, 4:355–360, 1993.

[83] N. Alon, C. Avin, M. Koucký, G. Kozma, Z. Lotker, and M. R. Tuttle. Many random walks are faster than one. *Combinatorics, Probability & Computing*, 20:481–502, 2011.

[84] Klim Efremenko and Omer Reingold. How well do random walks parallelize? In Irit Dinur, Klaus Jansen, Joseph Naor, and José Rolim, editors, *Approximation, Randomization, and Combinatorial Optimization. Algorithms and Techniques*, volume 5687 of *Lecture Notes in Computer Science*, pages 476–489. Springer Berlin Heidelberg, 2009. ISBN 978-3-642-03684-2.

[85] C. Cooper, A. Frieze, and T. Radzik. Multiple random walks in random regular graphs. *SIAM Journal on Discrete Mathematics*, 23:1738–1761, 2009.

[86] B. Shah and K.-I. Kim. Towards enhanced searching architecture for unstructered peer-to-peer over mobile ad hoc networks. *Wireless Personal Communications*, 77: 1167–1189, 2014.

[87] H. Sivaraj and G. Gopalakrishnan. Random walk based heuristic algorithms for distributed memory model checking. *Electronic Notes in Theoretical Computer Science*, 89:1–17, 2003.

[88] R. Pelánek, T. Hanžl, I. Černá, and L. Brim. Enhancing random walk state space exploration. In *Proceedings of the 10th international workshop on formal methods for industrial critical systems*, pages 98–105, 2005.

[89] M. D. Jones and J. Sorber. Parallel search for LTL violations. *International Journal on Software Tools for Technology Transfer*, 7:31–42, 2005.

[90] Yaniv Altshuler and Alfred M. Bruckstein. Static and expanding grid coverage with ant robots: Complexity results. *Theoretical Computer Science*, 412(35):4661 – 4674, 2011. ISSN 0304-3975.

[91] G. Berkolaiko and S. Havlin. Territory covered by N Lévy flights on d-dimensional lattices. *Physical Review E,* 55:1395–1400, 1997.

[92] D. W. Sims, N. E. Humphries, R. W. Bradford, and B. D. Bruce. Lévy flight and Brownian search patterns of a free-ranging predator reflect different prey field characteristics. *Journal of Animal Ecology*, 81:432–442, 2012.

[93] F. Bartumeus, E. P. Raposo, G. M. Viswanathan, and M. G. E. da Luz. Stochastic optimal foraging: Tuning intensive and extensive dynamics in random searches. *PLoS ONE,* 9:e106373, 2014.

[94] Ronald E Walpole, Raymond H Myers, Sharon L Myers, and Keying Ye. *Probability and statistics for engineers and scientists*, volume 5. Macmillan New York, 1993.

[95] G. Technitis, W. Othman, K. Safi, and R. Weibel. From A to B, randomly: a point-to-point random trajectory generator for animal movement. *Int. J. Geogr. Inf. Sci.*, 29:912–934, 2015.

[96] S. N. Majumdar and H. Orland. Effective Langevin equations for constrained stochastic processes. *Journal of Statistical Mechanics: Theory and Experiment*, 2015:P06039, 2015.

[97] M. E. Wosniack, E. P. Raposo, G. M. Viswanathan, and M. G. E. da Luz. A parallel algorithm for random searches. *Computer Physics Communications*, 196:390–397, 2015.

[98] M. de Jager, F. J. Weissing, P. M. J. Herman, B. A. Nolet, and J. van de Koppel. Lévy walks evolve through interaction between movement and environmental complexity. *Science*, 332:1551–1553, 2011.

[99] A. Ferran, M. Ettifouri, P. Clement, and W. J. Bell. Sources of variability in the transition from extensive to intensive search in coccinellid predators (Homoptera: Coccinellidae). *Journal of Insect Behavior*, 7:633–647, 1994.

[100] R. C. Tyson, J. B. Wilson, and W. D. Lane. Beyond diffusion: modelling local and long-distance dispersal for organisms exhibiting intensive and extensive search modes. *Theoretical Population Biology*, 79:70–81, 2011.

[101] S. Hill, M. Burrows, and R. Hughes. The efficiency of adaptive search tactics for different prey distribution patterns: a simulation model based on the behaviour of juvenile plaice. *Journal of Fish Biology*, 63:117–130, 2003.

[102] B. A. Nolet and W. M. Mooji. Search paths of swans foraging on spatially autocorrelated tubers. *Journal of Animal Ecology*, 71:451–462, 2002.

[103] M. B. Sokolowski. *Drosophila*: Genetics meets behaviour. *Nature Reviews Genetics*, 2:879–890, 2001.

[104] B. C. Clarke. The evolution of genetic diversity. *Proceedings of the Royal Society of London B*, 205:453–474, 1979.

[105] T. J. Ehlinger and D. S. Wilson. Complex foraging polymorphism in bluegill sunfish. *Proceedings of the National Academy of Sciences (USA)*, 85:1878–1882, 1988.

[106] K. Kiontke. Evolutionary biology: patchy food may maintain a foraging polymorphism. *Current Biology*, 18:R1017–R1019, 2008.

[107] M. B. Sokolowski, H. S. Pereira, and K. Hughes. Evolution of foraging behavior in *Drosophila* by density-dependent selection. *Proceedings of the National Academy of Sciences (USA)*, 94:7373–7377, 1997.

[108] S. A. Graf and M. B. Sokolowski. Rover/sitter *Drosophila melanogaster* larval foraging polymorphism as a function of larval development, food-patch quality, and starvation. *Journal of Insect Behavior*, 2:301–313, 1989.

[109] C. Tortorici, A. Brody, and W. J. Bell. Influence of spatial patterning of resources on search orientation of adult *Drosophila melanogaster*. *Animal Behaviour*, 34: 1568–1570, 1986.

[110] A. H. Edelsparre, A. Vesterberg, J. H. Lim, M. Anwari, and M. J. Fitzpatrick. Alleles underlying larval foraging behaviour influence adult dispersal in nature. *Ecology Letters*, 17:333–339, 2014.

[111] J. G. Burns, N. Svetec, L. Rowe, F. Mery, M. J. Dolan, W. T. Boyce, and M. B. Sokolowski. Gene-environment interplay in *Drosophila melanogaster*: Chronic food deprivation in early life affects adult exploratory and fitness traits. *Proceedings of the National Academy of Sciences*, 109:17239–17244, 2012.

[112] R. K. Vijendravarma, S. Narasimba, and T. J. Kawecki. Evolution of foraging in respose to chronic malnutrition in *Drosophila melanogaster*. *Proceedings of the Royal Society B*, 279:3540–3546, 2012.

[113] R. Kaun, K, C. A. L. Riedl, M. Chakaborty-Chatterjee, A. T. Belay, S. J. Douglas, A. G. Gibbs, and M. B. Sokolowski. Natural variation in food acquisition mediated *via* a *Drosophila* cGMP-dependent protein kinasi. *The Journal of Experimental Biology*, 210:3547–3558, 2007.

[114] A. Gomez-Marin, G. J. Stephens, and M. Louis. Active sampling and decision making in *Drosophila* chemotaxis. *Nature Communications*, 2:441, 2011.

[115] A. Gomez-Marin and M. Louis. Multilevel control of run orientation in *Drosophila* larval chemotaxis. *Frontiers in Behavioral Neuroscience*, 8:38, 2014.

[116] D. Berrigan and D. J. Pepin. How maggots move: Allometry and kinematics of crawling in larval diptera. *Journal of Insect Physiology*, 41:329–337, 1995.

[117] B. Risse, S. Thomas, N. Otto, T. Löpmeier, D. Valkov, X. Jiang, and C. Klämbt. FIM, a novel FTIR-based imaging method for high thrthrough locomotion analysis. *PLoS ONE*, 8:e53963, 2013.

[118] B. Gaveau and L. S. Schulman. Multiple phases in stochastic dynamics: Geometry and probabilities. *Physical Review E*, 73:036124, 2006.

[119] B. Gaveau, L. S. Schulman, and L. J. Schulman. Imaging geometry through dynamics: The Observable Representation. *Journal of Physics A: Mathematical and General*, 39:10307–10321, 2006.

[120] S. B. Nicholson, L. S. Schulman, and E. J. Kim. Deciphering interactions of complex systems that do not satisfy detailed balance. *Physics Letters A*, 377:1810–1813, 2013.

[121] B. Gaveau and L. J. Schulman. A general framework for non-equilibrium phenomena: the master equation and its formal consequences. *Physics Letters A*, 229: 347–353, 1997.

[122] B. Gaveau and L. J. Schulman. Theory of non-equilibrium first-order phase transitions for stochastic dynamics. *Journal of Mathematical Physics*, 39:1517–1533, 1998.

[123] L. S. Schulman. Mean-field spin glass in the Observable Representation. *Physical Review Letters*, 98:257202, 2007.

[124] L. S. Schulman. Transition matrix from a random walk. *ArXiv e-prints*, May 2016.

[125] I. Sachs, S. Sen, and J. Sexton. *Elements of Statistical Mechanics with an Introduction to Quantum Field Theory and Numerical Simulation*. Cambridge University Press (Cambridge), 2006.

[126] R. Aldrovandi. *Special Matrices of Mathematical Physics: Stochastic, Circulant and Bell Matrices*. World Scientific (Singapore), 2001.

[127] A. P. Hendry and M. T. Kinnison. An introduction to microevolution: rate, pattern, process. *Genetica*, 112-113:1–8, 2001.

[128] D. M. Raup and J. J. Sepkoski. Periodic extinction of families and genera. *Science*, 231:833–836, 1986.

[129] P. D. Gingerich. Rates of evolution on the time scale of the evolutionary process. *Genetica*, 112-113:127–144, 2001.

[130] D. N. Reznick and R. E. Ricklefs. Darwin's bridge between microevolution and macroevolution. *Nature*, 457:837–842, 2009.

[131] A. W. Simons. The continuity of microevolution and macroevolution. *Journal of Theoretical Biology*, 15:688–701, 2002.

[132] R. V. Solé, S. C. Manrubia, M. Benton, S. Kauffman, and P. Bak. Criticality and scaling in evolutionary ecology. *TREE*, 14:156–160, 1999.

[133] R. V. Solé, S. C. Manrubia, M. Benton, and P. Bak. Self-similarity of extinction statistics in the fossil record. *Nature*, 388:764–767, 1997.

[134] S. J. Gould and N. Eldredge. Punctuated equilibria: The tempo and mode of evolution reconsidered. *Paleobiology*, 3:115–151, 1977.

[135] P. Bak, C. Tang, and K. Wiesenfeld. Self-organized criticality. *Physical Review A*, 38:364–374, 1988.

[136] P. Bak and S. Boettcher. Self-organized criticality and punctuated equilibria. *Physica D*, 107:143–150, 1997.

[137] M. Paczuski, S. Maslov, and P. Bak. Avalanche dynamics in evolution, growth, and depinning models. *Physical Review E*, 53:414–443, 1996.

[138] D. L. Stein and C. M. Newman. *Spin Glasses and Complexity*. Princeton University Press, 2013.

[139] P. Bak and K. Sneppen. Punctuated equilibrium and criticality in a simple model of evolution. *Physical Review Letters*, 71:4083–4086, 1993.

[140] S. A. Kauffman and S. Johnsen. Coevolution to the edge of chaos: Coupled fitness landscapes, poised states and coevolution avalanches. *Journal of Theoretical Biology*, 149:467–505, 1991.

[141] B. Drossel. Biological evolution and statistical physics. *Advances in Physics*, 50: 209–315, 2001.

[142] J. Bascompte, P. Jordano, and J. M. Olesen. Asymmetric coevolutionary networks facilitate biodiversity maintenance. *Science*, 312:431–433, 2006.

[143] J. M. Montoya and R. V. Solé. Small world patterns in food webs. *Journal of Theoretical Biology*, 214:405–412, 2002.

[144] K. Christensen, S. A. di Collobiano, M. Hall, and H. J. Jensen. Tangled Nature: A model of evolutionary ecology. *Journal of Theoretical Biology*, 216:73–84, 2002.

[145] M. Hall, K. Christensen, S. A. di Collobiano, and H. J. Jensen. Time-dependent extinction rate and species abundance in a tangled-nature model of biological evolution. *Physical Review E*, 66:011904, 2002.

[146] S. A. di Collobiano, K. Christensen, and H. J. Jensen. The Tangled Nature model as an evolving quasi-species model. *Journal of Physics A: Mathematical and Theoretical*, 36:883–891, 2003.

[147] N. Goldenfeld and C. Woese. Life is physics: Evolution as a collective phenomenon far from equilibrium. *Annual Reviews of Condensed Matter Physics*, 2:375–399, 2011.

[148] S. Kirkpatrick, C. D. Gelatt Jr, and M. P. Vecchi. Optimization by simulated annealing. *Science*, 220:671–680, 1983.

[149] P. E. Anderson and H. J. Jensen. Network properties, species abundance and evolution in a model of evoevolutionary ecology. *Journal of Theoretical Biology*, 232:551–558, 2005.

[150] D. L. DeAngelis and J. C. Waterhouse. Equilibrium and nonequilibrium concepts in ecological models. *Ecological Monographs*, 57:1–21, 1987.

[151] J. M. Tylianakis, E. Laliberté, A. Nielsen, and J. Bascompte. Conservation of species interaction networks. *Biological Conservation*, 143:2270–2279, 2010.

[152] E. J. O'Gorman and M. C. Emmerson. Perturbations to trophic interactions and the stability of complex food webs. *Proceedings of the National Academy of Sciences*, 106:13393–13398, 2009.

[153] P. Jordano, J. Bascompte, and J. M Olesen. Invariant properties in coevolutionary networks of plant-animal interactions. *Ecology Letters*, 6:69–81, 2003.

[154] R. Albert, H. Jeong, and A. L. Barabási. Error and attack tolerance of complex networks. *Nature*, 406:378–383, 2000.

[155] M. Heo, L. Kang, and E. I. Shakhnovich. Emergence of species in evolutionary "simulated annealing". *Proceedings of the National Academy of Sciences*, 106:1868–1874, 2009.

[156] M. S. Tyler. *Developmental Biology, a guide for experimental study*. Sinauer Associates, Inc., 2000.

[157] M. B. Sokolowski. Foraging strategies of *Drosophila melanogaster*: A chromossomal analysis. *Behavior Genetics*, 10:291–302, 1980.

Appendix A

A Survey on Probability and Statistics

We dedicate this appendix to the definitions and discussion concerning the probability and statistics tools used in the thesis. We will restrict our discussion to continuous random variables, in agreement with the tools used in the development of the thesis.

A.1 Definitions

In probability, we call an *experiment* any process of trial and observation. If the outcome of the experiment is unknown, it is a *random experiment* and the collection of all possible elementary outcomes is the *sample space* Ω. These outcomes are called elementary since every time the experiment is performed exactly one of the outcomes will be observed. *Sample points* are the elementary outcomes of the sample space and are denoted by $w_i, i = 1,2,\ldots$ and for n possible outcomes we write $\Omega = \{w_1, w_2, \ldots, w_n\}$. In the case where either a prescribed outcome is observed or any of a number of possible outcomes is observed, we call it an *event*, that is a subset of the sample space.

A.1.1 Random variables

Consider a random experiment with sample space Ω and w a sample point in Ω. We will assign a real number to each $w \in \Omega$. A *random variable* $X(w)$ is a single-valued real function that assigns a real number (the value of $X(w)$) to each sample point $w \in \Omega$. We will denote a random variable by a single capital letter X instead of the function $X(w)$ to adequate the notation to the common practice in the literature. The sample space Ω is called the *domain* of the random variable X. The collection of all numbers that are values of X is the *range* of X.

Consider now X a random variable and x a fixed real value. Let A_x be the event that defines the subset of Ω consisting of all real sample points to which X assigns the number x. Mathematically, we express this as:

$$A_x = \{w|X(w) = x\}. \tag{A.1}$$

Since A_x is an event, it will have a probability to occur, which we define as follows:

$$p = P(A_x). \tag{A.2}$$

A.1.2 Cumulative distribution function

Let X be a random variable, x a number, and consider the event $[X \leq x] = \{x|X(w) \leq x\}$. The *cumulative distribution function* (CDF) of X if defined as:

$$F_X(x) = P(X \leq x), \quad -\infty < x < \infty, \tag{A.3}$$

that is, $F_X(x)$ corresponds to the probability that X takes on a value that is less than or equal to x. The most important properties of $F_X(x)$ are the following:

1. $F_X(x)$ is a non-decreasing function: if $x_1 < x_2$, then $F_X(x_1) \leq F_X(x_2)$;
2. $0 \leq F_X(x) \leq 1$;
3. $F_X(\infty) = 1$ and $F_X(-\infty) = 0$;
4. $P(a < X \leq b) = F_X(b) - F_X(a)$;
5. $P(X > a) = 1 - P(X \leq a) = 1 - F_X(a)$.

A.1.3 Continuous random variables and the probability density function

A random variable X is a *continuous random variable* if there exists a non-negative function $f_X(x)$, defined for all real $x \in (-\infty, \infty)$, having the property that for any set A of real numbers,

$$P(X \in A) = \int_A f_X(x)\mathrm{d}x. \tag{A.4}$$

The function $f_X(x)$ is the *probability density function* (PDF) of the random variable X and is defined by:

$$f_X(x) = \frac{\mathrm{d}F_X(x)}{\mathrm{d}x}. \tag{A.5}$$

The properties of the probability density function are listed below:

1. $f_X(x) \geq 0$;

2. $\int_{-\infty}^{\infty} f_X(x)\mathrm{d}x = 1$;

3. $P(a \leq X \leq b) = \int_a^b f_X(x)\mathrm{d}x$, and it implies that $P(X = a) = \int_a^a f_X(x)\mathrm{d}x = 0$;

4. $P(X < a) = P(X \leq a) = \int_{-\infty}^{a} f_X(x)\mathrm{d}x = F_X(a)$.

A.1.4 Moments of random variables

Let X be a continuous random variable. The *expected value* or *mean* of X, denoted by $E[X]$ or $\overline{X}$, is defined by:

$$E[X] = \int_{-\infty}^{\infty} x f_X(x)\mathrm{d}x. \tag{A.6}$$

The expected value of X is a weighted average of the possible values that X can assume: each value is weighted by the probability that X takes that value.

The nth *moment* of the random variable X, denoted by $E[X^n]$, is defined as:

$$E[X^n] = \int_{-\infty}^{\infty} x^n f_X(x)\mathrm{d}x, \quad n = 1,2,3,\ldots \tag{A.7}$$

so the expected value of X corresponds to the first moment.

The nth *central moment* of a random variable X is defined as:

$$E[(X-\overline{X})^n] = \int_{-\infty}^{\infty} (x-\overline{X})^n f_X(x)\mathrm{d}x, \tag{A.8}$$

and for $n = 2$ the central moment is called the *variance* of X.

A.1.5 Characteristic functions

Let $f_X(x)$ be the probability density function of the random variable X. We define the characteristic function of X by:

$$\varphi_X(w) = E\left[\mathrm{e}^{iwX}\right] = \int_{-\infty}^{\infty} \mathrm{e}^{iwx} f_X(x)\,\mathrm{d}x, \tag{A.9}$$

and we recover $f_X(x)$ from $\varphi_X(w)$ by:

$$f_X(x) = \frac{1}{2\pi}\int_{-\infty}^{\infty} \varphi_X(w)\mathrm{e}^{-iwx}\,\mathrm{d}w. \tag{A.10}$$

The most important properties of the characteristic function are listed below:

1. $\varphi_X(0) = 1$;
2. $|\varphi_X(w)| \leq 1$;
3. Given a and b constants, $\varphi_{aX+b}(w) = \mathrm{e}^{iwb}\varphi_X(aw)$;
4. If X and Y are independent random variables, then $\varphi_{X+Y}(w) = \varphi_X(w)\varphi_Y(w)$ (valid for n random variables);
5. $\varphi_X(w)$ is uniformly continuous.

A.1.6 The central limit theorem

The central limit theorem (CLT) concerns the sum of random variables and is very important in Statistics. The theorem states that as the number of independent identically distributed random variables with *finite* mean and variance increases, the distribution of their sum becomes normal regardless of the shape of the distribution of the random variables. We will present a proof that relies in the following important result, the Lévy's continuity theorem, that connects the convergence in distribution of a sequence of random variables with pointwise convergence of their characteristic functions.

Theorem A.1.1 (Lévy's continuity theorem). *Let F_n, $n \geq 1$ distribution functions with respective characteristic functions φ_n, $n \geq 1$. If $F_n \xrightarrow[n\to\infty]{} F$ in the continuity points of F, then $\varphi_n(w) \xrightarrow[n\to\infty]{} \varphi(w)$ for all $w \in \mathbb{R}$, and φ is the characteristic function corresponding to F. Conversely, if $\varphi_n(w) \xrightarrow[n\to\infty]{} \varphi(w)$ for $w \in \mathbb{R}$ is a continuous function in $w = 0$, then $\varphi(w)$ is the characteristic function of a probability density F.*

Proof. The proof can be found on [20]. □

Theorem A.1.2 (The Central Limit Theorem). *Consider* $\{X_n\}$ $(n \geq 1)$ *random variables that are independent and identically distributed with expected value* μ *and variance* σ^2 $(0 < \sigma^2 < \infty)$*. Then, for* $S_n = X_1 + X_2 + \cdots + X_n$*, we have:*

$$\frac{S_n - n\mu}{\sigma\sqrt{n}} \to N(0,1). \tag{A.11}$$

Proof. Without loss of generality, assume that $\mu = 0$. If that is not the case, define $Y_n = X_n - \mu$, so that Y_n has $\mu = 0$. Also, since the variables are identically distributed we will simplify the notation using $\varphi_{X_i} = \varphi$. Writing the characteristic function for $S_n/\sigma\sqrt{n}$ and using the properties listed in subsection A.1.5, we get:

$$\varphi_{S_n/\sigma\sqrt{n}}(w) = \varphi_{S_n}(w/\sigma\sqrt{n}) = \prod_{i=1}^{n} \varphi(w/\sigma\sqrt{n}) = \left(\varphi(w/\sigma\sqrt{n})\right)^n. \tag{A.12}$$

Using the Taylor expansion around zero until the second order,

$$\varphi(w/\sigma\sqrt{n}) = \varphi(0) + \frac{w}{\sigma\sqrt{n}}\varphi'(0) + \frac{1}{2}\left(\frac{w}{\sigma\sqrt{n}}\right)^2 \varphi''(0) + o\left(\frac{w^2}{n}\right). \tag{A.13}$$

According to the properties of φ, we have $\varphi(0) = 1$, $\varphi'(0) = i\mu = 0$ and $\varphi''(0) = i^2\sigma^2 = -\sigma^2$. Applying these properties to the last equation,

$$\varphi(w/\sigma\sqrt{n}) = 1 - \frac{w^2}{2n} + o\left(\frac{w^2}{n}\right) = 1 - \frac{w^2}{2n}\left[1 - \frac{o\left(\frac{w^2}{n}\right)}{\frac{w^2}{n}}\right]. \tag{A.14}$$

Now, notice that since $\lim_{x\to 0} \frac{o(x)}{x} = 0$, we have

$$\lim_{n\to\infty}\left[1 - \frac{o\left(\frac{w^2}{n}\right)}{w^2/n}\right] = 1. \tag{A.15}$$

Also, applying the following limit:

$$\lim_{n\to\infty} c_n = c \implies \lim_{n\to\infty}\left(1 - \frac{c_n}{n}\right)^n = \mathrm{e}^{-c}, \tag{A.16}$$

we finally have:

$$\lim_{n\to\infty} \varphi(w/\sigma\sqrt{n}) = \lim_{n\to\infty} \left\{1 - \frac{w^2}{2n}\left[1 - \frac{o(w^2/n)}{w^2/n}\right]\right\}^n = \mathrm{e}^{-w^2/2}. \tag{A.17}$$

By the Lévy's continuity theorem, the convergence on the characteristic functions in Eq.(A.17) implies in the convergence of the distributions. Since $e^{-w^2/2}$ is the characteristic function of the Normal distribution, we have $\frac{S_n}{\sigma\sqrt{n}} \to N(0,1)$. □

Appendix B

The experimental acquisition of *Drosophila* data

In this appendix we will describe the experimental work done in the acquisition of the *Drosophila*'s larvae movement data.

B.1 The *Drosophila melanogaster* Larvae

The fruitfly *Drosophila melanogaster* is a model organism widely used in biological research, in studies ranging from genetics to physiology and behavior. It is an animal species very easy to take care for, breeds quickly, lays many eggs and has four pairs of chromosomes. The fruitfly lifespan is about 30 days at 29^{o}C, and its development period varies with temperature: the development is faster in higher temperatures. The *Drosophila* life cycle is comparatively short, and involves a complete metamorphosis with three distinct stages: larva, pupal and adult. The female *Drosophila* lays its eggs and after one day of fertilization the embryo is formed into larva and hatches. During the larval stage, the larva consumes food continuously and therefore grows until reaching the pupal stage. The larval stages of *Drosophila* last 3 days and are summarized in Table B.1. After about five days, the fly emerges from the pupa case and 12 hours later is sexually matured and fertile.

A very important feature of *Drosophila* is its capacity to demonstrate many of the phenotypes that are observed in more complex organisms including mammals. The behavior phenotypes expressed by *Drosophila* are very complex and stand at the interface between the organism and its surrounding environment. One of the first works that

Table B.1 Larval stages of *Drosophila* (reproduced from [156]).

Time after fertilization	Developmental event (at 25°C)
24h (1 day)	hatching from egg; fist instar larva begins
49h (2 days)	second instar larva begins
72h (3 days)	third instar larva begins
120h (5 days)	puparium formation
216h (9 days)	adult ready to emerge from pupa case

studied *Drosophila* larval behavior addressed the foraging task, measuring the path length traveled by the larva in a food substrate [157].

The locomotion in *Drosophila* larvae is very simple: it consists of straight crawls interrupted by pause turns in a low speed. The first experimental assays to study larval movement consisted of microscope setups. However, nowadays it is possible to track the crawling larvae using a simple camera setup and record high contrast images that are analyzed with softwares that are automated to this task [115, 117]. In the next section we will describe the experimental methodology in our tracking experiments.

B.2 The Tracking Experiment

In the experiments we used 3rd instar *Drosophila* larvae from two different strains: rovers (for^R) and sitters (for^S). The rovers and sitters populations came from Marla Sokolowski's laboratory in Toronto (Canada). The larvae were reared in standard laboratory food inside incubators that kept them at constant temperature (25^oC). In order to specify the stage of each set of animals, we changed the flies from the rearing bottles every two hours in the day for three times. Once in a new bottle, the flies will lay eggs that will develop according to Table B.1. Then, every experiment with a given bottle was scheduled to happen 96h after the bottle was made, since our tracking was optimized for third instar larvae.

Before a tracking experiment, 10 larvae from the desired strain were taken from the rearing bottle. They were chosen according to their size, so we have similar animals in each experiment. The handling of each larva was made using a paint brush and they were gently transferred from the bottle to an acrylic plate, where they were rinsed in distilled water. This eliminates the food in their bodies. Next, the larvae were placed in an agar plate for 15min, before being transfered to the experimental arena.

The tracking arena is a squared acrylic plate (24cmx24cm) covered with a thick layer of agar. In experiments with food, the patches (diameter of 8.5cm and 4.2cm) were filled

with food in the following way. A circular region of agar inside the arena was removed and filled with different food solutions with the same density of agar. The process was done very carefully to avoid spilling agar over the patches.

In the behavior studies of the larvae foraging we tested different food recipes, that are described in the next subsection. The rover and sitter larvae interact with food performing chemotaxis, orientating their bodies towards the source of smell (apple juice and/or sucrose in our experiments). The results presented in this thesis correspond to the low quality food.

B.2.1 The food recipes

The agar was prepared boiling a solution of 2g of agar in 500ml of distilled H_2O until the solution looked homogeneous and the agar was totally melted. The proportion of agar in water (0.4%) was kept the same in all the foods prepared, so we have the same density in all the solutions. One important feature of the food solution was the transparency: this was required by the image acquisition technique described in the next section. Thus, we did not use yeast solutions, the most used food in behavior assays of *Drosophila* larvae, because of its yellowish color and opacity. The following food solutions were boiled in the microwave before used (to melt the agar), and were prepared every day before the experiments.

1. High quality food: 50ml of apple juice, 3.42g of sucrose, 0.8g of agar and 150ml of distilled H_2O.

2. Low quality food: 5ml of apple juice, 0.342g of sucrose, 0.8g of agar and 195ml of distilled H_2O.

3. High sucrose concentration food: 3.42g of sucrose, 0.8g of agar and 200ml of distilled H_2O.

4. Low sucrose concentration food: 0.342g of sucrose, 0.8g of agar and 200ml of distilled H_2O.

B.2.2 The acquisition of images

The arena with agar, food, and larvae was placed inside the incubator, kept in the dark at room temperature (25^oC). A structure of infrared LEDs was fixed around the acrylic glass plate. When the LEDs are turned on, infrared light (that is invisible to the larvae) is filled in the arena (this is the only light source inside the incubator). The image acquisition

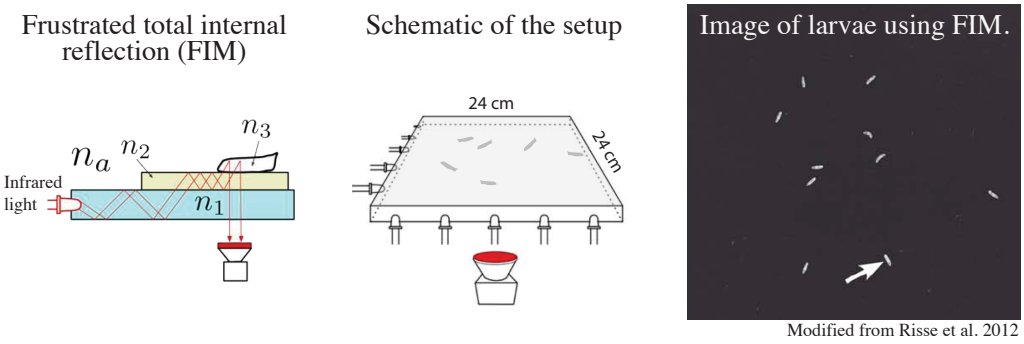

Figure B.1 The experimental methodology. In (a) the acrylic plate (refraction index n_1) is inundated with infrared red. The light is totally reflected in the agar interface (refraction index n_2), but the presence of the larva (refraction index n_3) frustrates the total internal reflection. Thus, the light is captured by the infrared camera positioned underneath the arena, schematized in (b). Finally, a very high contrasting image of the larvae is recorded by the camera (c). The image was modified from [117] by Berni, J.

technique uses frustrated total internal reflection (FTIR) to determine the contact surface between the larva and the agar substrate.

At the glass/agar interface, the infrared light experiences total internal reflection, because the refraction index of the agar (around 1.33) is smaller than the refraction index of the acrylic glass (1.5). However, the presence of the larvae above the agar (with a refractive index higher than the agar) frustrates the total internal reflection, so that light will enter the larval body. Here, light is reflected and the reflection angle will be smaller than the critical angle, so that light passes through all the layers and will be detected by the camera equipped with an infrared filter. This method, summarized in Fig. B.1 guarantees images with a very high contrast, that are ideal to use in the tracking software [117].

Appendix C

Properties of Stochastic and Real Symmetric Matrices

Stochastic matrices are very important in the study of Markov processes, Economics and operational research. Symmetric real matrices have the feature of being diagonalizable using an orthonormal basis from its eigenvectors. In the following we present important theorems concerning these two special types of matrices that will be used later.

C.1 Properties of stochastic matrices

A square $n \times n$ matrix $\mathbf{T}$ is a *stochastic matrix* when all its entries are non-negative real numbers and the sum of each column (or row) is a constant, that is,

$$\sum_{i=1}^{n} T_{ij} = a \quad \text{or} \tag{C.1}$$

$$\sum_{j=1}^{n} T_{ij} = a, \quad \text{with} \quad a \in \mathbb{R}. \tag{C.2}$$

When both row and column sums are constant (the same constant), the matrix is *doubly stochastic*. A transition matrix from a Markov process is always stochastic: a given state will make a transition to another one with probability one. So, in Markov process the stochastic matrix will have the column sum (or row sum) equal to one, as a conservation of probability consequence. In the following we will list a set of useful results concerning stochastic matrices.

Proposition C.1.1. *The product of two $n \times n$ stochastic matrices is a stochastic matrix.*

Proof. Let $\mathbf{T}$ and $\mathbf{Q}$ be $n \times n$ stochastic matrices with $\sum_{i=1}^{n} T_{ij} = \sum_{i=1}^{n} Q_{ij} = 1$. The product between $\mathbf{T}$ and $\mathbf{Q}$ is given by:

$$(\mathbf{TQ})_{ij} = \sum_{k=1}^{n} T_{ik} Q_{kj} = (T_{i1} Q_{1j} + \cdots + T_{in} Q_{nj}), \tag{C.3}$$

so the sum over a column will be:

$$\begin{aligned} \sum_{i=1}^{n} (\mathbf{TQ})_{ij} &= \sum_{i=1}^{n} \sum_{k=1}^{n} T_{ik} Q_{kj} \\ &= T_{11} Q_{1j} + \cdots + T_{n1} Q_{1j} + \cdots + T_{nn} Q_{nj} \\ &= Q_{1j}(T_{11} + \cdots + T_{n1}) \cdots + Q_{nj}(T_{1n} + \cdots + T_{nn}) \\ &= Q_{1j} + Q_{2j} + \cdots + Q_{nj} = 1, \end{aligned} \tag{C.4}$$

and $\mathbf{TQ}$ is a stochastic matrix. □

Theorem C.1.2. *If* $\mathbf{T}$ *is a stochastic matrix, then* $\mathbf{T}^k$ *is a stochastic matrix for all* $k \in \mathbb{Z}^+$.

Proof. We will use the principle of mathematical induction. For $k = 1$, the property is trivial. Now suppose that $\mathbf{T}^{k-1}$ is a stochastic matrix. Using the proposition C.1.1, we have that $(\mathbf{T}^{k-1}\mathbf{T}) = \mathbf{T}^k$ is a stochastic matrix. □

Theorem C.1.3. *If* $p(0) = (p_{01}, \ldots, p_{0n})$ *is an initial distribution for a stochastic process with transition matrix* $\mathbf{T}$*, then the distribution at a time* t *is* $p(t) = T^k p(0)$.

Proof. We will use the principle of mathematical induction. When $t = 0$, it is trivial, since $p(0) = \mathbf{T}p(0)$. Now assume that $p(k-1) = p_0 \mathbf{T}^{k-1}$. Then, $\mathbf{T}p(k-1) = \mathbf{T}^k p(0)$, so we just have to show that $p(k) = \mathbf{T}p(k-1)$. For the i component of this vector we have:

$$\begin{aligned} (\mathbf{T}p(k-1))_i &= \sum_{j=1}^{n} T_{ij} p(k-1)_j \\ &= \sum_{j=1}^{n} P(X_k = i | X_{k-1} = j) | P(X_{k-1} = j) \\ &= \sum_{j=1}^{n} P(X_k = i | X_{k-1} = j) \\ &= p(k)_i, \end{aligned} \tag{C.5}$$

which proves the statement. □

Thus, the distribution of states after k steps can be determined in terms of the initial distribution and the transition matrix raised to the k^{th} power.

Theorem C.1.4. *If* $\mathbf{T}$ *is a stochastic matrix* $n \times n$ *(columns sum to* 1*), then* $\lambda = 1$ *is an eigenvalue.*

Proof. It is necessary to solve the equation $\mathbf{xT} = \mathbf{x}$, and $\mathbf{x}$ is the left eigenvector assigned to $\lambda = 1$. Consider now that $x_i = 1$ for all $i = 1, \ldots, n$. Then,

$$\begin{aligned}(\mathbf{xT})_i &= \sum_{j=1}^{n} x_j T_{ji} \\ &= \sum_{j=1}^{n} T_{ji} \\ &= 1 \\ &= x_i. \end{aligned} \tag{C.6}$$

□

Theorem C.1.5. *If* $\lambda \in \mathbb{C}$ *is an eigenvalue of an* $n \times n$ *stochastic matrix* $\mathbf{T}$*, then* $|\lambda| \leq 1$.

Proof. Let $\mathbf{x}$ be the left eigenvector corresponding to λ and $x_k \equiv \max_{i \in [n]} x_i$. Since $\mathbf{xT} = \lambda \mathbf{x}$, we write:

$$\begin{aligned}(\lambda \mathbf{x})_k &= (\mathbf{xT})_k \\ &= (x_1 T_{1k} + \cdots + x_n T_{nk}). \end{aligned} \tag{C.7}$$

Now, taking the absolute value of Eq. (C.7) and using the triangle inequality $|\sum_{i=1}^{n} p_i| \leq \sum_{i=1}^{n} |p_i|$ we have:

$$\begin{aligned}|\lambda||x_k| &= |x_1 T_{1k} + \cdots + x_n T_{nk}| \\ &\leq |x_1 T_{1k}| + \cdots + |x_n T_{nk}| \\ &= T_{1k}|x_1| + \cdots + T_{nk}|x_n| \quad (\text{since} \quad T_{ij} \geq 0 \quad \forall i, j) \\ &\leq |x_k|(T_{1k} + \cdots + T_{nk}) \qquad (\text{the column sum is 1}) \\ &= |x_k|. \end{aligned} \tag{C.8}$$

Then, $|\lambda||x_k| \leq |x_k| \implies |\lambda| \leq |1|$. □

C.2 Properties of real symmetric matrices

A symmetric matrix $\mathbf{S}$ is a square matrix that is equal to its transpose, that is, $\mathbf{S} = \mathbf{S}^\top$. When the elements of a symmetric matrix $\mathbf{A}$ are complex numbers, we say that the matrix is a Hermitian matrix and $\mathbf{A} = \overline{\mathbf{A}^\top}$. Real symmetric matrices have important properties concerning its eigenvectors, that will be showed in the next theorems.

Theorem C.2.1. *If $\mathbf{S}$ is a real symmetric matrix, then its eigenvalues are real numbers.*

Proof. Let $\lambda \in \mathbb{C}$ be an eigenvalue of $\mathbf{S} \in \mathbb{R}^n \times \mathbb{R}^n$ and $\mathbf{u} \in \mathbb{C}^n$ its corresponding eigenvector. The eigenvalue equation can be stated as:

$$\mathbf{S}\mathbf{u} = \lambda\mathbf{u} \tag{C.9}$$

Taking the complex conjugate of Eq. (C.9) and using the fact that $S^* = S$, we have:

$$\mathbf{S}\mathbf{u}^* = \lambda^*\mathbf{u}^*. \tag{C.10}$$

Now multiplying both sides of Eq. C.9 by $(\mathbf{u}^*)^\top$,

$$(\mathbf{u}^*)^\top\mathbf{S}\mathbf{u} = \lambda(\mathbf{u}^*)^\top\mathbf{u}. \tag{C.11}$$

Using the associative property of matrix multiplication and the fact that $(\mathbf{AB})^\top = \mathbf{B}^\top\mathbf{A}^\top$:

$$\begin{aligned}\lambda(\mathbf{u}^*)^\top\mathbf{u} &= ((\mathbf{u}^*)^\top\mathbf{S})\mathbf{u} \\ &= (\mathbf{S}^\top\mathbf{u}^*)^\top\mathbf{u} \\ &= (\mathbf{S}\mathbf{u}^*)^\top\mathbf{u} \\ &= \lambda^*(\mathbf{u}^*)^\top\mathbf{u},\end{aligned} \tag{C.12}$$

resulting in the following relation:

$$(\lambda - \lambda^*)(\mathbf{u}^*)^\top\mathbf{u} = 0. \tag{C.13}$$

Now, since $\mathbf{u}$ is an eigenvector from $\mathbf{S}$, it must have at least one non-zero component, and then

$$(\mathbf{u}^*)^\top\mathbf{u} = \sum_{i=1}^{n} u_i^* u_i > 0. \tag{C.14}$$

Hence, to satisfy Eq. (C.13) we require that

$$\lambda = \lambda^*, \tag{C.15}$$

and λ is necessarily a real number. □

Theorem C.2.2. *The eigenvectors of a symmetric matrix are orthogonal.*

Another important property of symmetric matrices concerns the orthogonality of its eigenvectors.

Proof. Consider two eigenvectors $\mathbf{u_1}, \mathbf{u_2} \in \mathbb{R}^n$ from S with distinct eigenvalues $\lambda_1, \lambda_2 \in \mathbb{R}$. Their respective eigenvalue equations are given by:

$$\mathbf{S}\mathbf{u_1} = \lambda_1 \mathbf{u_1} \tag{C.16}$$

$$\mathbf{S}\mathbf{u_2} = \lambda_2 \mathbf{u_2}. \tag{C.17}$$

Multiplying both sides of the first equation above by $(\mathbf{u_2}^\top \mathbf{S})$ we have:

$$\begin{aligned} \lambda_1 \mathbf{u_2}^\top \mathbf{u_1} &= (\mathbf{u_2}^\top \mathbf{S}) \\ &= (\mathbf{S}^\top \mathbf{u_2})^\top \mathbf{u_1} \\ &= \lambda_2 \mathbf{u_2}^\top \mathbf{u_1}, \end{aligned} \tag{C.18}$$

resulting in the following condition:

$$(\lambda_1 - \lambda_2)\mathbf{u_2}^\top \mathbf{u_1} = 0. \tag{C.19}$$

Since we are considering distinct eigenvalues, $\lambda_1 \neq \lambda_2$ the only possibility to satisfy Eq. C.19 is

$$\mathbf{u_2}^\top \mathbf{u_1} = 0, \tag{C.20}$$

that is, $\mathbf{u_1}$ and $\mathbf{u_2}$ are orthogonal. □

Appendix D

The number of mutualistic pairs in the TN model

In this appendix we will define the interaction matrix J used in chapter 8. Then, we calculate the probability of large pairs, that is, the probability that both $J(x,y)$ and $J(y,x)$ are greater than some number α. As we discussed in chapter 8, the quasi-stable phases in the model are correlated to the presence of mutualistic interactions, corresponding to the large pairs in J.

D.1 Generation of the Interaction Matrix

The matrix J defines the relationship between the individuals in the tangled nature model. The interactions can be mutually positive ($J(x,y)>0$ and $J(y,x)>0$), mutually negative ($J(x,y)<0$ and $J(y,x)<0$), crossed ($J(x,y)>0$ and $J(y,x)<0$) or zero ($J(x,y)=0$ and $J(y,x)=0$). One individual does not interact with itself, thus $J(x,x)=0 \quad \forall x$. The interactions are fixed in the beginning of the simulation and do not change with time.

A pair of matrix elements, $J(x,y)$ and $J(y,x)$, is produced as follows [145]. There is a string of 0's and 1's associated with each of x and y, denoted as S_x and S_y. These can be associated with numbers n_x and n_y between 1 and 2^L by considering them to be binary coefficients. A third number, n_{xy}, can also be associated with the pair by forming $\mathrm{XOR}(S_x,S_y)$[1] and treating that string as binary coefficients.

Then, two sets of random numbers are produced, $f(n)$ and $g(n)$, $1 \le n \le 2^L$. The set $\{g(n)\}$ is taken to be uniform on the interval $[-1,1]$. For the set $\{f(n)\}$ we take some

[1] The exclusive or operation XOR compares two binary strings B and C and generates a third one that will have the element $A_i = 1$ if $B_i = 1$ and $C_i = 0$ or $B_i = 0$ and $C_i = 1$. Also, $A_i = 0$ if $B_i = C_i$.

$\theta \in (0,1)$ such that, with probability $1-\theta$, f is zero. If it is not zero (which occurs with probability θ) it is taken uniformly on the interval $[-1,1]$. In practice one selects f in the same way as g and then sets $f(n)$ to zero with probability $1-\theta$. In summary

$$P(g_0 \le g \le g_0 + dg) = dg/2, \tag{D.1}$$

while for f

$$P(f_0 \le f \le f_0 + df) = \theta\, df/2 \qquad \text{for } f_0 \neq 0. \tag{D.2}$$

With this notation,

$$J(x,y) = f(n_{xy})g(n_y) \text{ and } J(y,x) = f(n_{xy})g(n_x). \tag{D.3}$$

D.2 One Pair

We want the probability that both $J(x,y)$ and $J(y,x)$ are greater than some number α. This can be stated as:

$$p(\alpha) = \Pr(f(n_{xy})g(n_y) > \alpha \,\&\, f(n_{xy})g(n_x) > \alpha). \tag{D.4}$$

First consider the case where both f and g, for the selected numerical values, are positive. Call the associated probability $p^{(+)}(\alpha)$. For convenience, we write $r \equiv f(n_{xy})$ and $s_u \equiv g(n_u)$, $u = x, y$. We condition on r and sum over its possible values. Obviously it must be greater than α and less than 1. Using $\Pr(A|B) = \Pr(A\&B)/\Pr(B)$, we have

$$\begin{aligned} p^{(+)}(\alpha) &= \Pr(rs_y > \alpha \,\&\, rs_x > \alpha) \\ &= \sum_r \Pr(s_y > \alpha/r \,\&\, s_x > \alpha/r) * \Pr(r \le r_0 < r + dr) \\ &= \int_\alpha^1 dr\,(\theta/2)\Pr(s_y > \alpha/r \,\&\, s_x > \alpha/r) \\ &= \frac{\theta}{2} \cdot \frac{1}{4} \int_\alpha^1 dr\,(1-\alpha/r)^2\,. \end{aligned} \tag{D.5}$$

In the last term on the first line above r_0 is a dummy variable. The step from line 2 to line 3 is justified by s_x and s_y being independent (so that probabilities multiply) and the

fact that $\Pr(s_y > \alpha/r) = (1-\alpha/r)/2$. The integral in Eq. (D.5) is evaluated as follows.

$$I \equiv \int_\alpha^1 dr\,(1-\alpha/r)^2 = 1-\alpha-2\alpha\log r\,\Big|_\alpha^1 - \alpha^2\int_{1/\alpha}^1 ds\,, \tag{D.6}$$

where in the last term the substitution $s = 1/r$ has been made. Evaluating further gives

$$I = 1+2\alpha\log\alpha-\alpha^2\,. \tag{D.7}$$

Substituting

$$p^{(+)}(\alpha) = \frac{\theta}{8}\left(1+2\alpha\log\alpha-\alpha^2\right). \tag{D.8}$$

There is another way that both $J(x,y)$ and $J(y,x)$ can be large, namely if the corresponding f and g's are all negative. This has the same probability as the all-positive case, so the final answer is

$$p(\alpha) = \frac{\theta}{4}\left(1+2\alpha\log\alpha-\alpha^2\right). \tag{D.9}$$

D.3 Two Pairs

Two pairs involve the combination of 4 separate matrix elements. In this case we have two independent calculations and the probability that there are two unrelated pairs is just the square of what has already been calculated. Thus

$$p^{(2)}(\alpha) = \left[\frac{\theta}{4}\left(1+2\alpha\log\alpha-\alpha^2\right)\right]^2. \tag{D.10}$$

D.4 Three Pairs

We look for triplets, x, y, z, such that all six quantities, J_{xy}, J_{yx}, J_{xz}, J_{zx}, J_{yz} and J_{zy} exceed α. With each index and pair of indices we have associated S_u, $\mathsf{XOR}(S_u,S_v)$, n_u, n_{uv}, s_u, r_{uv}, as above, with $u,v \in \{x,y,z\}$. Note that not all these numbers are independent. Thus $\mathsf{XOR}(\mathsf{XOR}(S_x,S_y),\mathsf{XOR}(S_x,S_z)) = \mathsf{XOR}(S_y,S_z)$ (this is easily seen by considering $(S_x+S_y)+(S_x+S_z) = S_y+S_z$, all addition mod 2). However, this does not affect the independence of the variables in question, just as $f(n_{xy})$ was independent despite n_{xy} being dependent on x and y. This is because the f's and g's are all independent.

As before, we condition on values for $\{r_{uv}\}$ and generalize the previous notation. We integrate over the $\{r_{uv}\}$ values. First notice that the superscripts on the $p(\alpha)$'s have

different meanings. $p^{(2)}(\alpha)$ refers to 4 distinct genomes, while $p^{(3)}(\alpha)$ refers to only 3, but imposes conditions on the 6 possible combinations. For all 6 numbers positive, the desired quantity is:

$$\begin{aligned} p^{(3,+)}(\alpha) &= (\theta/2)^3 \int_\alpha^1 \int_\alpha^1 \int_\alpha^1 dr_{xy} dr_{xz} dr_{yz} \Pr\big(s_x > \alpha/r_{xy}\big) \Pr\big(s_y > \alpha/r_{xy}\big) \\ &\quad \times \Pr(s_x > \alpha/r_{xz}) \Pr(s_z > \alpha/r_{xz}) \Pr\big(s_y > \alpha/r_{yz}\big) \\ &\quad \times \Pr\big(s_z > \alpha/r_{yz}\big) . \end{aligned} \tag{D.11}$$

The case where some of these numbers are negative will be treated later. First we simplify the writing defining $\xi \equiv r_{yz}$, $\eta \equiv r_{xz}$ and $\zeta \equiv r_{xy}$. Then note that each s_u appears twice and depending on which α/r_{uv} is larger only the more stringent of these inequalities need be taken into account. To take advantage of this we note that there are 6 possibilities: $\xi > \eta > \zeta$, $\xi > \zeta > \eta$, etc. Therefore we integrate over only one of these and multiply the result by 6. It follows that

$$\begin{aligned} p^{(3,+)}(\alpha) &= 6\left(\frac{\theta}{2}\right)^3 \int_\alpha^1 d\xi \int_\alpha^\xi d\eta \int_\alpha^\eta d\zeta \Pr(s_x > \alpha/\zeta) \Pr\big(s_y > \alpha/\zeta\big) \\ &\quad \times \Pr(s_x > \alpha/\eta) \Pr(s_z > \alpha/\eta) \Pr\big(s_y > \alpha/\xi\big) \Pr(s_z > \alpha/\xi) \\ &= 6\left(\frac{\theta}{2}\right)^3 \int_\alpha^1 d\xi \int_\alpha^\xi d\eta \int_\alpha^\eta d\zeta \Pr(s_x > \alpha/\zeta) \Pr\big(s_y > \alpha/\zeta\big) \\ &\quad \times \Pr(s_z > \alpha/\eta) . \end{aligned} \tag{D.12}$$

Now make use of the properties of the random variables $\{s_u\}$ to get

$$p^{(3,+)}(\alpha) = 6\left(\frac{\theta}{2}\right)^3 \frac{1}{8} \int_\alpha^1 d\xi \int_\alpha^\xi d\eta \int_\alpha^\eta d\zeta \left(1-\frac{\alpha}{\zeta}\right)^2 \left(1-\frac{\alpha}{\eta}\right). \tag{D.13}$$

The ζ integral is just the "I" of Eq. (D.6),

$$\begin{aligned} p^{(3,+)}(\alpha) &= 6\left(\frac{\theta}{2}\right)^3 \frac{1}{8} \int_\alpha^1 d\xi \int_\alpha^\xi d\eta \left(1-\frac{\alpha}{\eta}\right) \int_\alpha^\eta d\zeta \left(1-\frac{\alpha}{\zeta}\right)^2 \\ &= \frac{3}{4}\left(\frac{\theta}{2}\right)^3 \int_\alpha^1 d\xi \int_\alpha^\xi d\eta \left(1-\frac{\alpha}{\eta}\right) \left[\eta - \alpha - 2\alpha \log\frac{\eta}{\alpha} + \alpha\left(1-\frac{\alpha}{\eta}\right)\right] \\ &= \frac{3\theta^3}{32} \int_\alpha^1 d\xi \int_\alpha^\xi d\eta \left(1-\frac{\alpha}{\eta}\right) \left[\eta - \frac{\alpha^2}{\eta} - 2\alpha \log\frac{\eta}{\alpha}\right]. \end{aligned} \tag{D.14}$$

We will shortly carry this forward, but already some observations can be made. For $\theta = 1/4$ the prefactor is $3/2048$, which is not far from $1/2^8$. Couple that with an integral that is quite small for α near 1, and you need quite large "L" to see this possibility play a role.

All integrations can be done explicitly and one gets the result

$$p^{(3,+)}(\alpha) = \frac{3\theta^3}{32}\left\{\frac{1}{6}(1-\alpha)[1+\alpha(7+22\alpha)] + \alpha\log\alpha\Big[1+\alpha(3+\alpha)+\alpha\log\alpha\Big]\right\}. \quad \text{(D.15)}$$

Now consider the possibility that the inequalities for the matrix elements are satisfied by having some of the f's and g's negative. Suppose $r_{xy} < 0$. Then both s_x and s_y must also be negative. But if $s_y < 0$, to satisfy the inequality for J_{yz} we need $r_{yz} < 0$. By this argument, all f's and g's must be negative. The probability integral for this possibility gives the same value as that for positive values, so all that is needed is a factor 2, as for the case of a single pair of matrix elements. Thus, finally

$$p^{(3)}(\alpha) = \frac{3\theta^3}{16}\left\{\frac{1}{6}(1-\alpha)[1+\alpha(7+22\alpha)] + \alpha\log\alpha\Big[1+\alpha(3+\alpha)+\alpha\log\alpha\Big]\right\}, \quad \text{(D.16)}$$

A remarkable feature of this expression is its expansion in $\bar{\alpha} \equiv 1-\alpha$,

$$p^{(3)}(\alpha) = \frac{3\theta^3}{16}\left[\frac{\bar{\alpha}^6}{90} + \frac{17\bar{\alpha}^7}{1260} + \frac{13\bar{\alpha}^8}{1008} + \frac{29\bar{\alpha}^9}{2520} + \mathrm{O}(\bar{\alpha}^{10})\right]. \quad \text{(D.17)}$$

If $\bar{\alpha} = 0.1$ ($\alpha = 0.9$), and we use a small L, there is no chance of success. But consider $L = 20$, for which there will be roughly $(2^{20})^2/2 = 2^{39}$ off diagonal matrix elements. Then the estimate above gives $\bar{\alpha}^6 \times 1.8 \times 10^7$; so for $\alpha = 0.9$ there will be about 20 triplets exceeding the 0.9 threshold.